

https://dspace.org/

Characterisation of the geothermal waters of South Africa

Safi, Musarrat

2025-02
University of the Witwatersrand, Johannesburg
https://hdl.handle.net/10539/49415
Safi, Musarrat. (2025). Characterisation of the geothermal waters of South Africa. [Master's dissertation, University of the Witwatersrand, Johannesburg]. WIReDSpace. https://hdl.handle.net/10539/49415

Downloaded from a DSpace repository. https://dspace.org/

CHARACTERISATION OF THE GEOTHERMAL WATERS OF SOUTH AFRICA

by

Musarrat Safi
Student Number: 0312755V; ORCID: **0000-0002-1085-3942**

A dissertation submitted to the Faculty of Science, University of the Witwatersrand, Johannesburg, in fulfilment of the requirements for the degree of Master of Science.



WITS
UNIVERSITY

School of Geosciences

Supervisors: Professor Gillian Drennan
Dr Khuliso Masindi

21 February 2025

CANDIDATE'S DECLARATION

I declare that this dissertation is my own, unaided work. It is being submitted for the Degree of Master of Science at the University of the Witwatersrand, Johannesburg. It has not been submitted before for any degree or examination at any other University.



(Signature of candidate)

21st Day of February 2025

ABSTRACT

The lack of active volcanism in South Africa gives the impression that there are no geothermal energy sources. Conversely, there are 41 known geothermal water sites which are surface manifestations of geothermal energy in South Africa. By characterising the geothermal waters for their hydrochemical properties it is possible to investigate their potential as energy sources. Prior to the current investigation, there was insufficient regional data to properly characterise the geothermal waters as the South African energy nexus excluded geothermal energy.

This research presents the hydrochemical characterisation of the 41 geothermal waters of South Africa against the backdrop of their geological settings. Their physical properties (temperature, pH, electrical conductivity, salinity) were measured at the source. Chemical analyses (Cl^-, HCO_3^-, SO_4^{2-}, Na^+, Ca^+, Mg^{2+}, K^+, and Fe^{2+}, SiO_2) were conducted using induced coupled plasma-optical emission spectrometer. Stable isotopes (δO18 and δD) and radiogenic isotope-tritium were analysed using an isotope ratio mass spectrometer and laser water isotope analyser, respectively.

The results showed that the geothermal waters in South Africa are located in three main geological settings 1) basement/crystalline rock types, 2) orogenic belts and 3) intracratonic basins. Most of the geothermal waters display varying temperatures (25°C (Cradock) to 61°C (Brandvlei)), pH (3.5 (Badsfontein and Aliwal) to 9 (Warmbath1)) and electrical conductivity (2 µS/cm (Bricks) to 4930 µS/cm (Riemvasmaak)). Four types of geothermal waters were identified in order of decreasing abundance, Na-Cl, mixed, Mg-HCO3 and Na-HCO3 waters. Most of these geothermal waters exhibit silicate weathering, partial equilibration and appear to be associated with a seawater signature. The isotope signatures confirm that the geothermal waters are of meteoric origin and are mostly older than 70 years.

This study established that 20 out of the 41 geothermal water sites have low to medium enthalpy ranges of 432 to 624 kJ/kg, that could be harnessed for power generation. Furthermore, it was estimated that waters between 1.6 and 2.7 km deep are likely to reach temperatures ranging between 102°C and 148°C. Most of the favourable sites are associated with the basement/crystalline Archean granites and gneisses, and orogenic belts such as the Limpopo Mobile Belt (associated with Soutpansberg and Waterberg Groups), and the Namaqua Natal Province.

DEDICATION

To my loving family and friends that have supported me throughout my academic career thus far.

ACKNOWLEDGEMENTS

My sincere gratitude is to the Almighty who has given me the ability to learn and have fun while doing it.

I wish to express my gratitude to my supervisors for their supervision, Professor Gillian Drennan and Dr Khuliso Masindi.

You have my greatest thanks, Dr Taufeeq Dhansay for throwing me into hot waters where your continuous guidance and encouragement throughout this journey is greatly appreciated.

The work I am presenting would not have been possible without the support from the Council for Geoscience. I am grateful for the opportunity, time and funding received during this study.

I am grateful to my colleagues at the Council for Geoscience for their attention to detail, encouragement, support and the most enjoyable trips to all the geothermal water sites in South Africa. Those memories I will cherish forever.

I am deeply appreciative to all the owners, managers, community leaders and members for their trust, patience and understanding for allowing the sampling of geothermal waters.

My indebted gratitude to my village- all my loving family and friends who understood my apology of “I’m concentrating on my studies and can’t make it”. I am grateful for your understanding, prayers and humour. Your support means more than you realise.

I thank the great scientists of all times, for through their work mine was made possible.

May the Almighty reward you for your efforts, guidance, understanding, patience and kindness.

CONFERENCES AND WORKSHOP ATTENDED

Safi, M., Motlakeng, T., Ngamlana, S., Maja, F., Ngubana, M., Phahlane, I., and Dhansay, T. (2022). Energy under your feet. Oral presentation at the Green Energy Day held online, South Africa, 30 August 2022.

Safi, M., Motlakeng, T., Ngamlana, S., Maja, F., Ngubana, M., Phahlane, I., and Dhansay, T. (2023). Advances made in geothermal energy in South Africa. Oral presentation at the GeoCongress held in Stellenbosch, South Africa, 11-13 January 2023.

TABLE OF CONTENTS

CANDIDATE'S DECLARATION ii
ABSTRACT iii
DEDICATION iv
ACKNOWLEDGEMENTS v
CONFERENCES AND WORKSHOP ATTENDED vi
TABLE OF CONTENTS vii
LIST OF FIGURES xi
LIST OF TABLES xiv
LIST OF EQUATIONS xv
NOTATIONS xvi
ABBREVIATIONS AND ACRONYMS xvii
SAMPLE NOMENCLATURE xviii
LIST OF DEFINITIONS xix
CHAPTER 1 Introduction and scope of this dissertation 1
1.1 Current energy status in South Africa 1
1.2 Climate change mitigation 2
1.3 South Africa's shift toward renewable energy 3
1.3.1 South Africa's energy development 4
1.3.2 CO_2 sequestration and geothermal energy 6
1.4 Geothermal energy in South Africa 7
1.5 Characterising the geothermal waters in South Africa 8
1.5.1 Aims and specific objectives 10
1.6 Brief chapter overview 10
CHAPTER 2 Concepts of geothermal energy 11
2.1 The Earth's internal heat 11
2.2 Types of geothermal systems 13
2.2.1 Convective geothermal systems 15
2.2.2 Conductive geothermal systems 17
2.3 Harnessing geothermal energy 19
2.3.1 Dry steam power plants 20
2.3.2 Flash power plants 21
2.3.3 Binary plants 22
CHAPTER 3 Literature review 25

3.1 Characterisation of geothermal waters for power generation 25
3.2 Geology and structural controls of the geothermal waters in South Africa . 27
3.3 Physical and chemical properties of the geothermal waters in South Africa 31
3.3.1 Hydrochemical properties 32
3.3.2 Stable isotopes: Oxygen, hydrogen and radiogenic isotopes 34
3.3.3 Geothermometry 36
3.3.4 The potential geothermal energy from geothermal waters of South Africa 38
3.3.4.1 Research into the utilisation of geothermal waters in South Africa 39
3.3.5 Harnessing geothermal waters for power generation 40
CHAPTER 4 Materials and methods 43
4.1 Geological settings of the geothermal waters of South Africa 43
4.2 Hydrochemical sampling 44
4.2.1 Physical properties 44
4.2.2 Chemical properties 45
4.2.3 Stable and radiogenic isotopes 45
4.2.4 Methods for analysing the hydrochemistry of the geothermal waters . 46
4.2.5 Data presentation 46
4.2.5.1 Statistical presentation 47
4.2.5.2 Graphical presentation 47
4.3 Geothermometry 48
4.4 Estimating the enthalpy of the geothermal waters 51
4.5 Estimation of the circulation depth of the geothermal waters 51
CHAPTER 5 Results 52
5.1 Geological settings and structural controls 52
5.1.1 Archean granites and gneisses 53
5.1.2 Pongola Supergroup and Transvaal Supergroup 55
5.1.3 Limpopo Mobile Belt, Soutpansberg Group and Waterberg Group 55
5.1.4 Namaqua-Natal Province 57
5.1.5 Cape Fold Belt, Karoo Supergroup and Uitenhage Group 58
5.2 Hydrochemical Results 59
5.2.1 Physical properties 59
5.2.2 Chemical properties 64

5.2.3 Stable Isotopes: Oxygen 18 (δ18O) and deuterium (δD) results 77
5.2.4 Tritium (^3H) 78
5.3 Geothermometry 80
5.4 Enthalpy 83
5.5 Circulation depth estimations of geothermal waters with low to medium enthalpy range 85
CHAPTER 6 Discussion 87
6.1 Geological settings 87
6.2 Hydrochemistry classification 90
6.2.1 Physical properties 90
6.2.2 Chemical properties 92
6.2.2.1 Na-Cl-type waters 93
6.2.2.2 Na-HCO_3-type waters 95
6.2.2.3 Mg-HCO_3-type waters 96
6.2.2.4 Mixed-type waters 97
6.3 Fluid-mineral equilibria 97
6.4 Isotopic classification 99
6.4.1 Stable Isotopes 99
6.4.2 Radiogenic isotope tritium 102
6.5 Most suitable geothermal waters 103
CHAPTER 7 Conclusion and recommendations 107
7.1 Re-evaluation of the aims and objectives 107
7.2 Contributions and impact 109
7.3 Recommendations 110
References 111
Appendix A: A comprehensive list of the analyses of geothermal waters from Kent (1949); Waring (1965) and Olivier and Jonker (2013). 133
Appendix B: Steam tables- Thermodynamic data for water at saturated vapor pressures and temperatures (adopted from Henley et al., 1984). 138
Appendix C: Geothermometry (°C) for geothermal waters for current study. 139
Appendix D: Geothermal gradients (sourced from Dhansay et al., 2017) for the geothermal waters of South Africa. 143
Appendix E: Measured temperatures (°C), quartz geothermometry temperatures (°C) and circulation depths (km) for the 41 geothermal waters of South Africa. 145
Appendix F: The geological domains, geothermometry, circulation depths and low-medium enthalpy of the geothermal waters in South Africa. 147

Appendix G: Conference Abstracts 148

LIST OF FIGURES

Figure 1: The current and planned energy usage shows a decrease in coal (from 89% to 51%), (modified from Department of Mineral Resources and Energy, 2019). 2

Figure 2: A comparison of energy supplied from various sources showing a steady decrease in coal powered energy and increase in renewable resources (modified from CSIR, 2022). 3

Figure 3: South Africa's load-shedding history from 2007 to December 2022. The dotted line shows the percentage of increase in load-shedding (modified from CSIR, 2022). 4

Figure 4: The location of the geothermal waters within geological regions of the current study (modified from Dhansay et al., 2017). 9

Figure 5: Chapter overview of this dissertation. 10

Figure 6: Plate boundaries of the world (Moeck, 2014). 13

Figure 7: Conditions needed for a geothermal reservoir to form (modified from Nemzer et al., 2005). 14

Figure 8: Cross-section of the Earths' heat flow for each division (modified from Boden, 2017). 15

Figure 9: Convective geothermal systems adapted from Jolie et al. (2021).a) Active volcano. b) Magmatic rift. c) Extensional fault environment. 16

Figure 10: Lindal diagram showing the utilisation of geothermal resource at given temperatures and enthalpy range (modified from Anderson and Lund, 1980; Gudmundsson et al., 1985; Nemzer et al., 2005; Rubio-Maya et al., 2015; Zheng et al., 2015; Sveinbjörnsson, 2016; Chiasson, 2016; Boden, 2017). 19

Figure 11: The configuration of dry steam for geothermal power generation (Boden, 2017). 21

Figure 12: The configuration of flash plant for geothermal power generation (Boden, 2017). 22

Figure 13: The configuration of binary plant for geothermal power generation (Boden, 2017). 23

Figure 14: Overview of the research into the geothermal waters in South Africa. 27

Figure 15: Location of selected geothermal waters sites (in blue) investigated by various researchers (in black) in South Africa. 29

Figure 16: The process flow of the methods and tools applied for characterising the geothermal waters. 43

Figure 17: The geothermal water sampling sites in this study. Note the geothermal water are located across the country. The abbreviations of the sites are listed on the right. 44

Figure 18: The process flow for presentation of results of the geothermal waters in South Africa. 52

Figure 19: The geothermal waters in South Africa, underlying geology and tectonic domains (modified from Dhansay et al., 2017). 53

Figure 20: Illustration showing the inverse correlation of temperature (°C) (measured at surface manifestations) versus the electrical conductivity (EC) of the geothermal waters. The geothermal waters are colour coded per geological domain..... 62

Figure 21: Schoeller diagram showing the trend of the anions and cation analyses of the geothermal water sites sampled. The analyses are colour coded per geological domain (Schoeller, 1963). 65

Figure 22: Scatter plot showing the relationship of chlorine concentration to the total ion concentration in the 41 geothermal water sites of South Africa . The top plot (a) shows the zoomed area of the orange box from the bottom plot (b). The geothermal waters are colour coded per geological domain. 66

Figure 23: Piper diagram of the sampled geothermal waters in South Africa showing the cation and anion concentrations based on hydrochemical analyses (Piper, 1944; Bethke et al., 2022). The geothermal waters are colour coded per geological domain. 67

Figure 24: Bivariate scatter plot displaying the relationship Ca+Mg and SO_4+HCO_3 in the sampled geothermal waters. The top plot (a) shows the zoomed area of the blue box from the bottom plot (b). The silicate and carbonate weathering are delineated by an equiline plotted that has a ratio of 1:1 to the ions. The geothermal waters are colour coded per geological domain. 69

Figure 25: Bivariate scatter plot displaying the relationship Ca+Mg and Na+K (meq/l) in the sampled geothermal waters. The top plot (a) shows the zoomed area of the blue box from the bottom plot (b). The silicate and carbonate weathering fields are delineated by a line that has a ratio of 1:1 to the ions plotted. The geothermal waters are colour coded per geological domain..... 71

Figure 26: 10Mg/(Mg+Ca) versus 10K/(10K+Na) binary plot (Baioumy et al., 2015), of geothermal waters that were sampled for this study. The black line displays the equilibration line at various temperatures. The geothermal waters are colour coded per geological domain. 72

Figure 27: Ternary diagram of Na/1000, K/100 and square root of Mg ion analyses. The geothermal water ratios are plotted in the immature water field, partial equilibrium and full equilibrium fields as delineated. The geothermal waters are colour coded per geological domain. 74

Figure 28: Maps illustrating the hydrochemistry results from the sampled geothermal waters together with the major structural features (produced in ArcGIS Pro)..... 76

Figure 29: A plot of δD versus δ18O for the sampled geothermal waters, Local Meteoric Water Line (LMWL). The geothermal waters are colour coded per geological domain. 77

Figure 30: The equilibration graphs of quartz and chalcedony show exponential increase in silica ions (mg/l) and temperature (°C)..... 80

Figure 31: Computation comparison of the geothermometry (°C) representing various forms of silica. 81

Figure 32: Theoretical curves for the silica geothermometry compared to the calculated quartz (Fournier, 1977) geothermometer of the sampled geothermal waters..... 81

Figure 33: Computation comparison of the geothermometry (°C) utilising Na^+, K^+ and Mg^{2+} concentrations. 82

Figure 34: Circulation depth of the geothermal waters together with measured temperature of the geothermal waters at surface and quartz geothermometry temperatures (°C). 86

Figure 35: The current study process flow for the discussion of the results. 87

Figure 36: The various types of geological settings and heat transfer mechanism of the geothermal waters in South Africa (modified from Moeck, 2014). 89

Figure 37: Geothermal water sites sampled including the geology and structure of the areas. 90

Figure 38: A plot of δD versus δ18O for the South African geothermal waters and the Local Meteoric Water Line (LMWL). Previous isotope analyses plotted in red (Diamond and Harris, 2000) and black (Mazor and Verhagen, 1983). Colour coded per geological domain. 101

Figure 39: Overview of the major geological domains and tectonic structures across South Africa. The locations of the various potential geothermal waters for harnessing geothermal energy are marked on the map with enthalpy ranges denoted by circle size and calculated circulation depth of the geothermal waters. Produced in ArcGIS Pro and modified from Dhansay et al. (2017). 105

Figure 40: Schematic diagram of a conceptual model for harnessing geothermal energy in a cascading manner (Onyango and Varet, 2014). 106

LIST OF TABLES

Table 1: Temperature, enthalpy range and type of plants utilised for power generation (modified from Sveinbjörnsson, 2016). 24

Table 2: Analyses on the geothermal waters collected. 46

Table 3: Temperature (°C) equations for geothermometers. 50

Table 4: The geothermal waters sampled showing the temperatures (°C), pH and electrical conductivity (EC-(µS/cm) in South Africa. 60

Table 5: Pearson correlation matrix showing the relationships between physical properties and hydrochemical properties of the geothermal waters sampled in South Africa. Dark green indicates a strong to very strong correlation, green indicates a moderate correlation, while the pink to light pink the correlation is weak between the physical properties and hydrochemical properties. 63

Table 6: Tritium values for the geothermal waters of South Africa with analytical error of 0.2 tritium unit (TU)..... 79

Table 7: The enthalpy range (Figure 10) and calculated quartz geothermometry (°C) (Fournier, 1977). 84

LIST OF EQUATIONS

Equation 1: $\delta T \delta z = T2 - T1 \delta z$ 11

Equation 2: $Q = -\lambda\ \delta T \delta z$ 12

Equation 3: $T_{SiO2} = 13095.19 - \log Si - 273.15$ 50

Equation 4: $T_{SiO2} = 15225.75 - \log Si - 273.15$ 50

Equation 5: $T_{SiO2} = 53.50 + 0.011236Si + -0.5559x10 - 4Si2 + 0.1772 \text{ x } 10 - 7\ Si3 + 88.390 \log Si$ 50

Equation 6: $T_{SiO2} = 10324.69 - \log Si - 273.15$ 50

Equation 7: $T_{SiO2} = 11124.91 - \log Si - 273.15$ 50

Equation 8: $T_{SiO2} = 10004.78 - \log Si - 273.15$ 50

Equation 9: $T_{SiO2} = 7184.51 - \log Si - 273.15$ 50

Equation 10: $T_{SiO2} = 7314.52 - \log Si - 273.15$ 50

Equation 11: $T_{Na/K} = 856 \log NaK + 0.857 - 273.15$ 50

Equation 12: $T_{Na/K} = 1217 \log NaK + 1.483 - 273.15$ 50

Equation 13: $T_{Na/K} = 933 \log NaK + 0.993 - 273.15$ 50

Equation 14: $T_{Na/K} = 13901.750 + \log NaK - 273.15$ 50

Equation 15: $T_{Na/K} = 1289 \log NaK + 1.615 - 273.15$ 50

Equation 16: $T_{Na/K} = 876.3 \pm 26.26 \log NaK + 0.8775 \pm 0.0508 - 273.15$ 50

Equation 17: $T_{K/Mg} = 441014 + \log K2Mg - 273.15$ 50

Equation 18: $z = Tcalc\text{-}TavgG$ 51

NOTATIONS

°C/km	Degree Celsius per kilometre- Geothermal gradient
$Wm^{-1} K^{-1}$	Power per unit distance per unit temperature -Thermal conductivity
$W m^{-2}$	Watts per square meter-Heat flow

ABBREVIATIONS AND ACRONYMS

CCUS	Carbon Capture, Utilization and Storage
CO_2	Carbon Dioxide
CCGT	Combined cycle gas turbines
CGS	Council for Geoscience
COP	Conference of Parties
CSP	Concentrated solar power
EC	Electrical conductivity
GHG	Greenhouse gases
GW	Gigawatt
GWh	Gigawatt hour
HELE	High-efficiency, low-emissions
ICP-OES	Induced coupled plasma-optical emission spectrometer
IEP	Integrated energy plan
IRP	Integrated resource plan
kWe	Kilowatt electric power
LEDS	Low Emissions Development Strategy
LMWL	Local Meteoric Water Line
ml	Millilitre
meq/L	Milliequivalents per litre
mg/l	Milligrams per litre
Ma	Million years ago
MW	Megawatt
MWe	Megawatt electric power
NCCAS	National Climate Change Adaptation Strategy
P4C	Presidential Climate Change Coordinating Commission
pH	Potential of hydrogen
r	Correlation coefficient
SADC	Southern African Development Community
sal	Salinity
SETs	Sectoral Emissions Targets
SDG	Sustainable Development Goal
SDGs	Sustainable Development Goals
SMOW	Standard Mean Ocean Water
TDS	Total dissolved solids
Temp.	Temperature (°C)
TU	Tritium units
UN	United Nations
UNFCC	UN Framework Convention on Climate Change
USD	United States Dollar

SAMPLE NOMENCLATURE

GeoWs Site	Abbreviation
Badplaas	BPS
Natal	NTL
Wagendrift	WGD
Baleni	BAL
Sulphur-Spring	SUS
Machadodorp	MDP
Siloam	SILO
Mphephu	MPU
Tshipise	TSH
Sagole	SAG
Evangelina	EVGL
Môreson	MRS
Rhemardo	RHM
Warmbath1	BELA
Warmbath2	BELA 2
Warmbath3	BELA3
Loubad1	LBD1
Loubad2	LBD2
Loubad3	LBD3
Amanzintaba	AMZT
Zimthabi	ZMTB

GeoWs Site	Abbreviation
Riemvasmaak	RIEV
Skroef Se Bad	SKROEF
Lilani	LIL
Shu-Shu	SHU
Avalon	AVA
Baden Club	BAK
Toorwater	TOOR
Warmwaterberg	WARM
Calitzdorp	CAZ
Caledon	CALE
Brandvlei	BRA
Goudini	GOUD
The Baths	THE BATHS
Bricks	BRICKS
Florisbad	FLO
Badsfontein	BAD
Aliwal	ALW
Cradock	CRAC
Polile Tshisa	PTS
Thangami	TGM

LIST OF DEFINITIONS

Term	Definition/description
Aquifer	Aquifer occurs underground in a rock also unconsolidated sediment unit that yields enough water for use in a spring or well.
Flash steam	To reduce the pressure of a geothermal liquid producing steam.
Impermeable	A substance or strata that does not allow fluid to pass through.
Infiltration	When water from the surface moves into porous rock or soil.
Injection	Also known as reinjection when fluids are pumped back into the ground.
Kilowatt (kW)	A measure of energy, the rate at which power flows over time. 1000 joules per second =1kW.
Megawatt (MW)	A measure of energy, the rate at which power flows over time. 1 000 000 joules per second/ one thousand kilowatts=1MW
Permeability	A strata or substance that allows fluid to be transmitted. This is influenced by pressure of the strata or substance.
Porosity	The percentage of the volume of pore spaces to that of the entire substance or strata volume.
Recharge	Movement of unsaturated water below the surface vertically to an aquifer. Recharge involves pumping water back into the ground after extraction.

(IGA Service GmbH, 2014)

CHAPTER 1 INTRODUCTION AND SCOPE OF THIS DISSERTATION

1.1 Current energy status in South Africa

In 2018, the supply of energy in South Africa was made up of 89% coal, 6% nuclear, 2% hydropower, 1% solar photo-voltaic, 2% wind and the remainder from co-generated biogas and landfills (Akinbami et al., 2021). Coal-powered plants are the primary energy source contributing significantly to the emissions of carbon dioxide (CO_2) in the country (Department of Mineral Resources and Energy, 2019). The increase in CO_2 emissions increases the greenhouse effects, causing adverse effects on the climate while influencing all spheres of life (Zheng et al., 2015). The acceleration to adopt sustainable and renewable energy resources worldwide highlights the inherent need to protect the environment for future generations.

In December 2015, 196 nations responded to the threat of climate change by agreeing to support the global response to climate change. The countries agreed to pursue efforts to limit the global temperature rise well below 2°C and to improve the ability of countries to deal with climate change impacts known as the Paris Agreement on Climate Change, came into effect in 2016 (Department of Mineral Resources and Energy, 2019).

The South African government published the Integrated Resource Plan of 2019 (IRP 2019) to increase the use of renewable energy. In the IRP 2019, the Sustainable Development Goals (SDGs) of the United Nations (UN) 2030 Agenda for Sustainable Development are included. SDG 7, the transfer toward affordable and clean energy is emphasized to promote renewable energy generation (Department of Mineral Resources and Energy, 2019).

In 2019 policies and systems to support the change were developed and approved by the cabinet, including The National Climate Change Information System, the National Climate Change Adaptation Strategy (NCCAS), the Low Emissions Development Strategy (LEDS) and the Presidential Climate Change Coordinating Commission (P4C) (Xasa, 2021).

1.2 Climate change mitigation

The IRP 2019 is a firm commitment from the South African government to reduce Greenhouse Gases (GHG) emissions. The energy sector is the highest emitter of GHG. Consequentially from 2030 to 2050 decommissioning of at least 24 100MWe coal power plants are planned. Either these plants will need replacement with cleaner coal technologies or other forms of energy will be introduced to the energy resources nexus (Figure 1). The prediction is to reduce coal energy generation by 2030 to 51 % from 89%. Consequently, a significant reduction in the total amount of GHG emitted is expected, contributing positively to the environment (Department of Mineral Resources and Energy, 2019). The prediction is that gas/diesel, solar and wind energy generation will contribute 35% to the energy range by 2030 (Department of Mineral Resources and Energy, 2019).

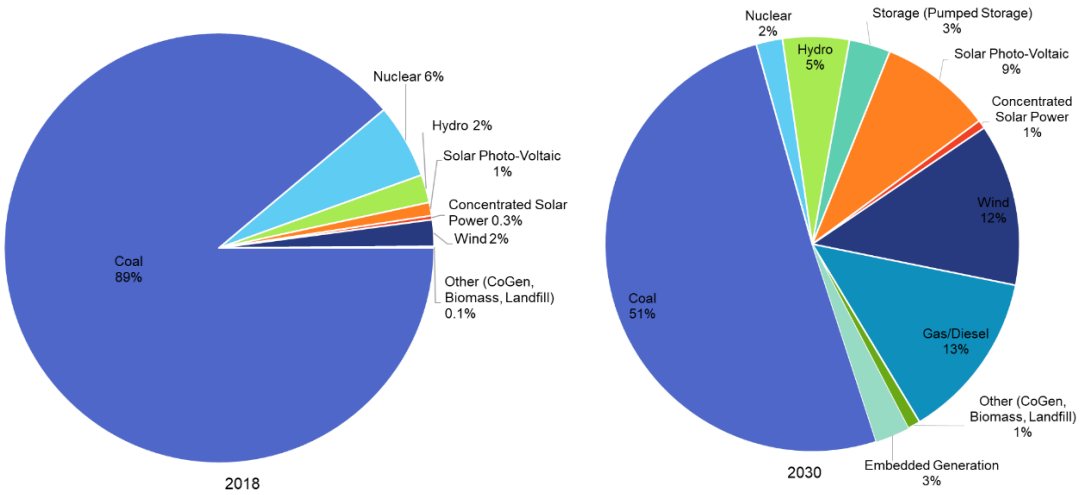

Figure 1: The current and planned energy usage shows a decrease in coal (from 89% to 51%), (modified from Department of Mineral Resources and Energy, 2019).

To support the reduction of GHG emissions the South African government is allocating Sectoral Emissions Targets (SETs), carbon budgets and a carbon tax for higher-emitting companies. The carbon tax was implemented in 2023, while the SETs framework was finalized in 2021/22. The carbon tax and budget will be aligned accordingly and is mandatory (Xasa, 2021).

In the UN Framework Convention on Climate Change (UNFCC) Conference of Parties (COP) 26 mentioned that South Africa is the largest emitter of CO_2 on the African continent. Consequently, a pledge of USD 8.5 billion was made by the International Partners Group of developed economies to assist South Africa in shifting towards a low-carbon economy (Mlaba, 2021).

1.3 South Africa's shift toward renewable energy

In South Africa, wind, biomass, solar and hydropower are the renewable energy sources that add to the energy grid. In the first half of 2021, the energy generation from renewable energy equated to 19% (Akinbami et al., 2021). South Africa's electricity production between 2010 and 2022 shows that energy supplied by coal decreased (Figure 2), while renewable energy sources have increased to 16TWh. Moreover, the overall energy generation decreased (CSIR, 2022).

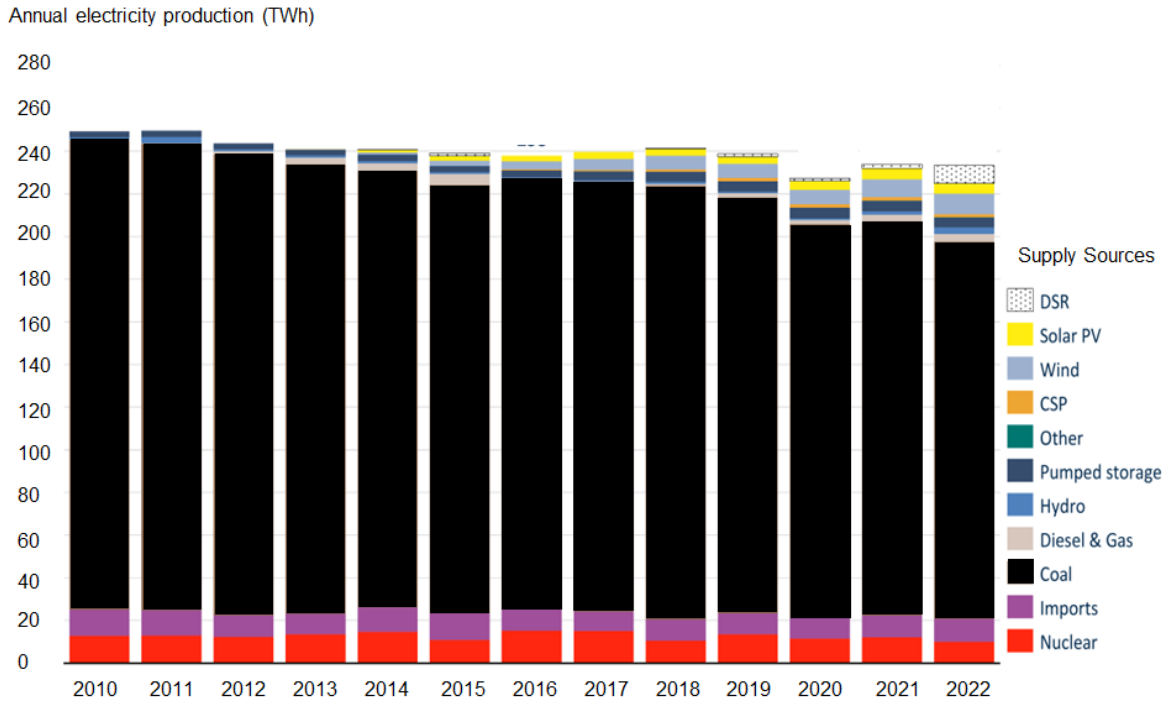

Demand Side Response (DSR) = Manual Load Reduction (MLR) + Interruptible Load Supply (ILS) + Interruption of Supply (IOS).
Solar PV= solar photovoltaics
CSP=concentrated solar power

Figure 2: A comparison of energy supplied from various sources showing a steady decrease in coal powered energy and increase in renewable resources (modified from CSIR, 2022).

In 2007, load-shedding was introduced to South Africans. Load-shedding relates to decrease of energy generated consequently power cuts in various parts of the country

for a given period. The term “Stage" was implemented in 2014 which refers to the number of hours of load-shedding, often between 1-4 hours at a time. Figure 3 displays the load-shedding history between 2007-2022, where in 2022 the load-shedding reached a high of 11 529GWh. This is a ~6450% increase from the initiation of load-shedding in 2007 (CSIR, 2022). Furthermore, reducing the load on the power grid will direct the power to the most needed regions in the country. Hence households were the first to have power reduced, thereafter communities, villages and towns

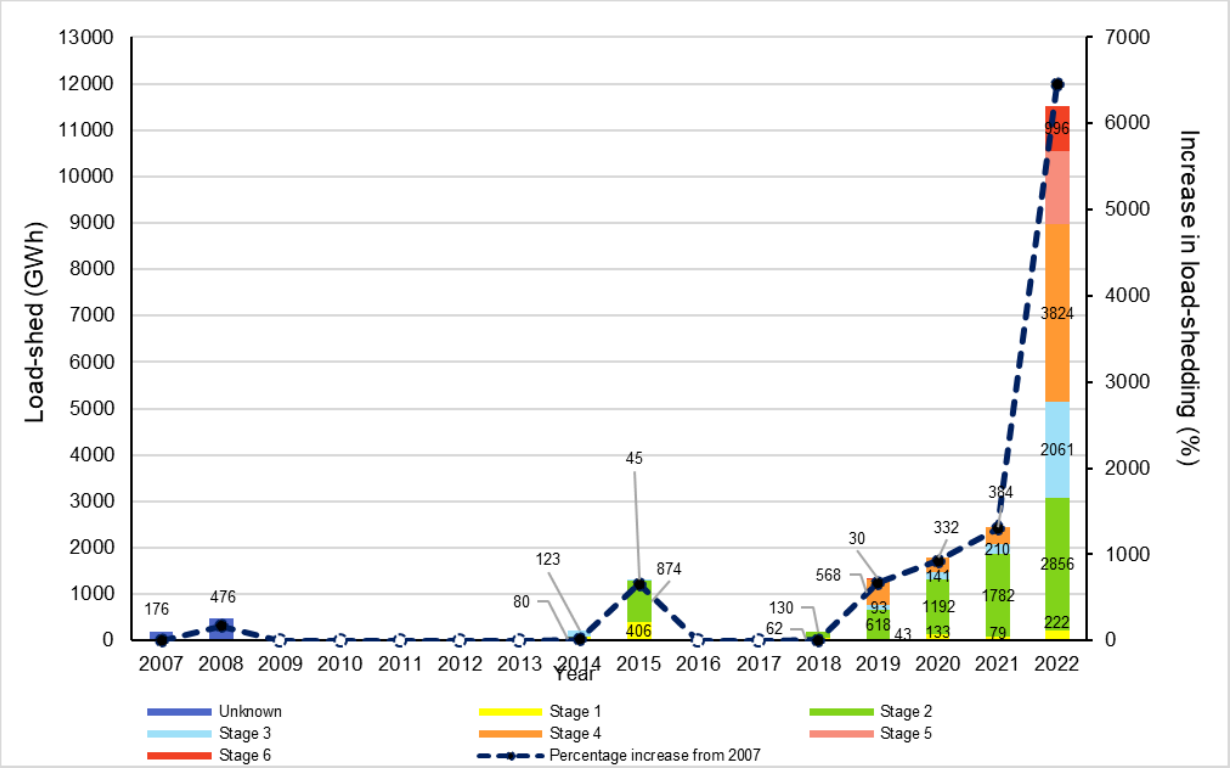

Figure 3: South Africa’s load-shedding history from 2007 to December 2022. The dotted line shows the percentage of increase in load-shedding (modified from CSIR, 2022).

1.3.1 South Africa’s energy development

The IRP 2019 shows that the South African government needs to invest in renewable resources while simultaneously cutting back on coal-powered plants. However, in the Annual Performance Plan 2020-2021 from the Department of Mineral Resources and Energy (DMRE), reported that “new investments must be made into efficient coal technologies. Cleaner coal technologies include High-Efficiency, Low-Emissions (HELE), supercritical and ultra-supercritical power plants and Carbon Capture, Utilization and Storage (CCUS) systems to comply with climate and environmental requirements” (Department of Mineral Resources and Energy, 2021, p12). This stance

indicates that the country will keep coal in the energy resources mix, whilst looking to establish strategic partnerships with organizations and countries that are experienced in the development of CCUS and HELE technologies.

The DMRE planned to implement 2500MW of nuclear power from 2020 to 2023 and is currently engaged in exploration of local shale and coastal gas (Department of Mineral Resources and Energy, 2021). In addition, the exploration of gas with neighbouring countries is under consideration for exploitation and beneficiation of the greater Southern African Development Community (SADC) region. Furthermore, the uptake of gas to market is being explored for short and long-term infrastructure in the SADC region. If gas is available the opportunity to convert the Combined Cycle Gas Turbines (CCGT) and run open-cycle gas turbine plants at Gourikwa (Mossel Bay), Dedisa (Coega IDZ), Avon (Outside Durban) and Ankerlig (Saldanha Bay) is a possibility (Department of Mineral Resources and Energy, 2021).

Harnessing biomass energy in the form of pulp, paper, and waste from the sugar industry in co-generation plants is also possible. Therefore, biomass energy should be able to deliver electricity at a competitive price, particularly in industrial centres for small (kW) to large (MW) scale generation (Department of Mineral Resources and Energy, 2021).

With the introduction of 6GW of renewable energy in the form of concentrated solar power (CSP), wind and gas, these systems do not have the required storage capacity or flexibility at present. Hence, storage solutions such as compressed air energy storage, hydrogen fuel cells, battery systems and flywheel energy storage could be used (Department of Mineral Resources and Energy, 2021). In addition to adding renewable resources, the implementation of the Integrated Energy Plan (IEP) together with the Integrated National Electrification Programme, provides a road map of the future energy landscape for South Africa . As the South African government adds renewable resources to the energy grid, it aims to reduce coal-powered plants to 51% by 2030 (Figure 1) showing South Africa’s effort to address climate change (Department of Mineral Resources and Energy, 2021).

From the above summary, DMRE has put forward a plan to mitigate climate change but has failed to explore or add geothermal energy as an alternate energy source to the IRP 2019 (Figure 1). Exploring geothermal energy would benefit the country, as it is stable, continuous, and independent of weather when compared to other forms of renewable energy such as wind and solar energy (Kaczmarczyk et al., 2020).

The installed capacity of geothermal energy increased by 27% from 2015 to 2020 worldwide. Countries such as the USA, Indonesia, Philippines, Turkey and Kenya have the most installed geothermal power generation (Huttrer, 2021). Of note in Indonesia, where an installed capacity of 2 289MW thermal energy has resulted in a reduction of 14.91million tons of CO_2 per year, geothermal power plants contributed 2130.6MW, in 2020. This geothermal energy indirectly reduces the amount of oil and gas imported into Indonesia equating to a saving of 100 778 barrels of oil equivalent per day (Kerjha, 2021; Huttrer, 2021).

Turkey accelerated geothermal energy from 397MW thermal energy in 2015 to 1152MW thermal energy in 2020 (Huttrer, 2021). Turkey planned to increase geothermal energy to 4000MW by 2023 (Idrissi et al., 2021) but managed to increase geothermal energy to 1691MW in this time period (Türkiye Sınai Kalkınma Bankası A.Ş, 2023). On the African continent, Kenya increased its geothermal energy output by doubling it in 2020 to 1193MW of thermal energy. Furthermore, the Kenyan government plans to have 5000MW online by 2030 (Huttrer, 2021).

1.3.2 CO_2 sequestration and geothermal energy

Renewable energy technology is advancing where hybrid systems are explored due to the initiatives to decreased CO_2 emissions. Such hybrid systems involve capturing CO_2, storage of the CO_2 and harnessing CO_2 as a power resource. The captured CO_2 is circulated underground in deep saline aquifers or hydrocarbon reservoirs. The CO_2 is naturally heated, transferred to the surface and expanded in a turbine to generate electricity. With the power plant at the surface, the CO_2 subsequently cooled (using wet cooling towers to increase the density), compressed, and then combined with any CO_2 stream from a CO_2 emitter before reinjection into the subsurface reservoir. The

continued CO_2 reinjection into the subsurface will build up into a plume and permanently store CO_2 underground. This cycle combines CO_2 sequestration with geothermal energy utilisation in low to medium enthalpy systems (Osman et al., 2021). Carbon Capture, Utilization and Storage (CCUS) forms part of the SA government's plans to mitigate climate change. Investment in CCUS might decrease the energy generation from coal, thus reducing harmful emissions.

1.4 Geothermal energy in South Africa

On a global scale, geothermal activity commonly occurs in regions at tectono-active plate boundaries and major fault zones. These areas are characterised by the extension or compression of crust coupled with high heat flow and widespread magmatism. Surface manifestations of geothermal activity include hotspots, transtensional pull-apart basins, magmatic arcs, as well as magmatic and amagmatic continental rifts (Jolie et al., 2021).

Currently productive geothermal plants occur in older volcanic or volcanoclastic systems with well-developed permeable lithologies and fracture networks (Anderson and Lund, 1980). In tectonically and/or volcanically active geothermal regions, heat is controlled by convection where geothermal gradients range from 150 to 300°C/km. The average geothermal gradient of the crust is 25-30°C/km of conductive heat transfer (Anderson and Lund, 1980; Jolie et al., 2021).

South Africa has no active volcanoes. Geologically most of the country is situated on the stable Kaapvaal Craton. The Kaapvaal Craton stabilised between 3700-2700 Ma and is marked by various intrusions and basin formation within the craton (De Wit et al., 1992). This stable continental region has low levels of seismicity, low heat flow and slight or no tectonic activity (Jones, 2017). Consequently, geothermal energy exploration in South Africa is limited. However, Boekstein (1998) published a visitors' guide to Hot Springs and Mineral Spa Resorts in Southern Africa. Furthermore, this is evidence of hot waters that are surface manifestations of geothermal energy at depth.

1.5 Characterising the geothermal waters in South Africa

Kent (1949) originally mapped the geothermal waters of South Africa, but a number of these have dried up since then due to over pumping of these geothermal waters (Olivier and Jonker, 2013). In addition, subsurface heat and tectonic investigations have highlighted numerous geological regions in South Africa that have some potential for geothermal energy (Dhansay et al., 2017).

The focal geological regions for potential geothermal energy sources include the Soutpansberg Basin, the Waterberg Basin, the Namaqua-Natal Province, the Cape Fold Belt and the Karoo Basin (Figure 4). Moreover, some of these regions could harness geothermal energy to support small-scale commercial and industrial heat pump systems (Tshibalo et al., 2015). However, fewer investigations and exploration have been undertaken for larger, baseload energy generation in South Africa (Dhansay et al., 2017).

The geological controls vary across regional (geological structures, heat flow and ground water dynamics) and local (physical and chemical properties, lithology and structural controls) geothermal water sites. Understanding the subsurface features controlling the geothermal waters is a challenge that requires investigations of geological, geochemical and geohydrological variations.

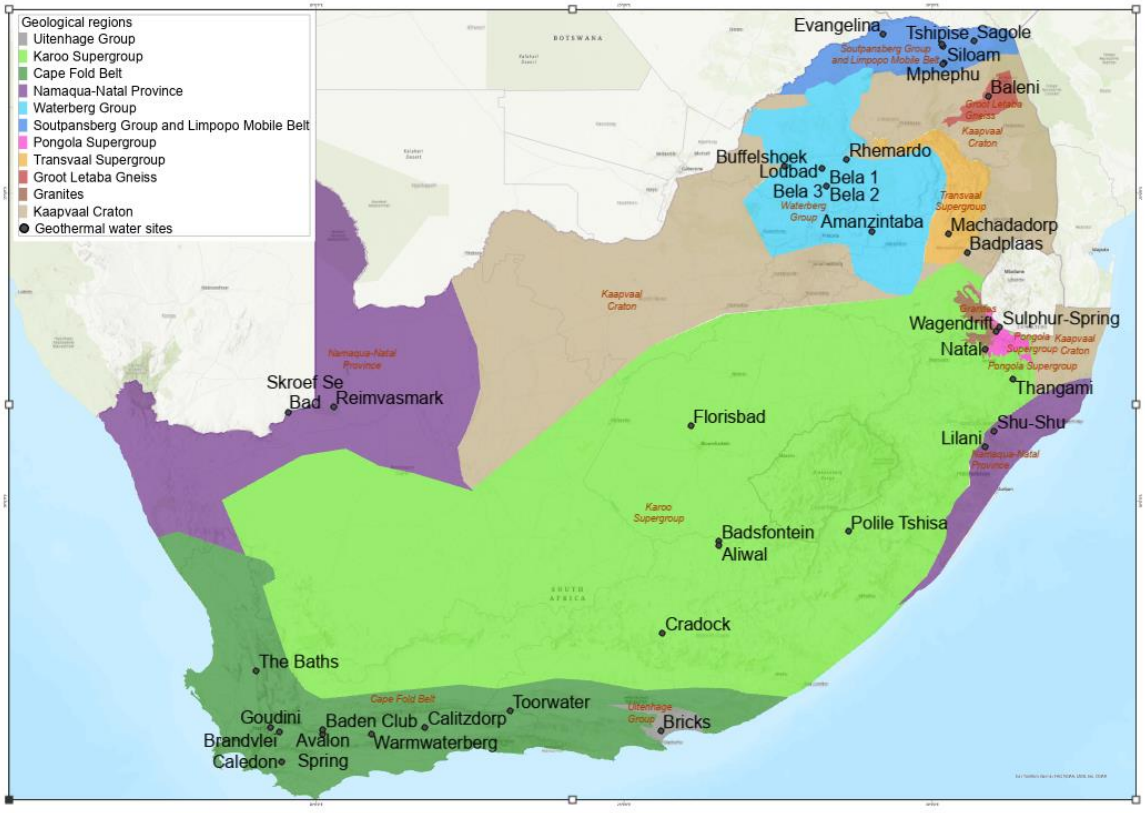

Figure 4: The location of the geothermal waters within geological regions of the current study (modified from Dhansay et al., 2017).

Anomalous geological heat sources in South Africa correlate with the occurrences of hot springs (geothermal waters), which further link to, and display underlying tectonic and chemical-lithostratigraphic controls on the subsurface heat flow (Dhansay et al., 2017).

Previously Tshibalo et al. (2015) updated the South African geothermal waters potential utilization (2010-2014) with a brief overview of the geology. These authors assessed the suitability of the hot springs in terms of bacterial and algal diversity and application. Tshibalo et al. (2015) had suggested that the government develop the geothermal waters in rural communities. Unfortunately, geothermal waters have not been harnessed as an energy source due to the lack of contribution for this type of energy in the Integrated Resource Plan 2019 (Department of Mineral Resources and Energy, 2019). Furthermore, geothermal water characterization on a country-wide scale is absent for the physical and chemical properties and their geological settings.

1.5.1 Aims and specific objectives

This research focuses on the physical and the major chemical constituents of the geothermal waters in South Africa to characterise the geothermal waters. To achieve this, the following essential investigations were undertaken:

1. Characterisation of physical and hydrochemical properties of the South African geothermal waters thereby increase the understanding and knowledge of such geothermal waters as a potential source of geothermal energy.
2. Conduct solute based geothermometry for temperatures of the geothermal water resources.
3. Identify possible moisture source(s) of the geothermal waters using stable isotopes and radiogenic isotope.
4. Calculate the enthalpy of the geothermal waters into low to medium enthalpy ranges.
5. Predict the depth of the geothermal resources.

The results of this research will facilitate a better understanding of geothermal energy resources in South Africa, which can then be incorporated into a revised roadmap for South Africa's renewable energy producers.

1.6 Brief chapter overview

The chapter overview of this dissertation is illustrated in Figure 5.

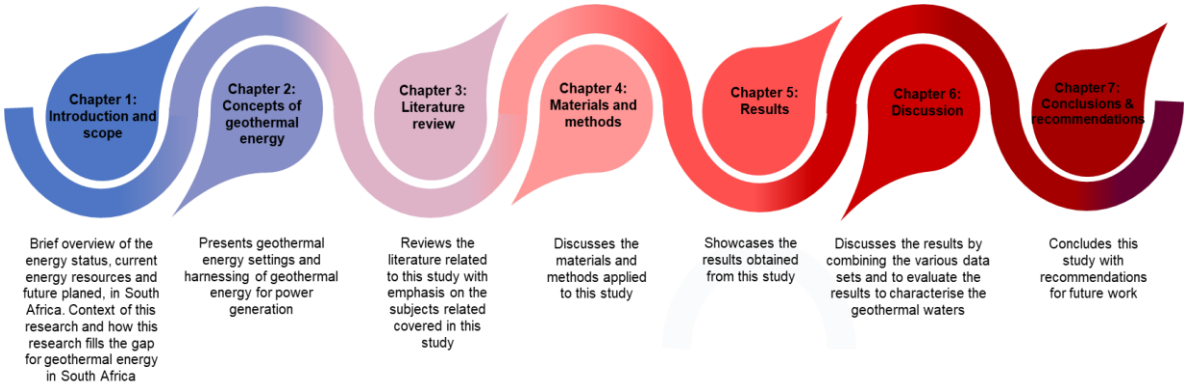

Figure 5: Chapter overview of this dissertation.

CHAPTER 2 CONCEPTS OF GEOTHERMAL ENERGY

Geothermal resources offer energy that is available on demand and renewable. Geothermal energy originates from the Greek word's 'geo' and 'thermos' translated to Earth and heat (Chand and Kumar, 2014). Geothermal energy is underground heat produced by the Earth. Undertsanding the geological settings of geothermal systems consequently the South African geothermal waters could be characterised.

2.1 The Earth's internal heat

The Earth has a few heat sources, such as residual primordial heat from its formation. This primordial heat is conserved energy as stated by the first law of thermodynamics. Heat is also produced from friction between rocks moving past each other along fault planes (Boden, 2017). Heat production also occurs when radioactive elements such as uranium (^{238}U), thorium (^{232}Th) and potassium (^{40}K) decay (Arnórsson et al., 2007). The radioactive elements concentrate within the Earth's crust as the pressure is lower when compared to the mantle. The mantle is bigger volumetrically with lower concentrations of radioactive elements than the crust but also contributes to crustal heat. Magma from the mantle produces heat that creates regions of high temperatures. Furthermore, another heat source is gravitational pressure which occurs when rocks are squeezed below the surface, heating up with depth (Anderson and Lund, 1980).

The rate of increase in temperature with depth in the Earth is called the geothermal gradient, which in shallow continental crust (<5 km) is typically 25-30°C/km (Anderson and Lund, 1980; Jolie et al., 2021). The deeper the geothermal source from the surface, the hotter the source. For a typical geothermal resource, the temperature should be 65-75°C at a depth of 2 km. Geothermal gradient is defined as the difference in temperature between two points (*T1* and *T2*) over distance (*δZ*) given by the equation below (Beardsmore and Cull, 2001):

$$\text{Equation 1: } \frac{\delta T}{\delta z} = \frac{(T2 - T1)}{\delta z}$$

The geothermal gradient (*t*) includes both magnitude and direction, expressed in terms of temperature per unit (Km^{-1}) (Beardsmore and Cull, 2001). Another manner of measuring the heat in the rocks is via heat flow. Rocks store heat and emit this heat

as thermal energy. Thermal energy emission occurs from every surface of the Earth by convection, molten rock and conduction through solid rock or by water movement (Anderson and Lund, 1980). Heat flow (Q) is when thermal energy moves vertically, measured as power per unit area (W m^{-2}) in a vector scale, between two points (δT) at a distance apart (δz) as shown in the equation (Beardsmore & Cull, 2001) :

Equation 2: $$Q = \frac{-\lambda \, \delta T}{\delta z}$$

The heat flow between two points is said to decrease in temperature hence, a negative sign in the heat flow equation (Equation 2), which is opposite to the geothermal gradient. Thermal conductivity relates the thermal gradient vector to the heat flow vector expressed as power per unit distance per unit temperature (Wm^{-1} K^{-1}). The thermal conductivity (λ) considers the physical property of a material. The thermal conductivity of the continental crust is 3 Wm^{-1} K^{-1} while the heat flow is between 30-70 mW m^{-2} (Beardsmore and Cull, 2001).

Areas have either lower or higher heat flow. Higher heat flow occurs near plate boundaries, in an area of concentration of radioactive elements and deeper within the Earth. High heat flow is evident on the surface as manifestations of volcanoes, hot springs (geothermal waters), fumaroles and geysers (Anderson and Lund, 1980). Geothermal systems are characterized by surface heat flow (conduction and convection), the nature of the heat source and plate tectonics. There are three main types of plate tectonic settings: convergent, divergent and transform plate boundaries (Figure 6) (Gehringer and Loksha, 2012).

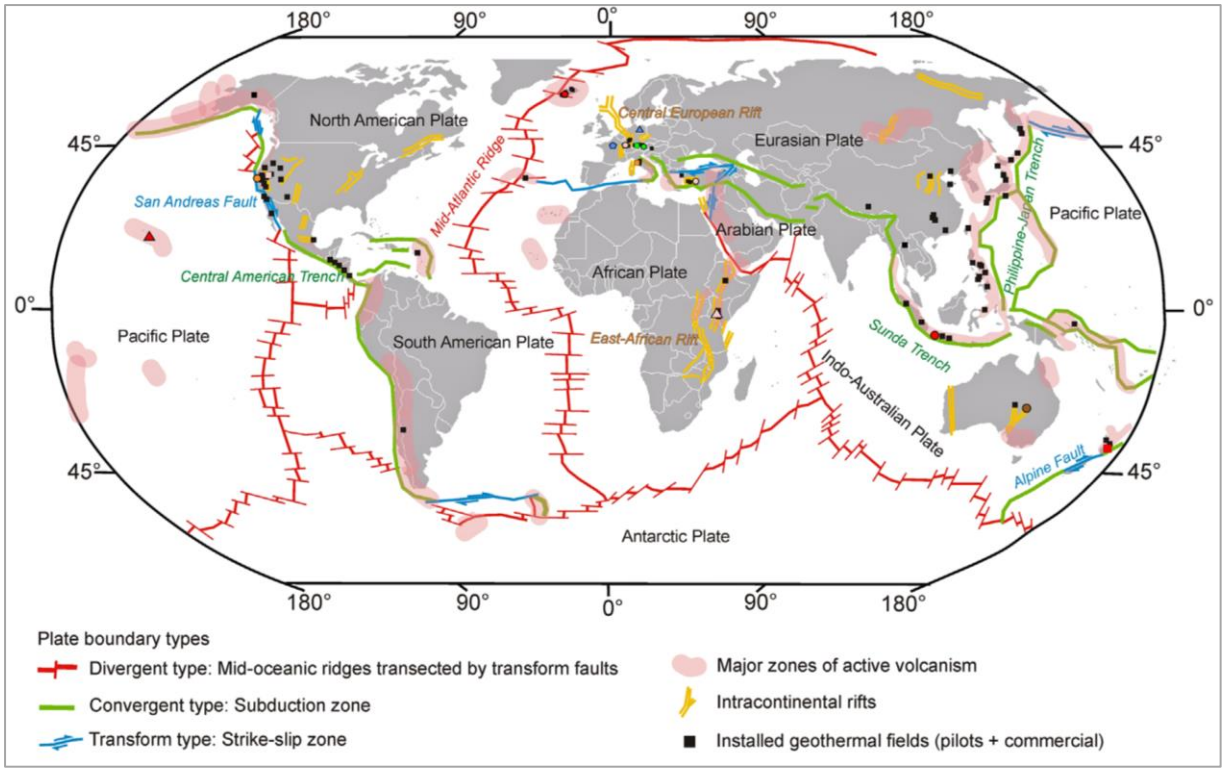

Figure 6: Plate boundaries of the world (Moeck, 2014).

2.2 Types of geothermal systems

According to the Best Practices Handbook for Exploration a description of geothermal systems is the interaction of a number of favourable combinations of heat source (high heat flow in the crust and thermal insulation such a thick sedimentary package), fluid transport and permeability structures (where fluids surface through fractures and fault networks), where heat flows to the surface from underground (Figure 7) (Nemzer et al., 2005; IGA Service GmbH, 2014; Jolie et al., 2021).

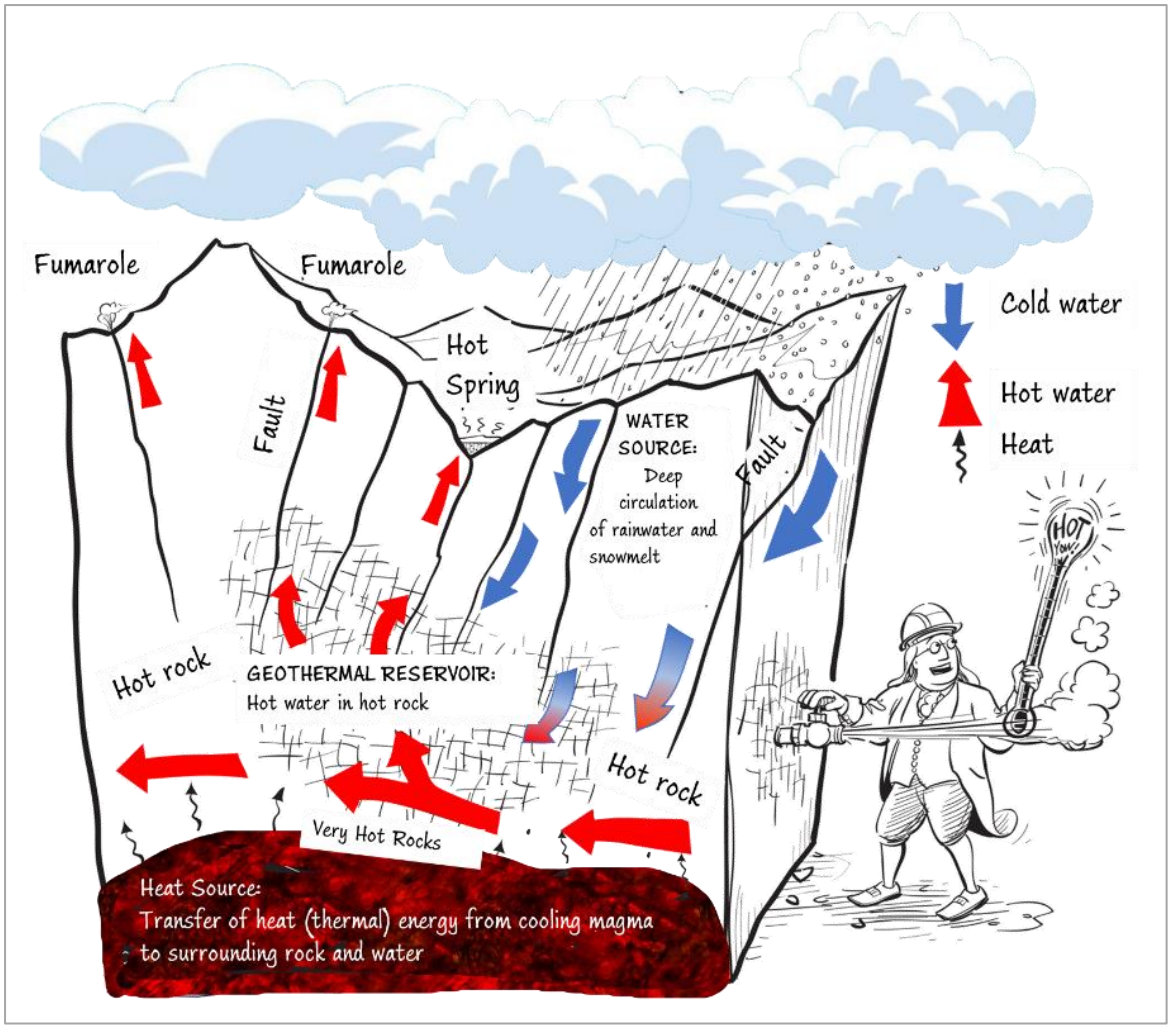

Figure 7: Conditions needed for a geothermal reservoir to form (modified from Nemzer et al., 2005).

Understanding the various geological features that control fluid flow and characterising the geothermal waters will assist with targeting geothermal waters for exploration and resource applications (Jolie et al., 2021). The chemical character of geothermal waters involves adsorption and desorption processes, dissolution of primary rock forming minerals and deposition of secondary minerals (Arnórsson et al., 2007).

Geothermal settings are subdivided according to their heat transfer mechanism (Figure 8) namely convection and conduction. Convection involves the transfer of heat through movement in liquid or gas forming a thermal gradient (Rybach, 1981; Boden, 2017).

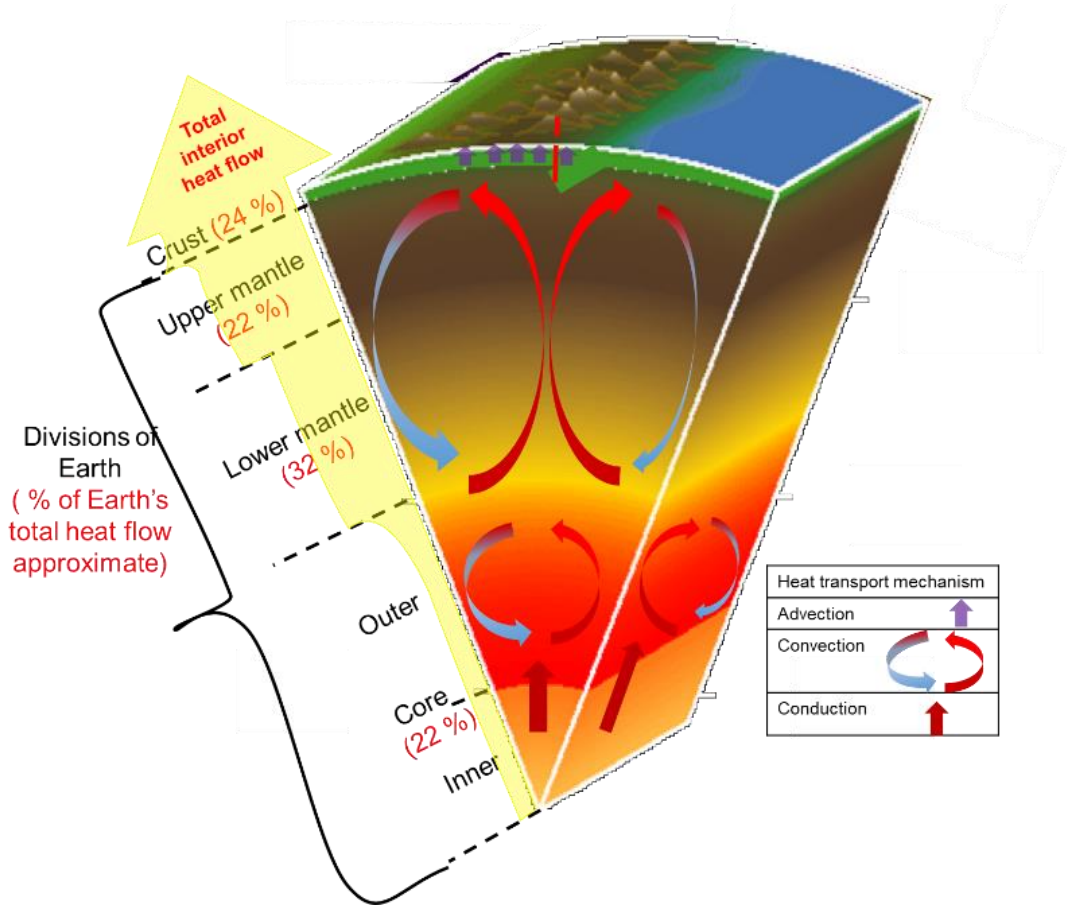

Figure 8: Cross-section of the Earths' heat flow for each division (modified from Boden, 2017).

2.2.1 Convective geothermal systems

Higher geothermal gradients, heat flow and fluid dynamics are characteristics of convective geothermal systems depicted in Figure 9 (Moeck, 2014; Jolie et al., 2021) The crustal plates either move apart or slide past each other in a convective environment. The plate boundaries are fractured and thinned out where lava extrudes at the surface and cools quickly. Fractures and faults develop around the intrusion where hydrothermal fluids circulate (Boden, 2017). The cold water circulates close to the magma, absorbing the heat and making the water hot; hotter water surfaces due to the density changes (Figure 9) (Moeck, 2014).

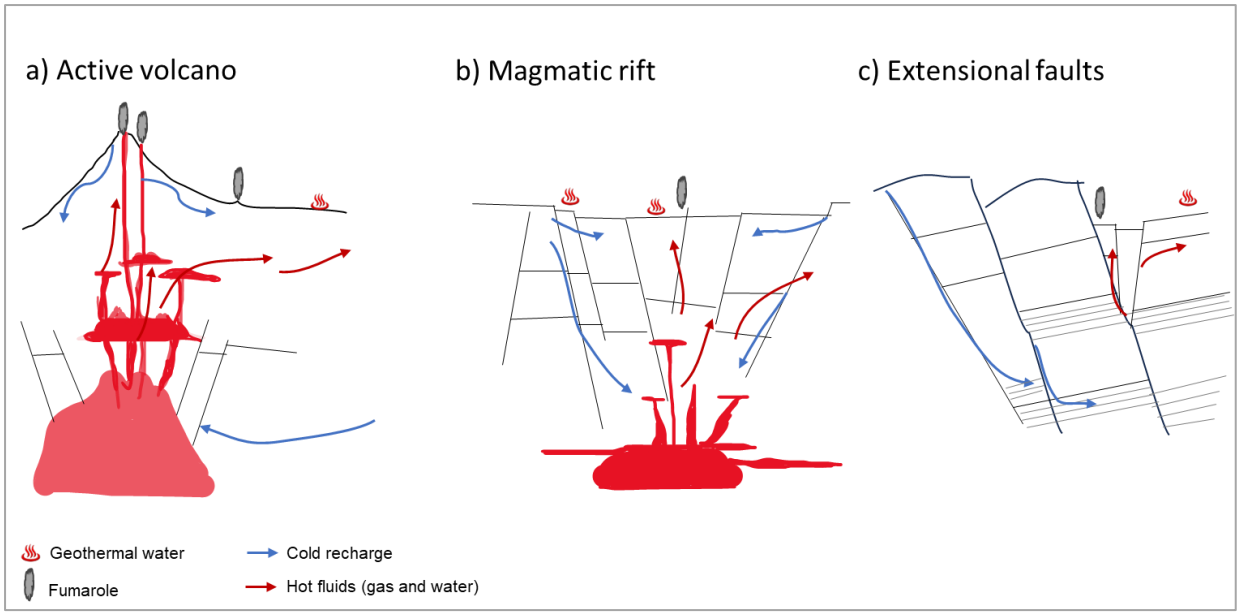

Figure 9: Convective geothermal systems adapted from Jolie et al. (2021).a) Active volcano. b) Magmatic rift. c) Extensional fault environment.

Another form of convective system is in areas where fluids circulate deeply along permeable zones in large volumes of rock. The fluids circulate in zones of fault and fracture networks or along stratigraphic beds. The fluid temperature is proportional to the heat flow in the area and the depth at which the fluid circulates (Figure 9) (Moeck, 2014).

Recharge to the geothermal source can occur along mountainous regions or valleys (Figure 9) (Anderson and Lund, 1980). In convection-dominated systems, structural controls, and high permeability (10-14 m^2; 10 mD) influence the fluid flow pathways for significant convection and increase fluid flow velocities (Moeck, 2014).

Typical tectonic environments where convection settings are present (Figure 9):

a) Convergent plate boundaries where magmatic arcs are present above the subduction zones (e.g. the Sunda Arc or the Philippine Japan Arc);
b) Divergent plate boundaries can be present in intracontinental settings such as the East African Rift or within the oceanic setting as in the Mid Atlantic Ridge;
c) Transform plate margins such as the strike-slip faults such as the San Andreas Fault or Alpine faults, and
d) Intraplate ocean islands such as hotspot magmatism in Hawaii (Moeck, 2014).

Major fault zones can cut across the lithosphere and connect the asthenosphere to the crust. The fluids from the asthenosphere use major faults as conduits for fluids to ascend towards the surface. The asthenosphere is described by upwelling of magma causing a bulge and tectonic denudation (metamorphic core complex terrains) (Moeck, 2014).

An example of oceanic ridge spreading and active volcanism occurs in Iceland. The Icelandic ridge which spreads at a rate of 18 mm/year is hosts to 33 geothermal systems (Wallis et al., 2018). This area produces 15-30% of the country's' power. The temperatures of these geothermal systems are >200°C at a depth of 1 km. Furthermore, in the Krafla region of Iceland, the geothermal source proves promising for direct heating by magma (Boden, 2017).

An example of a plate boundary where transform faults occur, associated with geothermal energy is in Indonesia at the Great Sumatra Fault. The Great Sumatra Fault is 1660 km long, and 30 geothermal systems have been identified, of which five have been developed. A series of volcanic centres is spatially coincident with the Great Sumatra Fault. Other geothermal systems in Indonesia appear to be related to volcanic arc systems (Wallis et al., 2018).

2.2.2 Conductive geothermal systems

The conduction of heat takes place in shallow continental crust with lower geothermal gradients (25-30°C/ km) (Anderson and Lund, 1980; Gehringer and Loksha, 2012; Jolie et al., 2021). Conductive geothermal systems are also characterised by low thermal conductive thick package of sediments covering granitic rocks that are generally enrich in radioactive elements (Anderson and Lund, 1980).

The radioactive elements decay giving off heat. The heat from the decay of elements may concentrate at the base of the sedimentary layers or may spread out depending on the thermal conductivity of the sediments. Deep regional aquifers occur in sedimentary basins where groundwater is accumulated and discharged in areas adjacent to highlands. Water moves through the aquifer and heats up with increase in

depth. At places in the sedimentary basin the fracture networks and faults form pathways for the water to ascend to the surface (Anderson and Lund, 1980).

Geopressured-geothermal systems form due to the lithostatic pressure of the overlying rocks, causing the heated fluids to rise to the surface along conduits. Occasionally waters intersect impermeable layers of rock, the waters are forced to ascend to surface via fracture and faults (Anderson and Lund, 1980).

An example of a conductive geothermal system is the Paris Basin, France. This is a 3 km thick intra-cratonic sedimentary basin, generating geothermal energy from 1970 to present day (Lopez et al., 2010). The geothermal waters range from 65-85°C to a circulation depth of 1.5 km- 2 km (Boden, 2017). Recently, in France, ten heating networks have been identified for utilization (Lopez et al., 2010). In France, geothermal energy for space heating sums up to 510MW (Lund and Toth, 2020).

2.3 Harnessing geothermal energy

The utilisation of geothermal energy is categorised by the temperature of the geothermal source into high (>852- 2107 kJ/kg), medium (>419 -852 kJ/kg) and low enthalpy(≤419 kJ/kg) as per Lindal diagram (Figure 10).

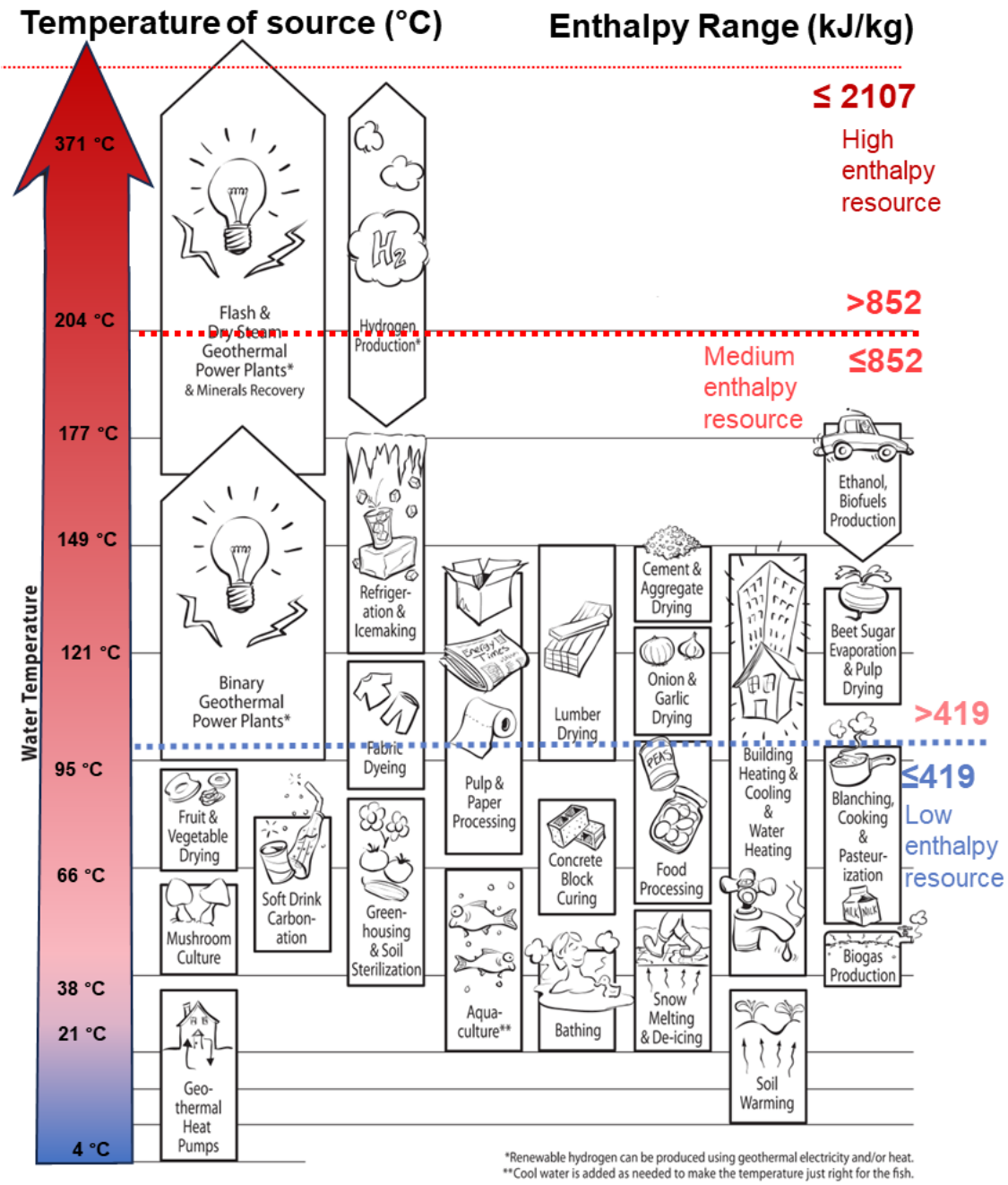

Figure 10: Lindal diagram showing the utilisation of geothermal resource at given temperatures and enthalpy range (modified from Anderson and Lund, 1980; Gudmundsson et al., 1985; Nemzer et al., 2005; Rubio-Maya et al., 2015; Zheng et al., 2015; Sveinbjörnsson, 2016; Chiasson, 2016; Boden, 2017).

Directly harnessing geothermal energy is the most common and efficient application to utilise geothermal water, with minimal energy losses. The temperature range for direct geothermal water usage is between 35°C and 95°C worldwide as shown in in the Lindal Diagram (Figure 10). Low to medium enthalpy (≤852 kJ/kg) resources are utilised for space heating, aquaculture, agriculture, food processing, recreational activities, balneology, industrial uses, snow melting and cooling spaces (Figure 10) (Anderson and Lund, 1980; Gudmundsson et al., 1985; Nemzer et al., 2005; Rubio-Maya et al., 2015; Zheng et al., 2015; Sveinbjörnsson, 2016; Chiasson, 2016; Boden, 2017). Medium to high enthalpy (≥852- 2107 kJ/kg) resources are utilised for power generation and hydrogen production. The investment risk is low as the geothermal resources is located in volcanic active regions (Gehringer and Loksha, 2012).

To optimise low to medium enthalpy geothermal resources a cascade model was developed in the mid-1980s. The cascading model consists of harnessing geothermal energy for power generation, thereafter for fish farming, green houses and completing the utilisation with district heating (Rybach, 1981; Rubio-Maya et al., 2015; Wallis et al., 2018; Jolie et al., 2021). One such example is in Canby, California, the geothermal power plant operates at 96.1°C to produce 50kWe, thereafter harnessing the energy for greenhouses, aquaculture, and district heating (Rubio-Maya et al., 2015).

In recent years, low to medium enthalpy ranges (≤852 kJ/kg) proved electricity generation is possible as technology advanced, but the initial cost of exploration is high and risk of return on investment is high. Various geothermal plant setups have been developed given the wide range of temperatures in geothermal systems. Such plant setups are discussed below.

2.3.1 Dry steam power plants

Dry steam power plants have a simple construction and design, making the high enthalpy (>852-2107 kJ/kg) resource the most desirable geothermal resource (Chiasson, 2016). A dry steam plant harnesses geothermal fluid in a superheated vapour state. The steam is converted into mechanical energy and thereafter into

electrical energy (Serpen and DiPippo, 2022) (Figure 11). A filter is added to the inlet pipe to ensure that solid and liquid particulates that might be present in the steam do not damage the turbine blades. A by-product of the dry steam plant is water, which is reinjected into the well to increase the geothermal resource lifespan (Chiasson, 2016).

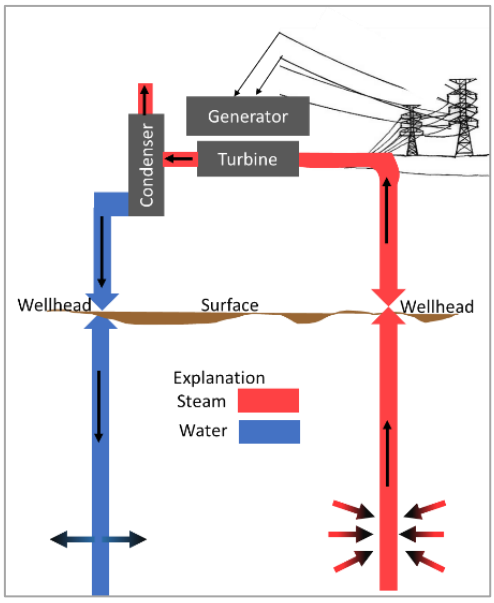

Figure 11: The configuration of dry steam for geothermal power generation (Boden, 2017).

The first dry steam plant for geothermal electricity generation was in 1904, in Larderello, Italy. After 11 years, Larderello generated enough power of 250kWe for commercialisation (Burgassi, 1999). Countries such as Mexico, United States of America and New Zealand set up experimental dry steam power plants. In California, an experimental dry steam plant was installed at The Geysers in 1932. The Geysers dry steam plant was commercialised in 1960 generating power to the local resort (Chiasson, 2016).

2.3.2 Flash power plants

Flash power plants operate from a high enthalpy liquid-dominated geothermal reservoir. In flash power plants, the system is a two-phase system separating the energy between the liquid and steam phases in the upper parts of the well when the water starts to boil or flash due to lower pressure. The steam moves into the turbine for electricity generation whilst the fluid is reinjected to maintain the geothermal reservoir pressure and to prevent contamination of the shallow groundwater source

(Figure 12) (Serpen and DiPippo, 2022). The steam temperature influences the amount of electricity produced. If the proportion of steam separated is high, the electricity production increases. Depending on the temperature of the incoming geothermal fluid, the fluid may undergo more than one flash, sometimes a triple flash process. In flash power plants, the pressure should be consistent at 6-7bar to yield 15-25% more power than a single flash cycle for the same geothermal fluid conditions. However, increasing the amount of flash cycles makes the plant build complex (Boden, 2017). In 1984 Kizildere, Turkey, installed and commissioned the first flash power plant producing 17.4MW electric power (Gokcen et al., 2004). In 2006, Turkey introduced the installation of an individual and a combination of binary and flash plants (Serpen and DiPippo, 2022).

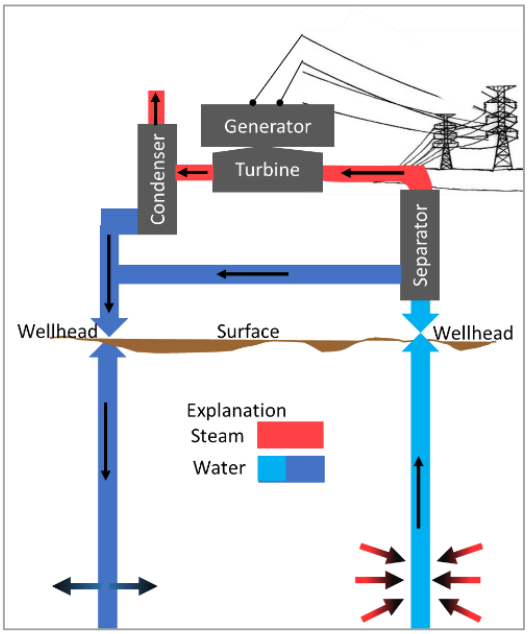

Figure 12: The configuration of flash plant for geothermal power generation (Boden, 2017).

2.3.3 Binary plants

Binary plants operate from geothermal reservoirs of low to medium enthalpy range (≤852 kJ/kg) and from a liquid-dominated geothermal resource (Chiasson, 2016: Boden, 2017). In the 1940s at the University of Pisa, a binary plant was designed. The design layout included a small Rankine Cycle unit which consists of low boiling temperature liquid driven by hot geothermal fluids from a geothermal reservoir (Figure 13) (Burgassi, 1999). The geothermal fluid heats the lower boiling point fluid. As the lower boiling point fluid heats, it expands to a gas state which is pumped through a

turbine to generate power. The lower boiling point fluid is condensed back to its liquid phase in a closed loop (Boden, 2017).

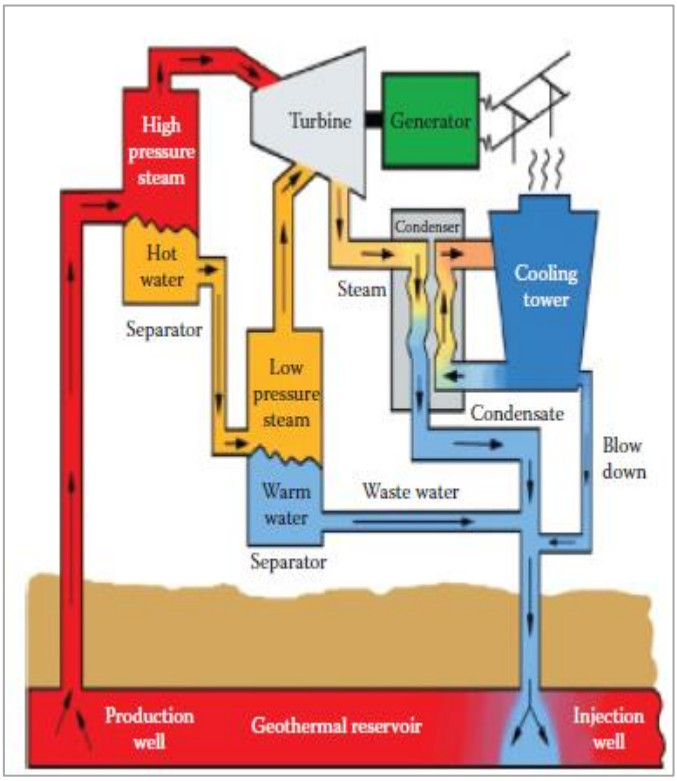

Figure 13: The configuration of binary plant for geothermal power generation (Boden, 2017).

The costs of operating binary plants are effective (Gehringer and Loksha, 2012). Binary plant installation can be as a single or multiple units. The single units are simple in a relatively small area with remote operation. In 1967, Russia's city of Paratunka, the first medium enthalpy binary plant produced 670kW for electricity and space heating. Since the 1980s, many successful binary plants have been installed worldwide (Serpen and DiPippo, 2022). In Turkey, the stand-alone unit power capacity ranges from about 2.5-3.0MW with reservoir temperatures between 160-240°C. The binary plants have smaller energy potential from lower enthalpy ranges. Even though the amount of electricity produced accounts for 6.3MWe, the binary power plant production increased to 12% (Boden, 2017). Table 1**Error! Reference source not found.** shows the temperature range of the geothermal sources, the enthalpy range and the type of power plant needed for power generation (modified from Sveinbjörnsson, 2016).

Some geothermal systems employ flash plants with binary plants. The binary plants are at the bottom of the flash plant. The binary plant heats the secondary working fluid to turn a separate turbine to increase the power output. The geothermal fluid input is hot enough to boil the secondary fluid in two loops (low-pressure and high-pressure loop). The loops connect to different turbines separated by a generator in the middle (Chiasson, 2016).

Table 1: Temperature, enthalpy range and type of plants utilised for power generation (modified from Sveinbjörnsson, 2016).

Temperature Range of source (°C)	Classified Enthalpy	Enthalpy Range (kJ/kg)	Type of plant power generation/uses
>374.15	High enthalpy resource	≤ 2 107	Dry (steam dominated) /Flash Steam Turbine (liquid dominated).
>200-374.14		> 852	Rankine t cycle.
> 100-200	Medium enthalpy resource	≤ 852	Binary Power Plants: Rankine Cycle
		> 419	
0< 100	Low enthalpy resource	≤ 419	Space heating and industrial uses.
0		0	Not for energy generation.

Apart from having a single power plant for a specific temperature range, various power plants setup can be combined to form a hybrid system. In addition, renewable energy like solar or sequestration of CO_2 (section 1.3.2) may be concurrently utilised with geothermal energy to optimise the resource (Rubio-Maya et al., 2015; Chiasson, 2016; Boden, 2017).

It is clear from the above discussion that the amount of background information gathered for any geothermal resource will determine the lifeline to developing a geothermal resource. In Chapter 3 the review on the research of how geothermal waters are characterised for power generation on a global scale. This also includes the review of South African geothermal waters to articulate the need for characterisation of the geothermal waters.

CHAPTER 3 LITERATURE REVIEW

This review examines the contributions of themes that are covered to characterise the geothermal waters for power generation across the globe. Included in the review are themes such as regional geology, structural controls and hydrochemistry of geothermal waters to characterise the of geothermal waters in South Africa. This review includes a review on the research on the utilisation of geothermal waters in South Africa.

3.1 Characterisation of geothermal waters for power generation

The development of geothermal energy for power generation historically relied on clear evidence of surface discharges of steam or hot water. For instance, in Larderello Italy, where shallow steam was observed at the surface is where the first geothermal electricity generation plant was developed (Burgassi, 1999; Gehringer and Loksha, 2012). It was only after the plant was established that the Larderello resource was investigated for its chemistry, geophysical properties, thermodynamics and production properties which involved both laboratory work and field work (Burgassi, 1999).

In the 1950s, in Wairakei, New Zealand surface manifestations of geysers are present, this is where a geothermal power plant was developed to harness geothermal energy (Gehringer and Loksha, 2012). The overview of Wairakei by Rosenberg et al. (2009) provided an update of data obtained from new drill holes, the geological and structural framework of the area and the system controls on fluid flow. Furthermore, Rosenberg et al. (2009) highlighted that iterative geological, hydrological, geochemical and geophysical investigation should continue for the next 50 years for further exploration and development. Hence, investigations are forecasted to continue even after development of a geothermal reservoir.

To harness geothermal energy in Iceland, research into subject matters such as geology, hydrochemistry, and geophysics were also investigated. Thereafter drilling had taken place where updates on the conceptual model, borehole geology, well logging, and hydrogeological modelling occurred. Even after production commenced geological monitoring and sustainable management of the geothermal reservoir is ongoing (ENGINE Coordination Action, 2008).

To be able to utilise geothermal energy, various phases need to be undertaken. The manner and quantity of the phases is not documented as a standard for utilisation of geothermal energy. However, a guide implemented by Gehringer and Loksha (2012) to develop geothermal energy employed eight phases. The eight phases include: preliminary survey, exploration, test drilling, project review and planning, field development, power plant construction, commissioning and operation. Of note is the exploration phase for geothermal energy which encompasses geological and surface studies, geochemical surveys and geophysical surveys (Gehringer and Loksha, 2012; Harvey et al., 2016; Boden, 2017; Scott et al., 2019).

An example of the various phases undertaken for developing geothermal energy are illustrated for the Eburru power plant in Kenya. Detailed surface research investigated six wells drilled to a depth of 2.5km, examining the geological setting, hydrothermal alteration of host rocks and hydrochemistry of the fluid system. These detailed investigations produced a complete extent of the reservoir in 1990 (Omenda and Karingithi, 1993). A pilot plant is presently operational (Omenda et al., 2020).

Rattanawong et al. (2020) investigated the characteristics of three geothermal waters in Thailand. The key subject maters of investigation were geological investigation of the site, chemistry (major ions and trace ions) and isotope ($\delta^{18}O$ and δD) analyses of the fluids. Jolie et al. (2021) highlighted that geology and chemistry are essential in characterising geothermal waters for power generation. Furthermore, assessing the temperature of the geothermal waters is a key tool for assessing the production characteristics of a geothermal resource (Section 2.3).

In summary, the information needed to properly characterise a geothermal resource includes geology of the site, geochemistry of fluids, reservoir characteristics (storage and surface flow), geophysical properties of the site (drill hole measurements) (Okoroafor et al., 2022). Only after characterising the geothermal waters, it is possible to begin the development of the reservoir (Burgassi, 1999; Gehringer and Loksha, 2012; Boden, 2017).

Hence the following sections review the geology and structural controls, hydrochemical properties (major ion and isotope analyses) and geothermometry of different sites and how these have contributed to the geothermal water research in South Africa. Therefore, the subsequent sections focus on studies completed in South Africa that have the potential for geothermal energy and harnessing of geothermal waters for power generation (Figure 14).

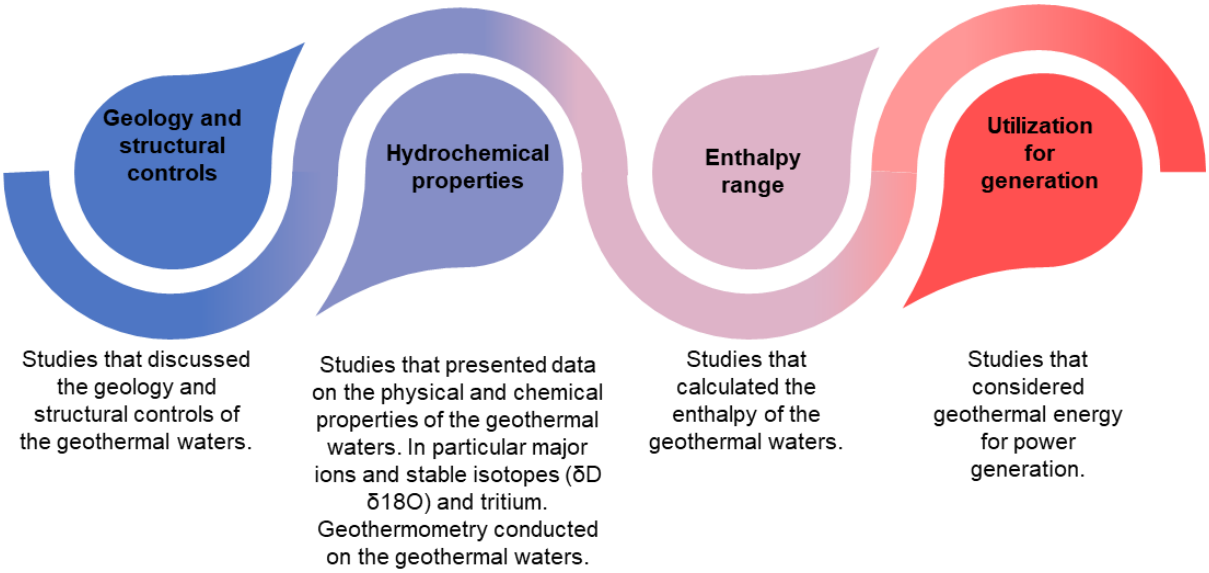

Figure 14: Overview of the research into the geothermal waters in South Africa.

3.2 Geology and structural controls of the geothermal waters in South Africa

Geothermal waters form springs at the surface as water percolates through pore spaces between granules and/or by migrating along conduits (faults, fractures and joints). Many studies discuss geothermal water compositions according to their geological location and stratigraphic distribution (Kent, 1949; Drogue et al., 2000; Tassi et al., 2006; Mohamed and Ehara, 2009; Baioumy et al., 2015; Yan et al., 2017; Zhenhua et al., 2018; Aydin et al., 2020; Chimeddorj et al., 2021; Temizel et al., 2021; Yu et al., 2022; Kiełczawa, 2023; Mahwa et al., 2023; Yin et al., 2023). Hence it is essential to understand the effect of the local geology on the geothermal waters and how this contributes to the characterisation of the geothermal waters.

The Geological Survey of South Africa, now known as the Council for Geoscience, initiated detailed investigations of the geothermal waters in South Africa between 1942 and 1981. This included the geology of the of the geothermal water sites and chemical analyses of the geothermal waters (Gevers, 1942, 1963; Kent 1946, 1962 b, 1979, 1980, 1981; Kent & Haughton, 1942; Kent & Russell, 1949; Von Backström, 1957,1962; Kent & Groeneveld, 1962 b; Kent et al., 1966; Temperley, 1975). Much later, individual studies by Gravelét-Blondin (2013); Madi et al. (2014); Fourie & Johnson (2017), Western Cape Branch of the Geological Society of South Africa, (2013) were conducted. Selected examples of these are discussed below.

Gevers (1942 and 1963) concentrated on the geothermal water Shu Shu and Lilani (Figure 15) in the Natal Sector of the Namaqua-Natal Province. Grevers (1942) studied the geology of Shu Shu and concluded that the geothermal water is capped by the impermeable Table Mountain Sandstone. A fault occurs in the area that strikes 63°E where it is infilled by calcite, thereafter, cemented by silica. At Shu Shu the hosts rocks are the Tugela Series composed of platy foliated black amphibolites and biotite-hornblende gneiss. Pyrite occurs as speck and veins in the hosts rock but does not contribute to the sulphurous odour at Shu Shu (Grevers, 1942). Gevers (1942) methodology for studying the geology is not documented in his work. Lilani has a few surface manifestations of geothermal waters which are located away from a major fault that trends E-W displacing the Table Mountain Series ~3 km. A dyke in the area acts as a conduit for the geothermal water to percolate at depth (Gevers, 1963).



Figure 15: Location of selected geothermal waters sites (in blue) investigated by various researchers (in black) in South Africa.

Kent (1946) showed that Loubads' (Figure 15) geothermal water flows through fractures and has no confining layer to constrain the geothermal water. Loubad exhibits low concentration of salts such as the Mn^{2+}, PO_4^{3-} and BO_2^{-}. Loubad surfaces between the contact of the sandstones of the Waterberg Group and Rooiberg felsites (Kent, 1946). Kent (1946) realised at the end of the study that the amount of information presented needed to be supplemented with further chemical analyses and geological investigations to better understand the mechanism that govern the geothermal water at Loubad. To date nothing has been published on Loubad geothermal water.

Kent and Russell (1949) studied the geothermal water at Buffelshoek (Zimthabi) (Figure 15) near Thabazimbi for chemical signatures of the geothermal water and geology of the area. Buffelshoek geothermal water consists of major of Na^{+}, K^{+}, Ca^{2+}, Mg^{2+} and $[SiO_2\ (OH)^2]^{2+}$. They concluded that the geothermal water flows underneath

between the contact of the Waterberg Group sediments and the Bushveld granite. A dyke serves as a conduit for the geothermal water to surface (Kent and Russell, 1949).

The Western Cape Branch of the Geological Society of South Africa and Council for Geoscience (2013) detailed the geology of Brandvlei. They concluded that Brandvlei geothermal waters descend relatively deeply into the Peninsula Formation where the fluids are heated. The geothermal water surfaces at a NE striking fault (Western Cape Branch of the Geological Society of South Africa, 2013).

Gravelét-Blondin (2013) studied Shu Shu geothermal water. Gravelét-Blondin (2013) reported the geology, hydrology and geothermal prospects of Shu Shu. The geothermal waters at Shu Shu descends to approximately 2 km and ascend to surface utilising the brittle structures in the area that trend N-NW (Gravelét-Blondin, 2013).

Aliwal and Polile Tshisa (Figure 15) site studies focussed on locating the source of individual geothermal waters employing geophysical methods (Madi et al., 2014; Fourie and Johnson, 2017). Madi et al. (2014) utilised magnetic and electromagnetic signatures at Polile Tshisa which included faults, fractures and dolerite dykes are the means for geothermal waters to surface. They further indicated that a neotectonic regional fault trending E-W connects the Badfontein, Aliwal and Polile Tshisa geothermal waters (Madi et al., 2014).

Fourie and Johnson (2017) mapped the geological structures at Aliwal where they employed existing geological maps from Council for Geoscience, remotely sensed images and conducted a magnetic survey. The results of this investigation showed that faults and a ring dyke serve as conduits for the groundwater to ascend to the surface. At Aliwal, the geothermal gradient is higher (~40°C/km) than average continental crust (~25-30°C/km) as methane gas and coalfields occur in the area. The authors recommended deploying both magnetotelluric and seismic surveys to locate the best drill hole site for harnessing geothermal energy for power (Fourie and Johnson, 2017).

Even though all the geothermal waters do not have detailed geological investigations, secondary information exists such as comparison of previous studies (Mazor and Verhagen, 1983; Hoole, 2000; Olivier, et al., 2008; Olivier, et al., 2010; Tshibalo et al., 2010; Olivier et al., 2011; Dhansay, 2012; Olivier and Jonker, 2013; Durowoju, 2015; Shabalala et al., 2015; Tshibalo and Tekere, 2015; Tshibalo et al., 2015; Durowoju et al., 2016; Jonker, 2016; Dhansay et al., 2017; Durowoju et al., 2018; Durowoju et al., 2019) which may be utilised as a base line for further research.

This literature review on the geology and structural controls of the geothermal waters identified the need for detailed geological investigations as this contributes to the chemical signature of the geothermal waters (Kent, 1949; Drogue et al., 2000; Tassi et al., 2006; Mohamed and Ehara, 2009; Baioumy et al., 2015; Yan et al., 2017; Zhenhua et al., 2018; Aydin et al., 2020; Chimeddorj et al., 2021; Temizel et al., 2021; Yu et al., 2022; Kiełczawa, 2023; Mahwa et al., 2023; Yin et al., 2023).

3.3 Physical and chemical properties of the geothermal waters in South Africa

Physical and chemical signatures of the geothermal waters will contribute towards characterising the South African geothermal waters and in understanding of the predominant hydrochemical processes operating in the geothermal systems (Kent, 1949; Drogue et al., 2000; Tassi et al., 2006; Mohamed and Ehara, 2009; Baioumy et al., 2015; Yan et al., 2017; Zhenhua et al., 2018; Aydin et al., 2020; Chimeddorj et al., 2021; Temizel et al., 2021; Yu et al., 2022; Kiełczawa, 2023; Mahwa et al., 2023; Yin et al., 2023). Therefore, it is important to review the previous research of geothermal waters in South Africa. This will assist with a longitudinal study to document changes in the geothermal waters over time and subsequently prompt further research.

Literature of the geothermal waters in South Africa dates to 1790, when Paterson documented a detailed account of one of the hot springs in the Western Cape Province, Swartberg Mountains being 56°C hot. Remarkably Paterson's (1790) journey of the geothermal water produced a map of the Cape area corresponding to the existing map of the geothermal waters in Cape area. Additional contributions from Lichtenstein (1811-1812), Methuen (1846) and Murray and Jameson (1850) on the geothermal waters are also documented (Waring, 1965). The literature review on the

hydrochemical properties of the geothermal waters of South Africa is investigated below.

3.3.1 Hydrochemical properties

The hydrochemistry, physical and medicinal properties of the geothermal waters were of interest to the International Society of Medical Hydrology because of the healing properties attributed to natural hot springs. The geothermal waters of South Africa were classified using the temperature and total dissolved solid concentrations of compounds for example chloride, carbonates or hydrocarbonate ions, bicarbonates of calcium and magnesium ions rather than ions only (Jonker, 2016). According to Jonker (2016), Juritz (1908) first attempted to classify the geothermal waters for use in locomotive boilers.

In the South African literature, analytical records were initially reported in grains per gallon by Rindl (1916). In 1930, reporting of groundwater and hot springs properties was standardised. Furthermore, this prompted Rindl (1930) to convert his results for several geothermal waters (Rindl 1916, 1918 and 1928) into the standardised manner. These standard reports also mentioned the geology of the geothermal waters.

Numerous researchers describe the geothermal waters for their chemistry such as Rindl (1931, 1932, 1934,1937,1940); Kent (1949, 1962 a-b, 1979, 1980 and 1981); Kent and Russell (1949); Kent and Groeneveld (1962 b); Gevers (1942); Von Backström (1957 and 1962); Temperley (1964 and 1975); Kent et al., (1966) and Hoffman (1979). Although the specific methods employed in these chemical analyses are not discussed in the literature, the results serve as a foundational reference point for this current study. Kent (1949) compiled the chemical analyses of his and co-workers' previous work with new data from seventeen additional geothermal waters for comparative analyses.

Kent (1949) reported that transporting geothermal water samples was challenging because the dissolved material in geothermal waters would precipitate out, forming residues on the sample bottles before they could be analysed. Kent (1949) concluded

that the hydrochemistry of the geothermal waters was closely associated with the geological features in which they occur. As the geothermal waters analyses were limited, Kent (1949) relied on accurate data of temperature, gases and precipitates for his research. Waring (1965) compiled the chemical constituents of thermal springs worldwide based on the data supplied by various researchers. This compilation included temperature (°C), flow (gallons per day), total dissolved solids (ppm), and principal chemical constituents and associated geology (Waring, 1965).

Renewed geothermal water research into individual occurrences restarted in 2008 when the Council for Geoscience collaborated with the University of South Africa and the Water Research Council for the chemical characterisation and utilisation of the geothermal waters. This collaboration resulted in characterising the geothermal waters in the Limpopo Province where the utilisation and human consumption played a focal role. Olivier and Jonker, (2013) updated the chemistry of the geothermal water in the Limpopo Province. They noted that several geothermal waters (Winburg, Icon, Stindal and Masequa) had dried up due to over extraction, while some have been renamed. Jonker (2016) had managed to document the geothermal waters name changes that made it easier to locate the geothermal waters for the current study. Jonker (2016) found some of the geothermal waters but could not be sampled as they were dried up, while others could not be located. Data collected by Jonker (2016) excluded factors such as the soil type, levels of local air pollution, vegetation in and around the geothermal water source, that could impact the geothermal water chemistry. Jonker (2016) concluded that the geothermal water chemistry is valuable when assessing the geothermal water for balneology factors (Jonker, 2016). Jonker (2016) highlighted that the updated chemical analyses from the various geothermal waters does not exist as a single dataset. Hence, a comprehensive list of the analyses of geothermal waters over time was compiled in Appendix A from the records of Kent (1949); Waring (1965); Olivier and Jonker (2013), as these authors incorporated the individual studies that occurred between these time periods showing the environmental variations with time (Jonker, 2016).

Previous investigations conducted by Douglas (2001); Olivier et al., (2008); Tshibalo (2010-2015); Boekstein (2012); Gravelét-Blondin (2013); Baiyegunhi et al. (2014); Murray et al. (2015); Duworoju (2015); Jonker (2016), Duworoju et al. (2016, 2018, 2019) discussed the hydrochemistry of the various geothermal waters. Important contributions by Murray et al. (2015) are detailed below.

Murray et al. (2015) distinguished between shallow and deep geothermal water. The geothermal waters sampled were from Florisbad, Aliwal and Cradock all located in the Karoo Supergroup. They concluded that the deep geothermal water were Na-Cl-type water, with lower δ18O and δD values than those that occur at shallow depths. The low alkalinity of the geothermal water could be due to precipitation of calcium carbonate at higher pH values. The analyses were conducted using the Induced Couple Plasma Mass Spectrometer. The Liquid Water Isotope Laser Analyser was utilised to measure the stable isotope (δ18O and δD) concentrations. Murray et al. (2015) detailed the sampling, transporting and analysing of the geothermal waters.

3.3.2 Stable isotopes: Oxygen, hydrogen and radiogenic isotopes

Oxygen-18 analysis refers to the stable isotope ratio of $^{18}O/^{16}O$ (δ18O (‰)) in the water molecule. In addition, deuterium analysis refers to the stable isotope ratio 2H/1H (δD (‰)) in the water molecule. Analysing isotopes in geothermal waters provides information on the physical parameters and responses of the geothermal waters that are difficult to obtain by other methods. As meteoric water infiltrated the ground to deeper aquifers, the behaviour of δ18O and δD is almost stable, thus forming unique groundwater tracers (Henley et al., 1984).

The radiogenic isotope tritium (^3H) was also analysed. Tritium radioactively fractionates to produce ^3He where the half-life of tritium is 12.33 years (Mazor, 2003; Michel, 2004; Murray et al., 2015). In the 1950's nuclear weapons tests introduced large amounts of tritium that is found in groundwater presently. The tritium values can assist with distinguishing pre-1950 water from younger water (Weaver et al., 1999) and serves as a useful indicator for age.

The temperature of the geothermal waters, seasonal rainfall patterns in the area and continental position of the geothermal waters influence the δ18O and δD isotopes in groundwater (Mook, 2000). A few of the geothermal waters' stable isotopes in South Africa were analysed (Mazor and Verhagen, 1983; Diamond and Harris, 2000; Olivier and Jonker, 2013; Gravelét-Blondin, 2013; Durowoju et al., 2019) which highlights the significant gap of over a decade between analyses. This highlights the need for continued research to advance the understanding of the geothermal waters. Mazor and Verhagen (1983) sampled 17 geothermal waters but failed to mention the details employed for sampling and analysing the geothermal waters. Diamond and Harris (2000) sampled 13 geothermal waters at the source, sometimes multiple times. These authors utilised a mass spectrometer adding a standard sample for quality control. These results were reported as Standard Mean Ocean Water (SMOW). Furthermore, Olivier and Jonker (2013) mention that the geothermal water samples were collected at source and analyses for stable isotopes were done, however details regarding the methods employed were lacking. Nevertheless, these results are still valuable for comparison through time.

Durowoju et al. (2019) had studied isotopes for Sagole, Tshipise, Mphephu and Siloam that were collected seasonally. Their results showed that Sagole, Tshipise, Mphephu and Siloam were more depleted in δ18O in the winter compared to the summer. Durowoju et al., (2019) also mentioned that Mphephu and Siloam are located at higher altitudes that could be a contributing factor to the depleted δO18 signature for these waters. Stable isotopic compositions further confirm the significant role of evaporation on the groundwater chemistry of the geothermal waters studied (Durowoju et al., 2019).

Detail stable isotope (δO18 and δD) analyses were conducted by Gravelét-Blondin (2013) from Shu Shu geothermal water and the Tugela River water, exhibiting a variation in the stable isotopes for different seasons. This variation may have been from the local recharge or seasonal recharge, (Gravelét-Blondin, 2013). The Shu Shu stable isotopes published by Gravelét-Blondin (2013) are the only isotope data recorded to date.

From the above, it is apparent that the fractionation processes of δO18 and δD are influenced by factors such as temperature, seasonal rainfall pattern and continental position which in turn can produce variations in these isotopes of groundwater in different localities (Mook, 2000).

3.3.3 Geothermometry

Understanding the chemical signatures of the geothermal waters will provide insight into the source rock and water-rock interaction. However, this does not predict the temperature of the water, hence the need to perform solute-based geothermometry to establish geothermal resource temperatures. As documented by Ellis (1979) certain considerations are considered when applying solute based geothermometry:

a) In the rock-water system the elements or species present are available to interact with the environment,

b) the water-rock reactions should equilibrate at depth within a certain time frame,

c) the reaction rates should be slow enough for the reaction between water-rock to re-equilibrate as the water ascends to the surface.

For the South African geothermal waters, Cave and Clarke (2003), computed temperatures for the geothermal waters in the Western Cape Province namely: Brandvlei, Caledon, Calitzdorp, Goudini, Montagu (known as Avalon), Warmbad (known as Warmwaterberg). The quartz and chalcedony geothermometers computed the most likely and suitable geothermal resource temperatures that ranged between 60°C and 105°C. Cave and Clarke (2003) mentioned that the Na-K-Ca geothermometers even after considering correction factors of molar proportions were high (183°C -302°C) or below the surface temperature (from -9°C to -40°C) of the geothermal waters.

Dhansay et al. (2017) gathered geochemistry, heat flow, and heat-producing rock data from previous researchers such as Kent (1949); Jones (1988); Hoole (2000); Olivier et al. (2011); Boekstein (2012) and Olivier and Jonker (2013) to produce a geothermal energy map of South Africa. Dhansay et al. (2017) computed geothermometry from Si

or Na and K concentrations of the geothermal waters from secondary sources of information. The supplementary data does not tabulate the ion content but rather the source, hence, reproducing the geothermometry is cumbersome. Dhansay et al. (2017) highlighted the five anomalous high heat-producing areas in the country where the estimate of the depths to reservoirs of the geothermal waters was between 2 and 5 km. The five heat producing areas are the Limpopo Mobile Belt, Bushveld Basin near the Thabazimbi-Murchison Lineament, the boundary of the Kaapvaal Craton and Namaqua-Natal Belt, Cape Fold Belt and the southern Karoo (Dhansay et al., 2017).

Gravelét-Blondin (2013) utilised the ($[SiO_2(OH)_2]^{2+}$), Na^+, Ca^{2+}, K^+ and Li^+ concentration from Shu Shu for geothermometry with predicted temperature range from 58°C to -157°C. Some of the temperatures computed were below Shu Shu surface temperature and were excluded from Gravelét-Blondin's (2013) analyses. Gravelét-Blondin's (2013) proposed a conceptual model for Shu Shu that located the geothermal water circulation depth of 1825-2153 m, is recharged 130 km away and takes 60 years to surface (Gravelét-Blondin, 2013).

Murray et al. (2015) computed the depth of several geothermal water resources within the Karoo Supergroup region by assuming the geothermal gradient of 1.5°C/100m and a surface temperature of 20°C. The calculated circulation depths were 470 m to 1150 m, for the geothermal waters to be as hot as it is on surface. Murray et al. (2015) suggested that long-term monitoring and sampling of the geothermal waters is required to understand the systems and would have increased the confidence in the geothermometers obtained.

Geothermometry is a common practice used to produce a preliminary conceptual model of a geothermal water site for the potential of harnessing geothermal energy (Rattanawong et al., 2020). Pang and Reed (1998) proposed that aluminium be accounted for in the geothermometry field by fixing the aluminium value. Their experiment utilised synthetic water that made up of minerals present with aluminium in their structure. The estimated temperatures were taken as a converging point on

the calculated geothermometry graphs. Pan and Reeds' (1998) proposed geothermometry calculation was applicable to geothermal waters lacking Al analysis and for waters with an incorrect Al analysis.

In Kizildere, Türkiye, a geothermal reservoir that produces energy displays actual temperatures (202°C) that are similar to the calculated quartz geothermometer temperatures (204°C -213°C) according to a study by Gökgöz (1998).

In China, a 4 km geothermal well was drilled in Cangzhou City. The silica and Na-Mg geothermometers (Feng et al., 2012) accurately estimated the reservoir temperature (107°C-108°C) to the measured temperature from the borehole (108°C) (Kai et al., 2020). The Na-Mg geothermometer is suitable for low temperature geothermal fluids and reaches equilibrium quickly in solution (Hongmei et al., 2006).

3.3.4 The potential geothermal energy from geothermal waters of South Africa

Rubio-Maya et al. (2015) classified enthalpy into high, medium and low enthalpy (Table 1). One can determine the enthalpy range of each reservoir if the reservoir temperature is known at depth and used in conjunction with the Henley Table (Appendix B) (Henley et al., 1984; Mohamed and Ehara, 2009). Dhansay et al. (2017) mentioned that low to medium enthalpy resources occur in areas with geothermal gradients of 40°C/km, producing five anomalous high heat-producing areas in the country. However, the work by Dhansay's et al. (2017) falls short in providing information on the depth and temperature of geothermal water reservoirs. Depth of the geothermal water reservoirs rely on the assumption that the geothermal waters have reached thermal equilibrium. The calculated temperatures are justified as the subsurface fluid flow is steady and slow with high thermal conductivity of rocks (Feng et al., 2012). Research on the enthalpy range of geothermal waters is limited to temperatures based on geothermometry. Previously, heat flow measurements have been inconsistent with measurements concentrated on the Kaapvaal Craton. A study by Dhansay (2012) published a heat flow map of the Karoo Supergroup that covers a large area of the country. This heat flow map displays higher heat flows (80 mW m-2) for northern Lesotho and the boundary between the Kaapvaal Craton and the Namaqua-Natal Province and the western boundary between the Cape Fold Belt and

the Namaqua-Natal Province (Dhansay, 2012). Additional work such as exploratory wells are commonly used to measure the geothermal reservoir and the geothermal gradient as demonstrated by Gökgöz (1998); Sveinbjörnsson (2016) and Kai et al., (2020) for low to medium enthalpy systems.

3.3.4.1 Research into the utilisation of geothermal waters in South Africa

Hoole (2000) proposed that a tourist attraction for Lilani be considered. He emphasized that the development of a tourist attraction adopts a holistic approach where local participation in all aspects of development be considered .

Another form of harnessing the geothermal energy is by aquaculture. Joao, (2022) compared the efficiency of heat from heat pumps at Brandvlei geothermal waters for warm water aquaculture throughout the year. The heated water heats the pond that houses the fish. Therefore, the heated water does not enter the fishpond but rather maintains the heated water of the fishpond, making the chemical constituents of the geothermal water of little impact. The heat from the geothermal waters is 55% efficiently utilised compared to heated water via a heat pump experiment (Joao, 2022). Joao (2022) study reaffirms what was mentioned by Tshibalo et al. (2015) that certain regions could harness geothermal energy to support small-scale commercial farming.

In South Africa, the notion of utilising geothermal energy for power generation was proposed by Dhansay (2012). A conceptual prefeasibility model with various parameters such as geological conditions affecting heat flow and heat productivity, were considered by Dhansay (2012). Furthermore, economic factors such as construction and maintenance costs were also considered for the hypothesized plant. This author proposed a low enthalpy-enhanced geothermal system in the Vhembe district, Limpopo Province. The plant would produce 75MW of power from 3 wells drilled 5-6 km deep over 30 years. (Dhansay, 2012).

By contrast, Gravelét-Blondin (2013) studied Shu Shu geothermal water and proposed that a binary 400kW power plant could provide sufficient power for 625 rural homes.

This proposed binary plant at Shu Shu was based on work done on the Chena Hot Springs data drawing on a liner relationship on the parameters utilised for power generation. However, Gravelét-Blondin, (2013) did not consider the enthalpy range of Shu Shu and fell short in deploying geophysics survey for Shu Shu to locate the subsurface geothermal resource.

Olivier and Jonker (2013) showcased the potential of the geothermal waters in South Africa. They indicated that all the geothermal waters were suitable for agriculture, aquaculture, mining of minerals and tourism. According to Olivier and Jonker (2013) high temperature (>50°C) and high flow rate (126 l/s) classified Brandvlei a suitable site to harness geothermal energy for power generation. Siloam exhibits a high temperature (>50°C), but the flow rate is lower than Brandvlei. To increase the flow rate from Siloam a borehole would be needed to harness geothermal energy for power generation. Other geothermal waters were noted to have potential for power generation based on their high temperatures (>50°C) alone, such as Shu Shu, Calitzdorp, Warmbaths and Badplaas (Olivier and Jonker, 2013).

Olivier and Jonker (2013) highlighted that, based on subsurface heat and tectonic investigations numerous geological regions in South Africa exhibit some potential for geothermal energy. However, exploration for baseload energy generation has been limited (Dhansay et al., 2017) compared to other countries that have increased their geothermal energy production.

3.3.5 Harnessing geothermal waters for power generation

People are drawn to geothermal waters for medicinal, hygiene and tourism. Hence geothermal waters are areas that can benefit from tourism and hence the need for the energy (Boekstein, 1998). In 2015, 25 countries had set up geothermal power plants that converted geothermal energy to generate power (Bertani, 2015).

In 1904 in Larderello Italy, the first attempt to produce electricity from geothermal steam was conducted. By 1913, the first commercial plant, Larderello One started operating by producing 250kWe (also mentioned in section 2.3.1). By 1939, the completion of the first big geothermal power plant at Larderello boasted six 10 MW

units (Burgassi, 1999). The power generated was from a reservoir with medium to high permeability at ~270 °C with a reservoir pressure of 6 MPa. Furthermore, a second deep superheated steam reservoir is also present at temperatures of 300-350 °C with a pressure of 7 MPa (ENGINE Coordination Action, 2008). Other international examples take on a different facet such as the San Michkael Project in the Amatitlan area of Guatemala.

The San Michkael Project in the Amatitlan area of Guatemala is a low-enthalpy geothermal reservoir. Initially that was initially intended, the exploration of the San Michkael Project was for power production and direct use. This investigation research included geology, geophysics, geochemistry and shallow borehole datasets equating to an investment of USD2 -USD3 million investment. This project failed to produce a high enthalpy and instead the research results were published. Following the initial abandonment of the San Michkael Project, the resource was able to produce 20-25kW primary power with geothermal water temperatures of 90-120°C. For this to be accomplished site engineering involved optimising the geothermal reservoir as a cascading model to harness geothermal energy. The cascading model resulted in utilisation for power generation, candle making, dehydration, crop irrigation and pre-heating or cleaning plastic materials. The geothermal resource facilitates an industry that otherwise would have relied on traditional power producing methods. This project had knock-on benefits for the local communities, but these were not reported thus the benefit of geothermal energy to the local community is not apparent (Paiz Ramirez, 2021).

Zheng et al. (2015) used a novel data analysis system to analyse the geothermal energy utilisation trends worldwide. Their findings indicated that in the first phase direct use of geothermal energy for heating and cooling areas, food industry, snow melting, space cooling and recreational activities. Zheng et al. (2015) considered power generation in the second phase of their study. The final phase of their study was to harness geothermal energy in a hybrid model by a combination of various forms of energy or a cascade model (Section 2.3). These authors also predicted that the current

methods of geothermal energy utilisation would likely reach saturation by 2030, where newer technologies would need to emerge (Zheng et al., 2015).

To grasp the mechanism behind the geothermal waters, as future sources of energy production the geology of the geothermal waters needs in-depth research. However, for the current study, a general overview would suffice as the geothermal waters are located across the country. As discussed, the chemistry of a few geothermal waters has been reported at least once and the studies that followed referenced the previous work for comparison purposes. Hence, this current study updated the dataset of analyses forms a pillar in developing geothermal energy in South Africa.

CHAPTER 4 MATERIALS AND METHODS

Previous chapters outlined an association between productive geothermal energy and geological setting. In addition, the review of the literature conducted on geothermal waters in South Africa and the world provided the context of how this current research forms a pillar in further developing geothermal energy in South Africa. In this chapter, the intention is to describe the methods and tools applied to characterise the geothermal waters (Figure 16).

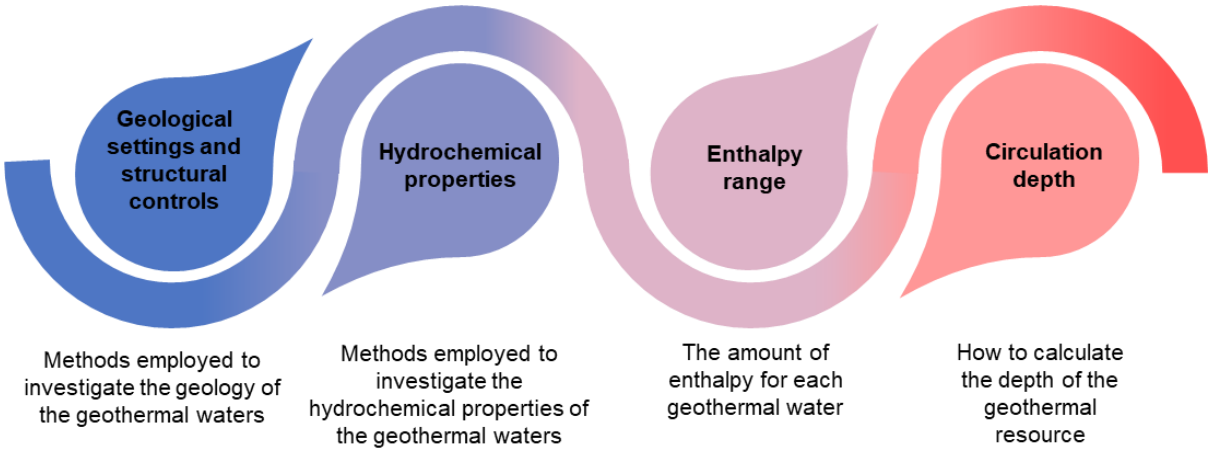

Figure 16: The process flow of the methods and tools applied for characterising the geothermal waters.

4.1 Geological settings of the geothermal waters of South Africa

For this study, the geology was investigated using a desktop study approach as the study area covers geothermal waters across South Africa, as the duration of this study was limited. A detailed study of the geology was therefore, beyond the scope of this research. Previous work on individual geothermal waters referenced maps from the Council for Geoscience to give context to the chemistry of the geothermal waters (as explained in Section 3.2). However, further investment into the geology of geothermal waters may add value to geothermal waters as a potential source of geothermal energy.

4.2 Hydrochemical sampling

In this study, 41 geothermal waters sites were sampled in South Africa as displayed in Figure 17. The methods employed for measuring the physical and chemical properties of the geothermal waters are discussed in detail below.

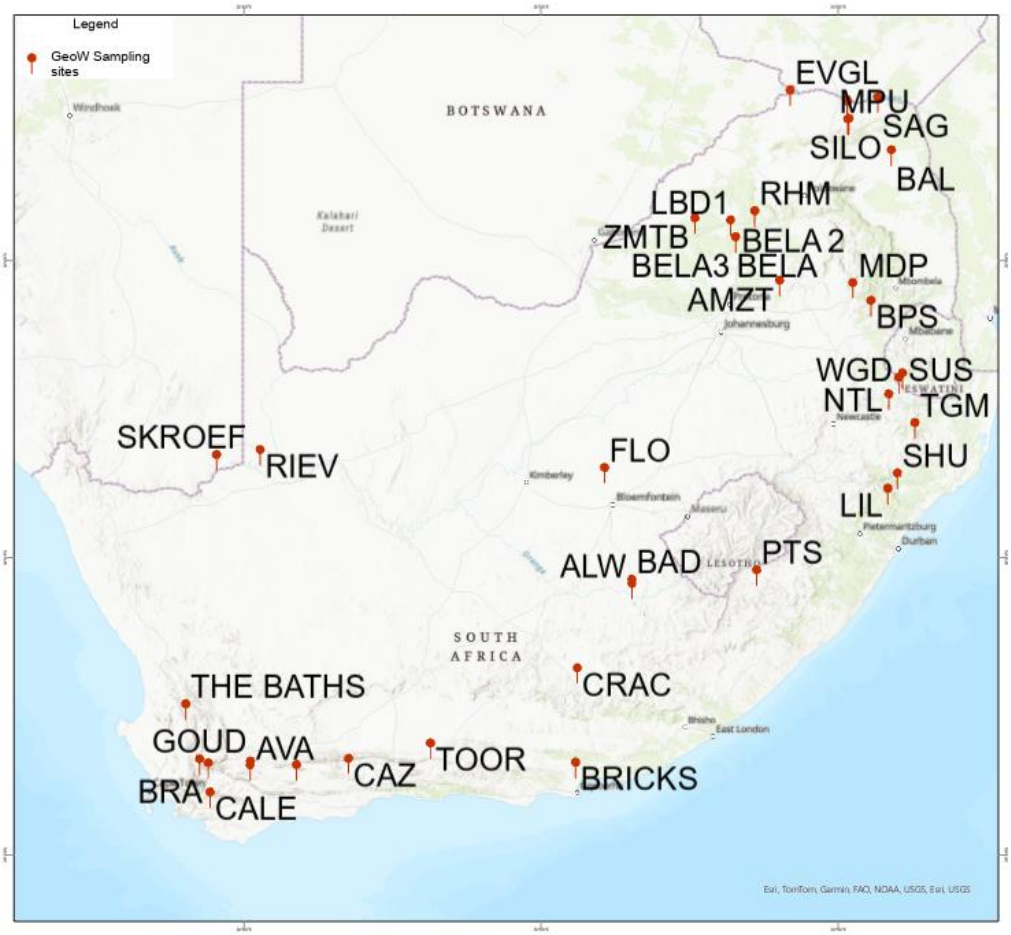

GeoWs Site	Abbreviation
Badplaas	BPS
Natal	NTL
Wagendrift	WGD
Baleni	BAL
Sulphur-Spring	SUS
Machadadorp	MDP
Siloam	SILO
Mphephu	MPU
Tshipise	TSH
Sagole	SAG
Evangelina	EVGL
Môreson	MRS
Rhemardo	RHM
Warmbath1	BELA
Warmbath2	BELA 2
Warmbath3	BELA3
Loubad1	LBD1
Loubad2	LBD2
Loubad3	LBD3
Amanzintaba	AMZT
Zimthabi	ZMTB
Riemvasmaak	RIEV
Skroef Se Bad	SKROEF
Lilani	LIL
Shu-Shu	SHU
Avalon Spring	AVA
Baden Club	BAK
Toorwater	TOOR
Warmwaterberg	WARM
Calitzdorp	CAZ
Caledon	CALE
Brandvlei	BRA
Goudini	GOUD
The Baths	THE BATHS
Bricks	BRICKS
Florisbad	FLO
Badsfontein	BAD
Aliwal	ALW
Cradock	CRAC
Polile Tshisa	PTS
Thangami	TGM

Figure 17: The geothermal water sampling sites in this study. Note the geothermal water are located across the country. The abbreviations of the sites are listed on the right.

4.2.1 Physical properties

Geothermal waters have diverse compositions and occur in an array of pressure and temperature environments (Figure 6). The hydrochemical characteristics of the geothermal waters are significant in comprehending the principal hydrochemical mechanisms in various geothermal systems. The hydrochemical mechanisms includes understanding the interaction between water and rocks and identifying the possible origins of the geothermal waters (Mohamed and Ehara, 2009). For these

reasons, the geothermal waters were sampled to understand the hydrochemical characteristics.

The physical properties of the geothermal waters are affected by the chemical properties of the geothermal waters and the chemistry of the host rocks (Stefánsson et al., 2013). Therefore, a portable multisensor probe was used to measure the temperature (°C), pH and total electrical conductivity (EC= µS/cm) and salinity (sal) of the geothermal waters. At each measurement site, the portable multisensor probe was calibrated according to the manufacturer's specifications. The measurements were taken at a flowing spring or borehole with an existing pump following the methods described by Weaver et al. (2007). Since most geothermal waters are associated with a name as per literature, the geothermal waters sample names were abbreviated to reflect the sampling site name, for example, Riemvasmaak (RIEM) or Tshipise (TSH) (Figure 17) in all the figures. All physical properties were recorded and collated for each site.

4.2.2 Chemical properties

Chemical properties included analyses for major ions (HCO_3^-, Cl^-, SO_4^{2-}, F^-, Na^+, Ca^{2+}, Mg^{2+}, K^+ and Fe^{2+}), silica ions ($[SiO_2(OH)_2]^{2+}$),stable isotopes and radiogenic tritium. Geothermal water samples were collected in clean plastic water bottles. These bottles were rinsed with the geothermal waters from the source before sampling to minimise possible contamination. The samples were collected by filtering geothermal waters using a 45µm filter and the samples were preserved with nitric acid in 200ml bottles. The samples were stored in a cooler box with ice packs, lowering the temperature of the samples to preserve the ions present. This procedure ensured that samples were not contaminated by the bottles used for sampling and that interaction time of the samples with the local environment was limited (Weaver et al., 2007).

4.2.3 Stable and radiogenic isotopes

Stable isotopes (δ8O and δ D) and radiogenic isotope (tritium) samples were collected in 2000ml bottles direct from the source. These bottles were rinsed with the geothermal water from the source before sampling to ensure the reliability of the

samples. The analytical precision is 0.5‰δ18O and 1.5‰δD, expressed relative to the Local Meteoric Water Line (LMWL). Stable isotopes are altered with the hydrological cycle. It is for this reason that the author assumes that geothermal waters have stable hydrochemical constituents in solution, such as Cl^-, 18O/16O and 2H/1H, while ion exchange is absent.

4.2.4 Methods for analysing the hydrochemistry of the geothermal waters

All the cations and anions (HCO_3^-, Cl^-, SO_4^{2-}, F^-, Na^+, K^+, Ca^{2+}, Mg^{2+} and Fe^{2+}) were analysed using an induced coupled plasma-optical emission spectrometer (ICP-OES) Silica ions were analysed using a spectrophotometer. Standards and duplicate samples were added to the analyses for quality control. The purpose of quality control was to maintain the integrity of the samples, improve the accuracy of the analytical data, and prevent any false positive readings caused by contamination.

The chemically active species such as Na^+, K^+, Ca^{2+}, Mg^{2+} and $[SiO_2\ (OH)^2]^{2+}$ react with the changing conditions underground. These ions react according to temperature, dependent on chemical interactions in the geothermal systems and are utilised to predict subsurface temperatures (Khosrawi, 1996).

The isotope analyses of hydrogen (δD and ^{3}H) and oxygen (δ18O) were analysed using an Isotope Ratio Mass Spectrometer or a Liquid Water Isotope Analyser. For quality control purposes, duplicate samples were included in the batch analyses. Table 2 shows the various analyses and the volume of water collected.

Table 2: Analyses on the geothermal waters collected.

Analyses	Bottle type	Bottle size(ml)	Filter	Preservative
Cations	Plastic	200	Yes	Yes HNO_3
Anions	Plastic	200	Yes	No
Silica ions	Plastic	200	Yes	No
Stable Isotopes	Plastic	2000	No	No
Blank	Plastic	2000	No	No

4.2.5 Data presentation

Physical and hydrochemical properties of the geothermal waters are represented statistically and graphically to characterise the geothermal waters . This data is presented in an objective and consistent manner.

4.2.5.1 Statistical presentation

A statistical method was employed known as the Pearson correlation. The Pearson correlation matrix measures the relationship between variables (physical and hydrochemical parameters) at 0=0.05 level of significance. This produces a correlation coefficient r, which is a measure of the strength and direction of the relationship between pairs of continuous variables. Ranges are between r=-1.00 and r=+1.00 where the closer the correlation is to either r=-1.0 or r=+1.0 the relationship is stronger (Boslaugh and Watters, 2008). The correlation coefficient r is described as very strong (r=0.80–1), strong (r=0.70–0.79) moderate (r=0.50–0.69) and weak (r=0.00–0.49). The Statistical Package for the Social Sciences software was used for this geothermal water correlation matrix.

4.2.5.2 Graphical presentation

Graphs representing the different physical properties are presented to establish relationships between the various properties. In addition, by plotting the Piper diagram the dominant types of water present, the chemical character of the geothermal waters and the water-rock interaction between the source areas of different geothermal waters can be displayed. A Piper diagram combines three fields of the chemical constituent concentration: two triangles and a rhombus display the chemical properties of the geothermal waters. One triangular field to the lower right includes the percentage reacting values of the three anion groups (HCO_3^-, Cl^- and SO_4^{2-}). The other triangular field to the lower left contains percentage reacting values of the three cation groups (Na^+, Ca^{2+} and Mg^{2+}). The ion triangles plot as a single point on each displaying a conventional trilinear coordinate. The rhombus in the middle plots all the chemical constituents of the waters as a single point, representing the intersection of points from the cation and anion triangles. The rhombus indicates the relative composition of the water in terms of the cation-anion pairs that correspond to the vertices of the field. The subdivision of the rhombus indicates the water-type categories (Piper, 1944). The current study used the Geochemical Workbench software to plot the chemical results (Bethke et al., 2022). Ions analyses are in mg/l but for the Piper plot and some of the bivariate scatter plots the analyses were converted to meq/l. In an attempt to group the geothermal waters, the geological settings are colour coded. The advantage of using the Piper diagram is that one can easily compare large datasets (Kent, 1979;

Kent, 1980; Duah, 2010; Ármannsson, 2012; Mohammed and Garba Abba, 2015; Masindi and Abiye, 2018; Mahwa et al., 2023).

The Schoellar diagram is presented as log concentration of the major ions, which connect to form trends of the geothermal waters. This leads to an interesting anomaly where two adjacent springs may differ significantly regarding their chemical properties (Schoellar, 1963). To understand the ion exchange process in the geothermal waters, the Ca+Mg vs SO_4+HCO_3 and Ca+Mg vs Na+K bivariate plots show the distribution of geothermal waters between carbonate and silicate weathering (Durowoju et al., 2019; Henry, 2020; Mahwa et al., 2023).

The Na-K-Mg geoindicator by Giggenbach (1986) reveals the relationship of water to host rock, displayed as a ternary diagram with Na/1000, K/100 and the square root of Mg at the apices (Cave and Clarke, 2003; Ármannsson, 2012; Baioumy et al., 2015; Mohammed and Garba Abba, 2015; Cruz Pauccara, 2018; Mahwa et al., 2023). In addition, a bivariate plot of the major cations %Mg = 10Mg/(Mg+Ca) vs %K = 10K/(10K+Na) to indicate the isochemical dissolution (Abidin et al., 2005; Baioumy et al., 2015; Cruz Pauccara, 2018; Herzhegovina et al., 2020; Ayari et al., 2023). The signatures of the geothermal waterseither have an affinity to the crust or to seawater or are in equilibrium at a given temperature (Giggenbach, 1988 a, b).

To further characterise the geothermal waters, the relationship between the stable isotopic values (δ18O and δD) are plotted together with the Local Meteoric Water Line (LMWL) of various regions across South Africa to better understand the recharge of the geothermal waters (Gökgöz, 1998; Diamond and Harris, 2000; Gravelét-Blondin, 2013; Cruz Pauccara, 2018; Durowoju et al., 2019). Tritium values are regarded as an indicator of the age of the geothermal waters.

4.3 Geothermometry

For the geothermal waters to be hot at the surface, the geothermal waters should be hotter underground (as explained in Section 2.1). By performing solute-based geothermometry one can predict the geothermal resource temperatures.

Geothermometry calculates the resource temperature based on the concentration of ions ($[SiO_2\ (OH)^2]^{2+}$,Na^+, K^+ and Mg^{2+}) in the geothermal waters that predicts the resource temperature as determined by various researchers (Truesdell, 1976, Fournier, 1977; Arnórsson, (1983; 1985); Giggenbach, 1988 a, b; Verma and Santoyo, 1997; Santoyo and Díaz-González, 2010). Silica equations are based on the solubility of quartz in water that was determined from experimental data. Silica occurs in different forms such as quartz, cristobalite, chalcedony and amorphous silica. A recommended geothermal water surface temperature is needed to apply the equations because as the geothermal waters ascend to surface, the silica reacts to the temperature loss (Giggenbach, 1988 a, b; Güleç, 2005).

The equations for the geothermometers are presented in Table 3. The various geothermometers are utilized with caution as the geothermal waters occur in different geological settings while some processes may change the chemical signature of the geothermal waters. This collation is to have an idea of the temperature of the geothermal resource as many geothermal waters' geothermometry has not yet been undertaken to this extent in South Africa Since many of the South African geothermal waters geothermometry has not been investigated, this current study serves as a central data set for such a compilation.

The geothermometers are dated to 1977 but are still utilised to predict temperatures of geothermal resources (Drogue et al., 2000; Tassi et al, 2006; Mohamed & Ehara, 2009; Baioumy et al. 2015; Yan et al. 2017; Zhenhua et al. 2018; Aydin et al, 2020; Chimeddorj et al. 2021; Temizel et al. 2021; Yu et al. 2022; Kiełczawa, 2023; Mahwa et al, 2023; Yin et al. 2023). Kai et al., (2020) demonstrated that the Na-Mg and the average silica geothermometers accurately estimated the reservoir temperature for a drilled well. The only variable in the equations is the ion concentration (Table 3). Hence each of the geothermal water particular ion concentration was substituted in the equations.

Table 3: Temperature (°C) equations for geothermometers.

Geothermometer	Equation	Recommended Temp. (°C) Range	Reference
Quartz	Equation 3: $T_{SiO2}= \left(\frac{1309}{5.19-\log Si}\right) - 273.15$	0-250	Fournier, (1977)
Quartz-after steam loss	Equation 4: $T_{SiO2}= \left(\frac{1522}{5.75-\log Si}\right) - 273.15$	0-250	Fournier, (1977)
Quartz	Equation 5: $T_{SiO2}=53.50 + (0.011236Si) + (-0.5559x10^{-4}Si^2) + (0.1772 \text{ x } 10^{-7} Si^3) + (88.390 \log Si)$	*NR	Arnórsson, (1985) based on Fournier and Potter, (1982)
Chalcedony	Equation 6: $T_{SiO2}= \left(\frac{1032}{4.69-\log Si}\right) - 273.15$	0-250	Fournier, (1977)
Chalcedony	Equation 7: $T_{SiO2}= \left(\frac{1112}{4.91-\log Si}\right) - 273.15$	25-180	Arnórsson, (1983)
Alpha-Cristobalite	Equation 8: $T_{SiO2}= \left(\frac{1000}{4.78-\log Si}\right) - 273.15$	0-250	Fournier, (1977)
Opal-CT(Beta-Cristobalite)	Equation 9: $T_{SiO2}= \left(\frac{718}{4.51-\log Si}\right) - 273.15$	0-250	Fournier, (1977)
Amorphous silica	Equation 10: $T_{SiO2}= \left(\frac{731}{4.52-\log Si}\right) - 273.15$	0-250	Fournier, (1977)
Na-K	Equation 11: $T_{Na/K}= \left(\frac{856}{\log\left(\frac{Na}{K}\right)+0.857}\right) - 273.15$	*NR	Truesdell, (1976)
Na-K	Equation 12:$T_{Na/K}= \left(\frac{1217}{\log\left(\frac{Na}{K}\right)+1.483}\right) - 273.15$	0-250	Fournier, (1977)
Na-K	Equation 13:$T_{Na/K}= \left(\frac{933}{\log\left(\frac{Na}{K}\right)+0.993}\right) - 273.15$	*NR	Arnórsson, (1983)
Na-K	Equation 14:$T_{Na/K}= \left(\frac{1390}{1.750+\log\left(\frac{Na}{K}\right)}\right) - 273.15$	*NR	Giggenbach, (1988 a, b)
Na-K	Equation 15:$T_{Na/K}= \left(\frac{1289}{\log\left(\frac{Na}{K}\right)+1.615}\right) - 273.15$	*NR	Verma and Santoyo, (1997)
Na-K	Equation 16: $T_{Na/K}= \left(\frac{876.3(\pm 26.26)}{\log\left(\frac{Na}{K}\right)+0.8775(\pm 0.0508)}\right) - 273.15$	*NR	Santoyo and Díaz-González, (2010)
K-Mg	Equation 17: $T_{K/Mg}= \left(\frac{4410}{14+\log\left(\frac{K2}{Mg}\right)}\right) - 273.15$	*NR	Giggenbach, (1988 a, b)

*NR-Not Reported

4.4 Estimating the enthalpy of the geothermal waters

The geothermometry temperatures were investigated as an indication of the most realistic temperatures of the geothermal resource. These temperatures of the geothermal waters were applied to the Henley Steam table (Henley et al., 1984) (Appendix B) to determine the amount of heat each geothermal waters resource would be able to produce.

4.5 Estimation of the circulation depth of the geothermal waters

The depth at which the geothermal waters circulate is built on the understanding that the geological settings and the geothermal gradient are stable. As the geothermal gradient of the geothermal waters is reported by Dhansay et al.(2017) (Appendix D), the depth of circulation can be calculated from solute geothermometry according to the equation below (Cave and Clarke, 2003; Shestakova et al., 2018; Chimeddorj et al., 2021).

Equation 18: $z = \frac{Tcalc\text{-}Tavg}{G}$

Where *z* is the geothermal resource depth in meters Tcalc is the temperature (°C) calculated by a reliable geothermometer, T avg is the yearly average air temperature (°C) of the sampling locality, G is the mean geothermal gradient (Cave and Clarke, 2003; Shestakova et al. 2018; Chimeddorj et al. 2021). Solute geothermometry and depth estimates rely on the relative conductivity of rock materials and slow steady rates of subsurface fluid flow (Cave and Clarke, 2003). This is particularly relevant as the majority of South Africa occurs on basement rocks of the Kaapvaal Craton that is isolated from active tectono-thermal processes with slow steady rates of subsurface fluid flow (Jones and Scheiber-Enslin, 2022).

CHAPTER 5 RESULTS

The previous chapters discussed an association between productive geothermal energy, geological settings, methods and tools applied to characterise the geothermal waters. In this chapter, the intention is to present the results obtained from the methods and tools applied for characterising the geothermal waters (Figure 18).

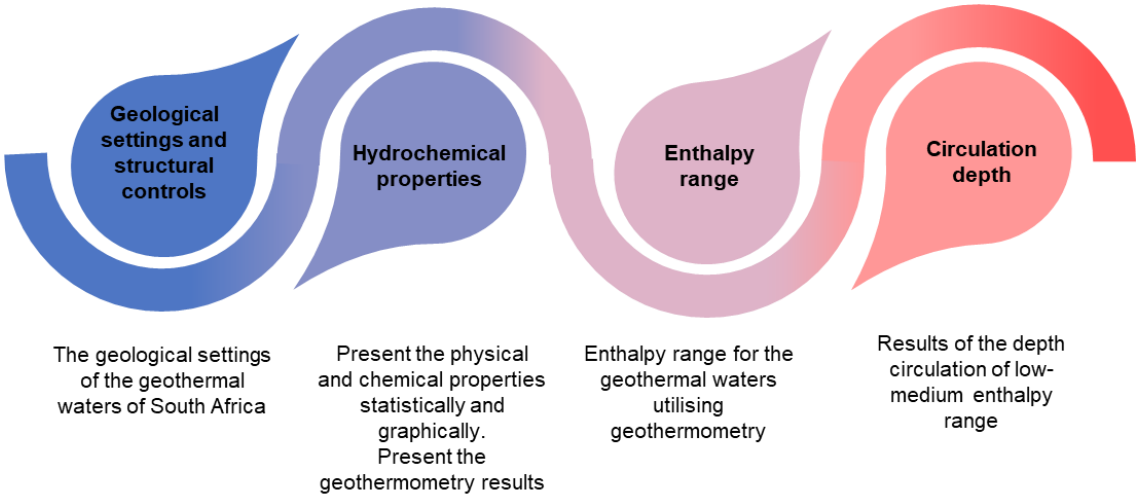

Figure 18: The process flow for presentation of results of the geothermal waters in South Africa.

5.1 Geological settings and structural controls

Figure 19 displays geothermal waters sites and their encompassing geological settings including the major tectonic structures in South Africa. The majority of the South Africa is underlain by granitic basement rocks of the Kaapvaal Craton. The Kaapvaal Craton formed by combining several fragments of ancient crust that stabilised during the early Archean eon (Poujol et al., 2003). This amalgamation of the ancient crustal fragments represents deep crustal discontinuities (Schmitz et al., 2004). Further to this, the Kaapvaal Craton is bordered by paleo-orogenic belts. These orogenic belts recorded continental collision events (Thomas, 1989; Linol and De Wit, 2016).

The geothermal waters in South Africa occur within these orogenic belts. Furthermore, the geothermal waters are often associated with high heat producing plutonic rocks linked to tectonic accretionary processes for example recorded in the Kaapvaal

Craton. Geothermal waters are controlled by brittle features (faults, joints, fractures) that enable subsurface fluid migration and concentration. This further links to and provides evidence for underlying tectonic and chemical-lithostratigraphic controls on the subsurface heat flow. The geothermal waters in South Africa are located in Archean granites and gneisses, the Limpopo Mobile Belt associated with the Soutpansberg Group, the Waterberg Group and the Bushveld Igneous Complex, the Namaqua-Natal Province, the Cape Fold Belt and its association with the Karoo Supergroup and Uitenhage Group (Dhansay et al., 2017) (Figure 19). However, fewer geothermal waters are associated with rocks of the Transvaal Supergroup and Pongola Supergroup (Figure 19).

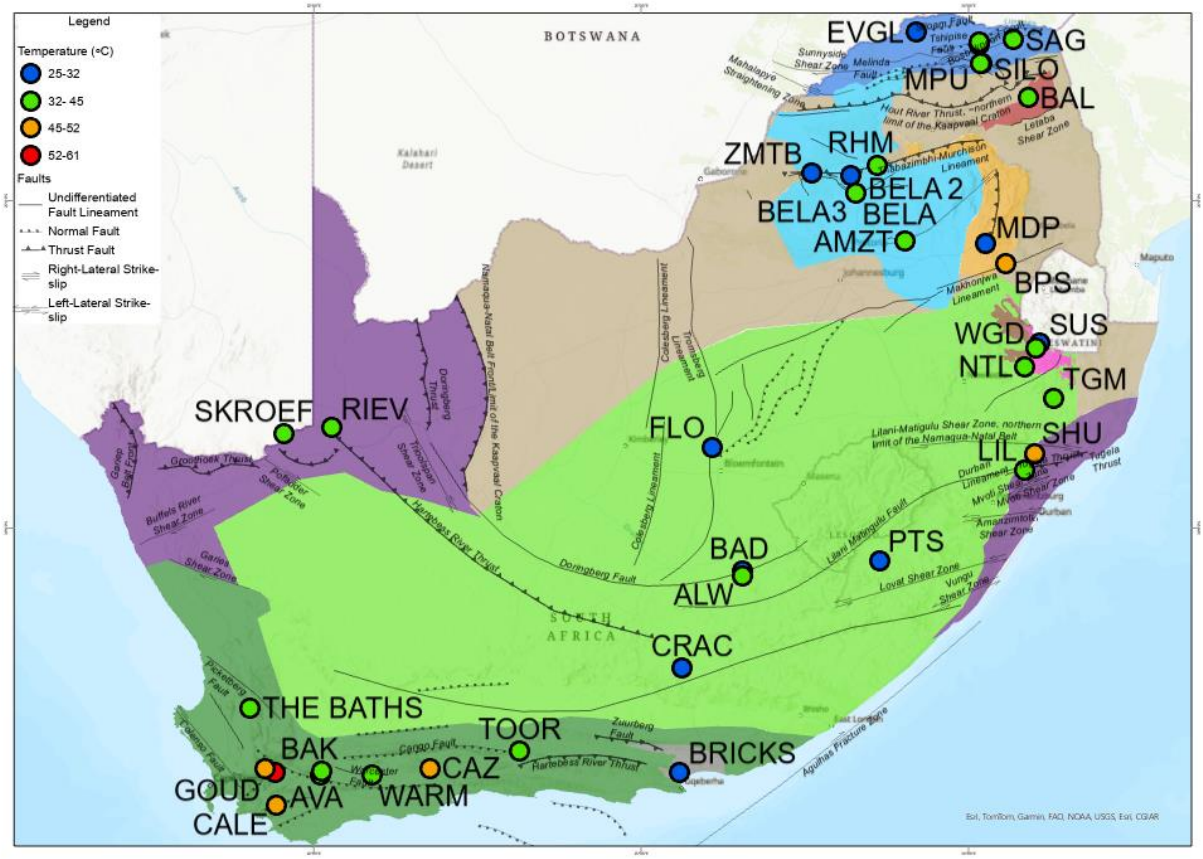

Figure 19: The geothermal waters in South Africa, underlying geology and tectonic domains (modified from Dhansay et al., 2017).

5.1.1 Archean granites and gneisses

There are four geothermal waters associated with the Archean granites and gneisses namely Badplaas (BPS), Natal (NTL), Wagendrift (WGD) and Baleni (BAL). Badplaas

(BPS) is associated with the Nelshoogte Gneiss in the Mpumalanga Province. Natal (NTL) and Wagendrift (WGD) occur in the Anhalt Suite (Figure 19) in KwaZulu-Natal Province. Baleni (BAL) is in the Groot Letaba Gneiss, Limpopo Province.

The Archean granites and gneisses intruded into greenstone belt terrains at various periods (Johnson et al., 2006). The Nelshoogte Gneiss comprises of trondhjemite gneiss and intruded into the host rocks ~3230 Ma (Matsumura, 2014). The Nelshoogte Gneiss exhibits low heat production of <2 μWm^{-3} with Th/U ratio of 4.6 representing average crustal signatures. Continued regional magmatism led to granites with higher signature of Th/U ratio of 7.3. Widespread sedimentation followed the period of magmatism further burying the trondhjemites and gneisses, insulting the heat at depth (Robb et al., 2021). In the trondhjemites and gneisses the concentration of Th=19.9-99ppm and U=58-339ppm is significantly high (Wang et al., 2020). As the Kaapvaal Craton stabilised, further deposition of overlying sediments occurred (De Wit et al., 2018).

Apart from the heat produced at Badplaas, the structural junction between the Mawelawela and Stolzburg-Moodies Faults is located at Badplaas. These faults bound the Inyoni Shear Zone characterised by brittle-ductile shear zones in the area along which water is able to ascend to surface (De Wit et al., 2018).

The Anhalt Suite is made up of granodiorites, quartz monzonites and trondhjemites. This suit of granitoids intruded into host rock ~3267 ± 21 Ma ago (Mukasa et al., 2013). Research into the Anhalt suite is limited but the White Mfolozi granitoid representing an A-type granite similar to Anhalt Suite was studied. The White Mfolozi granitoid may be used as a proxy to the Anhalt suite. The concentration of Th is between 11-26ppm and U is between 1-8ppm for White Mfolozi granitoid. Supracrustal rocks of the Pongola Supergroup overlie the Anhalt Suite, insulating the heat (Misra et al., 2017). A dyke crosscuts the area where the Natal (NTL) geothermal waters is located which could act as a conduit for water to surface (Stedman and Hunter, 1990).

The Groot Letaba Gneiss is made up of tonalities and trondhjemite, which intruded into country rock ~2960-2860 Ma with concentration of Th=1-17ppm and U=<1-8ppm

contributing to the heat at Baleni (Moyen et al., 2024). In the Baleni area, NE-SW faults align with regional faults that occur in the Giyani and Murchison greenstone belts. It is likely that the geothermal waters utilise these structures to ascend to surface (Johnson et al., 2006). The heat flow on the Kaapvaal Craton is mostly in the range of 35 to 55 mW m^{-2} (Jones, 2017) however U=170-424ppm and Th= 42-110ppm concentration is high in places such as the central Kaapvaal Craton (Baughman and Flowers, 2020).

5.1.2 Pongola Supergroup and Transvaal Supergroup

Two geothermal waters are located in the Mpumalanga Province: Sulphur Springs (SUS) is associated with the Pongola Supergroup and Machadodorp (MDP) is associated with the Transvaal Supergroup (Figure 19).

Sulphur Springs (SUS) occurs in the Pongola Supergroup composed of sediments and volcanic rocks, broadly constrained to 3000-2800 Ma (Hicks and Gold, 2020). Several phases of deformation in the Pongola Supergroup produced strike slip shear zones. One such shear zone is the Mahamba Shear Zone associated with Sulphur Springs (SUS) enabling geothermal waters to surface (Johnson et al., 2006). The Pongola Supergroup formed in a rift-to-intracratonic-sag-type environment (Moore et al., 2001). The faults in the region strike NE-SW (Kent, 1949). Sulphur Springs is located in an area where various heat producing igneous intrusions (Dhansay et al., 2017) have formed such as the Anhalt Suite (Section 5.1.1). The Anhalt Suite could be a heat source for Sulphur Springs. Furthermore, the overlying Pongola Supergroup (~9100 m thick sequence) (Wilson et al., 2013) could act as an insulator of heat. Machadodorp (MDP) is situated in the Pretoria Group of the Transvaal Supergroup comprised of clastic sediments and volcanic rocks formed between 2650 and 2050 Ma (Johnson et al., 2006). Sills intruded into the Transvaal Supergroup that could have fractured the surrounding rock enabling water to surface (Reczko, 1994).

5.1.3 Limpopo Mobile Belt, Soutpansberg Group and Waterberg Group

Figure 19 illustrates the geothermal waters sampled for the current study in the Limpopo Mobile Belt and Soutpansberg Group areas namely Siloam (SILO), Mphephu (MPU), Tshipise (TSH), Sagole (SAG), Evangelina (EVG), and Môreson (MRS). The Limpopo Mobile Belt, Soutpansberg Group and Waterberg Group outcrop in the

Limpopo, North-West and Gauteng Provinces of South Africa (Figure 19). The Limpopo Mobile Belt formed as the Kaapvaal Craton collided with the Zimbabwe Craton (Coward, 1976). The junction between the two cratons is located along the Palala Shear Zone (Kramers et al., 2011). The Limpopo Mobile Belt covers an expansive high-grade terrain of gneisses. The Limpopo Mobile Belt deposition, deformation and metamorphism of sediments span a billion years (~ 3300 to ~ 2200 Ma) (Brandl, 1981; Boshoff, 2008). The Palala Shear Zone, Tshipise Fault, Siloam Fault and Bosbokpoort Fault are structures within the Limpopo Mobile Belt and Soutpansberg Group with a NE-SW trend (Figure 19). These faults could act as conduits for water to surface.

In the Limpopo Mobile Belt a conductive body is located 10 km below the Archean gneiss (Khoza et al., 2013). The heat from the conductive zone is insulated by the overlying Archean gneisses. Average concentrations of U=2ppm and Th=14ppm in the Limpopo Mobile Belt (Andreoli et al., 2011). Heat flow in the Limpopo Mobile Belt is averaged at 55 mW m^{-2} (Jones, 2017).

The Soutpansberg Group developed and is preserved along the extension of the Palala Shear Zone (Dorland et al., 2006). The Soutpansberg Group rests unconformably on Archean granulite-grade gneisses (Johnson et al., 2006). The Soutpansberg Group geology is composed of sedimentary and volcanic lithologies located in the northern region of South Africa (Brandl, 1981). The age of the Soutpansberg Group is 3937 Ma-1831 Ma (Geng et al., 2014). The Soutpansberg Group is intensely fractured. Fracture analyses and magnetic lineaments corroborate these tectonic evolution phases with the predominance of ENE-WSW fractures across the Soutpansberg Group (Stettler et al., 1989). The Xmas Fault and the Kranspoort Fault are ENE-WSW trending faults that occur close to the geothermal water enabling water to surface

The Waterberg Group is bounded by the Melinda Fault in the north. The Melinda Fault represents the re-activated structure along the Palala Shear Zone. The Waterberg Group is an extension of the Soutpansberg Group (Jansen, 1982). The rocks from the Waterberg Group rest unconformably on the Blouberg Formation, the Bushveld

Igneous Complex and Archean granites and gneisses. The Waterberg Group is characterised by clastic sedimentary rocks where deposition is influenced by the underlying crustal discontinuities (Callaghan et al., 1991). The deposition of the Waterberg Group took place between 2054 and 2051 Ma. The Waterberg Group can reach u to ~5 km thickness in places (Dorland et al., 2006). The sheer volume of rock in the area would be able to provide the insulation for heat in the area. Within the Waterberg Group the uranium concentration is between 69 and 1574ppm and Th concentration is between 26 and 1030ppm. Limited minor northwest trending brittle faults transacted the Waterberg Group while post-Waterberg Group faults trend ENE with downthrown blocks to the south (Mtimkulu, 2009). Furthermore, these faults enable water to ascend to surface. The geothermal waters in the Waterberg Group sampled for the current study are Rhemardo (RHM), Warmbaths (BELA), Loubad (LBD), Amanzintaba (AMZT) and Zimthabi (ZMTB). Three sites for Warmbaths and Loubad were sampled and are named numerically.

5.1.4 Namaqua-Natal Province

The Namaqua-Natal Province occurs in the KwaZulu-Natal Province (Natal Sector) and the Northern Cape Province (Namaqua Sector). Approximately 1200 to 1000 Ma ago Laurentia and Kalahari Cratons converged to form the massive orogenic Namaqua-Natal Province (Van Niekerk et al., 2022). The Namaqua-Natal Province is 1400 km long and 400 km wide, extending beneath the Phanerozoic Karoo Supergroup (Johnson et al., 2006). The Namaqua-Natal Province rocks comprise of both igneous and metamorphic rocks. The Kheis Province borders the Namaqua sector to the east and the Gariep Belt borders it to the west (Eglington, 2006). Deformation is preserved in broad-to-narrow shear zones and brittle faults showing penetrative foliage (Thomas et al., 1994). As seen in Figure 19, at the extremities of the Namaqua-Natal Province, geothermal waters occur around thrust faults. The voluminous intrusions in the Namaqua and Natal sectors provide a significant radiogenic source of heat producing elements (Dhansay et al., 2017). The heat flow in the Namaqua-Natal Province is between 50 to 75 mW m^{-2} (Jones, 2017). The sampled geothermal waters for the current study in the Namaqua Sector are Riemvasmaak (RIEV) and Skroef se Bad (SKROEF), and in the Natal Sector are Shu Shu (SHU) and Lilani (LIL).

5.1.5 Cape Fold Belt, Karoo Supergroup and Uitenhage Group

The geothermal waters sampled for the current study associated with the Cape Fold Belt are Avalon (AVA), Baden Club (BAK), Toorwater (TOOR), Warmwaterberg (WARM), Calitzdorp (CAZ), Caledon (CALE), Brandvlei (BRA), Goudini (GOUD) and The Baths (THE BATHS) (Figure 19).

The Cape Fold Belt occurs in the Western and Eastern Cape Provinces. This belt comprises sedimentary rocks (shales and quartzites) from the Palaeozoic Cape Supergroup (Linol et al., 2021). The Cape Fold Belt was compressed as the paleo-Pacific plate subducted northward beneath the southern margin of Gondwana between 276 Ma and 210 Ma (Hansma et al., 2016). Consequently, the Karoo Basin formed a foreland system (Thomas et al., 1994). This orogeny was defined by the formation of a north-verging fold and thrust (Pankhurst et al., 2006) potentially with a strike-slip component (Johnston, 2000; Linol and De Wit, 2016). Much of the strain generated during this orogeny would have been accommodated by deep basement structures (Viola et al., 2005; Paton et al., 2006) with many pre-existing fractures reactivated, including paleo strike-slip faults (Johnston, 2000; Paton et al., 2006). In Figure 19 most of the geothermal waters are located close to or on faults produced by the Cape orogeny. The Cape Granite Suite intruded into the Cape Supergroup between 552 and 510 Ma (Clemens and Stevens, 2021) generating with it average concentration of Th=18ppm and U=5ppm (García-Arias et al., 2024). The Karoo Supergroup overlies the Cape Supergroup. Presently, the Karoo Supergroup is in a state of relative tectonic quiescence and is principally affected by NE-SW-directed extension (Viola et al., 2005; Bird et al., 2006).

In general, the Cape Fold Belt and the southern Karoo regions share a dominant E-W fracture pattern that can be related to the N-S principal stress regime during the Mesozoic tectonic activity along the southern margin of Gondwana. However, further east, the pattern shows clear rotation toward ESE-WSW, which highlights the effect of the underlying boundary of the Namaqua-Natal Province (Riley et al., 2005). These fractures enabled water to move through the rocks of the Cape Supergroup before cementation destroyed the primary porosity (Diamond and Harris, 2000). Furthermore, the Karoo Supergroup hosts the Karoo Uranium Province (Kenan and Chirenje, 2016)

and is located close to the geothermal waters namely: Florisbad (FLO), Badsfontein (BAD), Aliwal (ALW) and Cradock (CRAC). Other geothermal waters that occur in the Karoo Supergroup are Polile Tshisa (PTS) and Thangami (TGM).

The Uitenhage Group overlying the Cape Fold Belt formed during the Mesozoic period along pre-existing faults associated with the Cape Fold Belt (Hattingh and Goedhart, 1997). The Uitenhage Group, also known as the Algoa Bay sub-basin is composed of conglomerates and sandstones that are intensely faulted (Johnson et al., 2006). The Zuurberg Fault borders the northern and eastern margin of the Uitenhage Group (Figure 19). Bricks (BRICKS) was sampled for this study in the Uitenhage Group. BRICKS surfaces close to the Coega Fault trending E-W in the Uitenhage Trough (Figure 19) that could be a conduit for geothermal water to surface. The Uitenhage Trough can be up to 2500 m thick (Makhubele & Bordy, 2021) that could act as insulator for heat.

5.2 Hydrochemical Results

5.2.1 Physical properties

Table 4 lists all the geothermal waters sampled, abbreviations for reference to the illustrations together with physical properties. In addition, the table groups the geothermal waters into similar geological domains. The illustrations are colour coded per geological domain.

The two hottest geothermal waters occur in the Cape Fold Belt Brandvlei (BRA at 60.5°C) and in the Limpopo Mobile Belt Tshipise (TSH at ~55°C). The coldest geothermal water occurs at Cradock (CRAC) at a temperature of 25.4°C associated with the Karoo Supergroup. On average, the temperature of the Limpopo Mobile Belt geothermal waters is 44°C from six sites measured. The Cape Fold Belt boasts nine geothermal waters that yield an average temperature of 44°C.

Table 4: The geothermal waters sampled showing the temperatures (°C), pH and electrical conductivity (EC-(µS/cm) in South Africa.

Geological setting	Geothermal water sites	Abbreviation	Temperature (°C)	pH	EC (µS/cm)
Archean granites and gneisses	Badplaas	BPS	49.4	7.5	581
	Natal	NTL	40.6	5.5	339
	Wagendrift	WGD	32.5	6.5	285
	Baleni	BAL	41.6	8.0	2*
Pongola Supergroup	Sulphur-Spring	SUS	29.7	5.5	188
Transvaal Supergroup	Machadodorp	MDP	28.8	6.5	377
Soutpansberg Group associated with the Limpopo Mobile Belt	Siloam	SILO	50.6	7.5	551
	Mphephu	MPU	43.4	7.2	357
	Tshipise	TSH	54.9	7.5	802
	Sagole	SAG	44.7	8.0	329
	Evangelina	EVGL	30.7	7.5	245
	Môreson	MRS	40.4	8.9	619
Waterberg Group	Rhemardo	RHM	36.5	7.6	356
	Warmbath1	BELA	49.0	9.2	627
	Warmbath2	BELA 2	35.4	6.5	14
	Warmbath3	BELA3	40.9	7.5	309
	Loubad1	LBD1	32.1	7.0	207
	Loubad2	LBD2	32.9	6.8	207
	Loubad3	LBD3	30.2	7.5	62
	Amanzintaba	AMZT	34.2	8.1	1156
	Zimthabi	ZMTB	31.0	7.6	939
Namaqua-Natal Province	Riemvasmaak	RIEV	38.4	4.0	4930
	Skroef Se Bad	SKROEF	45.0	6.0	344
	Lilani	LIL	40.0	6.0	434
	Shu-Shu	SHU	50.5	6.0	1445
Cape Fold Belt	Avalon	AVA	40.3	6.0	144
	Baden Club	BAK	38.5	6.0	82
	Toorwater	TOOR	41.8	5.5	198
	Warmwaterberg	WARM	44.0	5.5	239
	Calitzdorp	CAZ	49.0	5.5	209
	Caledon	CALE	48.8	5.5	198
	Brandvlei	BRA	60.5	5.5	74
	Goudini	GOUD	45.2	5.5	81
	The Baths	THE BATHS	43.0	5.5	82
Uitenhage Group	Bricks	BRICKS	27.0	8.0	144
Karoo Supergroup	Florisbad	FLO	26.8	7.5	4240
	Badsfontein	BAD	29.4	3.5	2120
	Aliwal	ALW	32.6	3.5	2160
	Cradock	CRAC	25.4	4.0	235
	Polile Tshisa	PTS	29.1	4.0	406
	Thangami	TGM	37.5	5.5	634

*Discussed further in Section 6.2.1.

The most conductive geothermal waters are from the Namaqua sector of the Namaqua-Natal Province (Riemvasmaak (RIEV=4930 µS/cm)) and in the Karoo Basin (Florisbad (FLO= 4240 µS/cm)). The least conductive geothermal waters is located in the Groot Letaba Gneiss (Baleni (BAL=2.0 µS/cm)). These trends are further elaborated in the discussion (Section 6.2.1).

The pH of all measured geothermal waters ranges from 4 to 9. The most acidic (pH=4) geothermal waters are in the south of the Karoo Supergroup namely Cradock (CRAC) and Polile Tshisa (PTS) and from Namaqua-Natal Province Riemvasmaak (RIEV) . The most alkaline geothermal water is Warmbaths (BELA) associated with Waterberg Group and the Limpopo Mobile Belt. The pH and electrical conductivity (EC) of the geothermal waters sampled were generally similar across the geological regions. The geothermal waters from the Karoo Supergroup (Florisbad (FLO) and Namaqua-Natal Province (Riemvasmaak (RIEV) and Skroef se Bad (SKROEF)) show an inverse correlation of EC values with temperature as illustrated in Figure 20. The geothermal waters are colour coded per geological domain. A comparison of the geothermal waters in the southern region of the Natal Sector of the Namaqua-Natal Province shows that Shu Shu (SHU) is hotter with higher EC values.

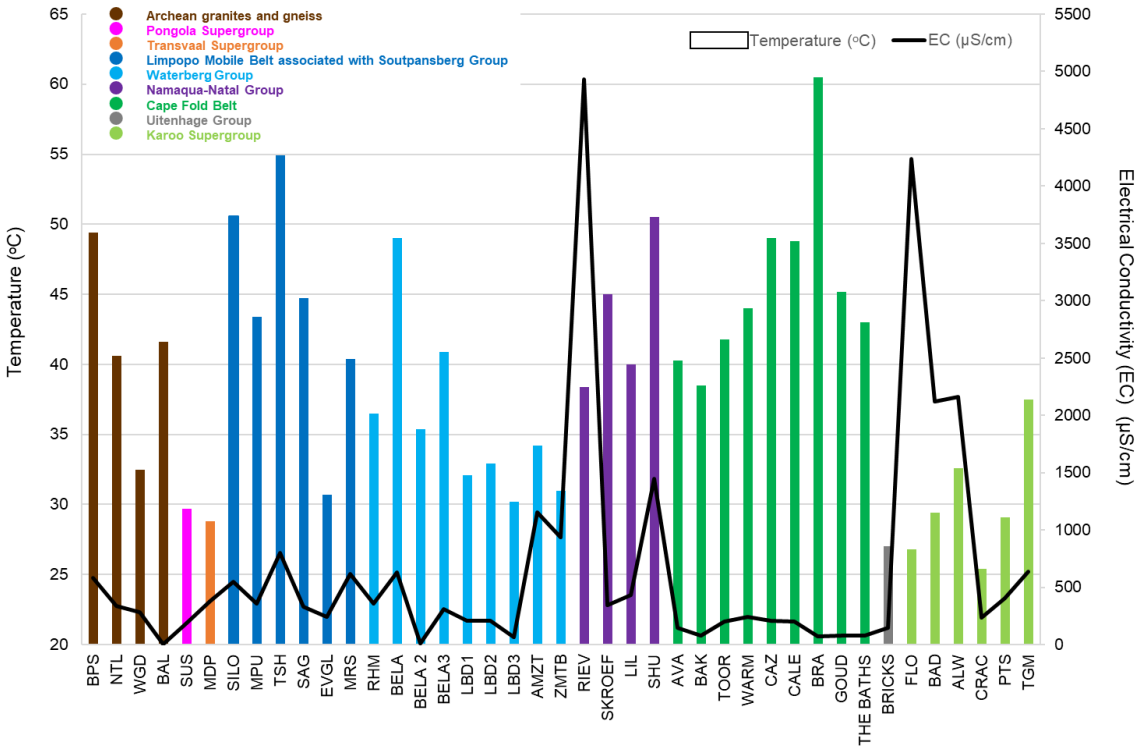

Figure 20: Illustration showing the inverse correlation of temperature (°C) (measured at surface manifestations) versus the electrical conductivity (EC) of the geothermal waters. The geothermal waters are colour coded per geological domain.

Lower EC and temperatures characterize the geothermal waters at Loubad (LBD) from the Waterberg Group. The relationships of physical properties in geothermal waters with hydrochemical properties were evaluated using the Pearson's correlation (Table 5). Based on the Pearson's correlation (Table 5) the relationship between EC and temperature are weak (r=-0.29).

Table 5: Pearson correlation matrix showing the relationships between physical properties and hydrochemical properties of the geothermal waters sampled in South Africa. Dark green indicates a strong to very strong correlation, green indicates a moderate correlation, while the pink to light pink the correlation is weak between the physical properties and hydrochemical properties.

	Temp. (°C)	pH	Ec (µS/cm)	Sal (%)	Bicarbonate Alkalinity $CaCO_3$ (mg/ℓ)	Chlorine Cl (mg/ℓ)	Sulphate SO_4 (mg/ℓ)	Fluoride F (mg/ℓ)	Silica SiO_2 (mg/ℓ)	Sodium Na (mg/ℓ)	Potassium K (mg/ℓ)	Calcium Ca (mg/ℓ)	Magnesium Mg (mg/ℓ)	Iron Fe (Dissolved) (mg/ℓ)	Manganese Mn (Dissolved) (mg/ℓ)
Temp. (°C)	1.00														
pH	0.16	1.00													
Ec (µS/cm)	-0.29	-0.25	1.00												
Sal (%)	-0.28	-0.13	0.81	1.00											
Bicarbonate Alkalinity $CaCO_3$ (mg/ℓ)	-0.06	0.05	-0.03	-0.01	1.00										
Chlorine Cl (mg/ℓ)	-0.35	0.09	0.33	0.97	0.06	1.00									
Sulphate SO_4 (mg/ℓ)	-0.04	0.03	0.20	0.63	0.12	0.72	1.00								
Fluoride F (mg/ℓ)	-0.05	0.10	0.15	0.09	0.58	-0.09	-0.04	1.00							
Silica SiO_2 (mg/ℓ)	0.49	0.19	-0.17	0.00	-0.10	-0.27	0.05	0.33	1.00						
Sodium Na (mg/ℓ)	-0.30	0.12	0.35	0.95	0.10	0.98	0.79	-0.05	-0.19	1.00					
Potassium K (mg/ℓ)	0.11	0.11	0.32	0.65	0.02	0.35	0.55	-0.07	0.18	0.40	1.00				
Calcium Ca (mg/ℓ)	-0.33	-0.02	0.46	0.90	0.02	0.86	0.82	-0.11	-0.18	0.87	0.59	1.00			
Magnesium Mg (mg/ℓ)	-0.23	0.17	-0.07	0.39	0.12	0.87	0.72	-0.17	-0.20	0.86	0.18	0.71	1.00		
Iron Fe (Dissolved) (mg/ℓ)	0.16	-0.15	-0.11	-0.16	-0.08	-0.10	-0.10	-0.25	-0.02	-0.13	0.13	-0.12	-0.05	1.00	
Manganese Mn (Dissolved) (mg/ℓ)	0.26	-0.17	-0.14	-0.18	-0.09	-0.06	-0.07	-0.30	0.02	-0.09	0.17	-0.11	0.01	0.71	1.00

The Pearson correlation reveals a weak correlation (r=0.00-0.49) between pH and temperature. The correlation between temperature and salinity (r=0.28) is negative. The EC and salinity show a very good positive correlation.

Salinity has a strong correlation with Cl^- (r=0.97), Na^+ (r=0.95), Ca^{2+} (r=0.90) while the correlation with K^+ and SO_4^{2-} is moderate (r=0.65 and r=0.63 respectively). The SO_4^{2-} correlates well with major ions Ca-SO_4 (r=0.82), Mg-SO_4 (r=0.72), Na-SO_4 (r=0.79), Cl-SO_4 (r=0.72) with a moderate correlation to K-SO_4 (r=0.55). Na^+, Cl^-, SO_4^{2-}, Mg^{2+} and Ca^{2+} have good correlations between each of the ions. Ca^{2+} shows very good correlation with Mg^{2+}(r=0. 71) but moderate correlation with K^+(r=0.59). Cl^- has strong correlations with Na^+(r=0.98), Mg^{2+}(r=0.87) and Ca^{2+}(r=0.86). F^- and HCO_3^- exhibit a moderate correlation (r=0.60). Silica ions have a weak correlation to temperature and carbonate (r=0.00-0.49). Fe^{2+} and Mg^{2+} have a good correlation (r=0.71).

5.2.2 Chemical properties

A Schoeller diagram (Schoeller, 1963) represents the hydrochemistry of the various geothermal waters in Figure 21. The most abundant ions in the geothermal waters sampled are Na^+ and Cl^-, while Mg^{2+}, Ca^{2+}, and SO_4^{2-} are the least abundant. Most geothermal water ion concentration trends are similar, outliers include the geothermal waters from the Karoo Supergroup (Polile Tshisa (PTS), Limpopo Mobile Belt (Môreson (MRS)) and Waterberg Group (Loubad (LBD)).

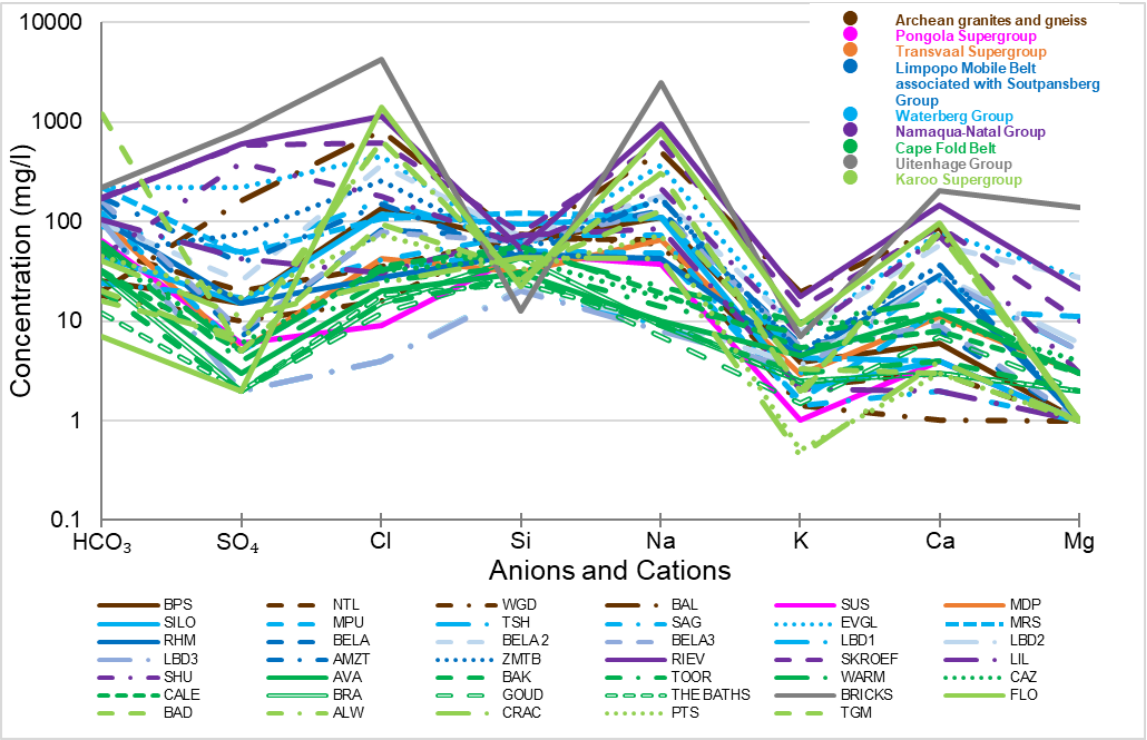

Figure 21: Schoeller diagram showing the trend of the anions and cation analyses of the geothermal water sites sampled. The analyses are colour coded per geological domain (Schoeller, 1963).

BRICKS from the Uitenhage Group exhibits the highest concentration of , Ca^{2+}, Mg^{2+}, Na^{+}, K^{+} and Cl from all the geothermal waters sampled. In Figure 22 the total amounts of cations display a good correlation for geothermal waters from the Karoo Supergroup. As the chlorine concentration increases, the total amount of cations increases. Hence, chlorine is a major anion in the geothermal waters sampled.

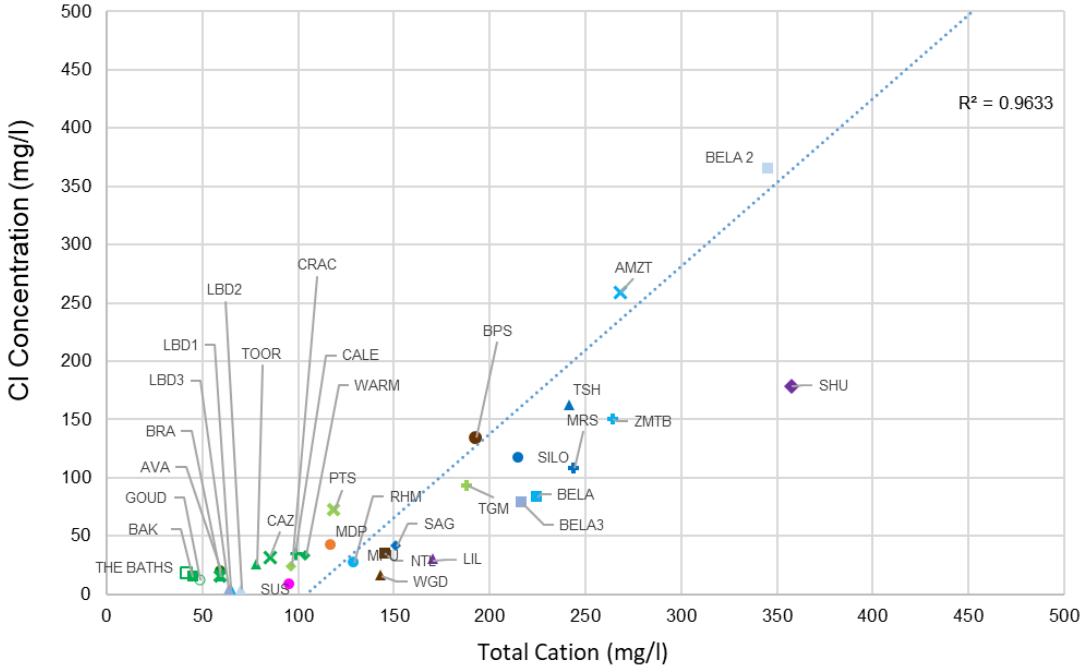

a)

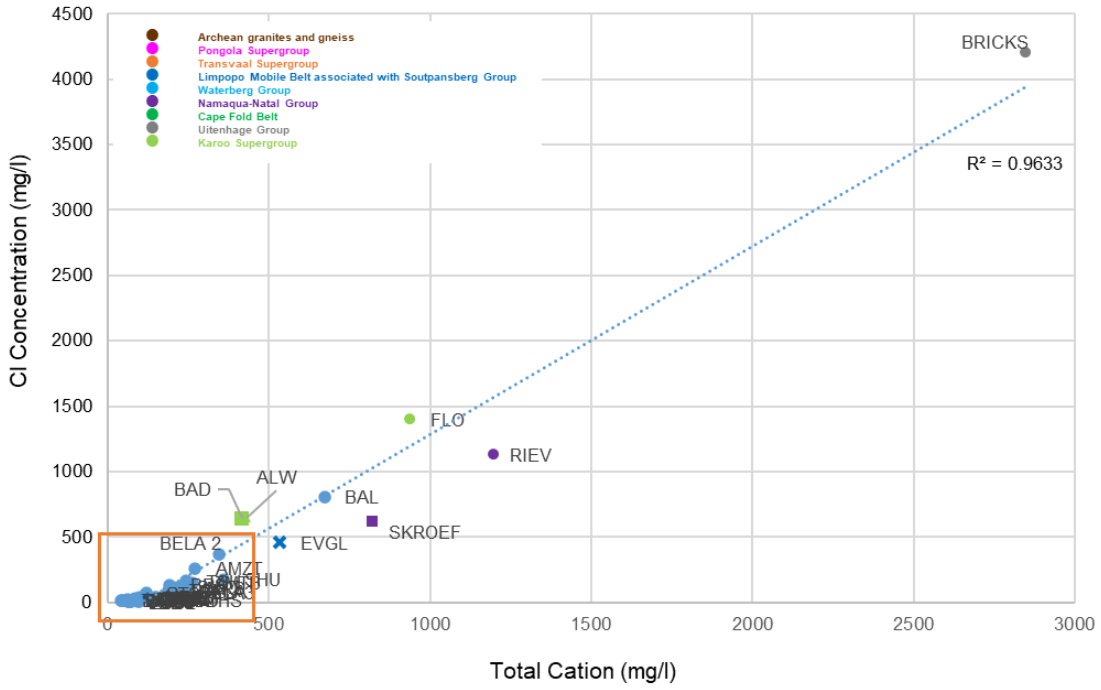

b)

Figure 22: Scatter plot showing the relationship of chlorine concentration to the total ion concentration in the 41 geothermal water sites of South Africa . The top plot (a) shows the zoomed area of the orange box from the bottom plot (b). The geothermal waters are colour coded per geological domain.

Figure 23 illustrates the water types of the 41 geothermal waters sampled in South Africa using a Piper trilinear diagram (Piper, 1944).

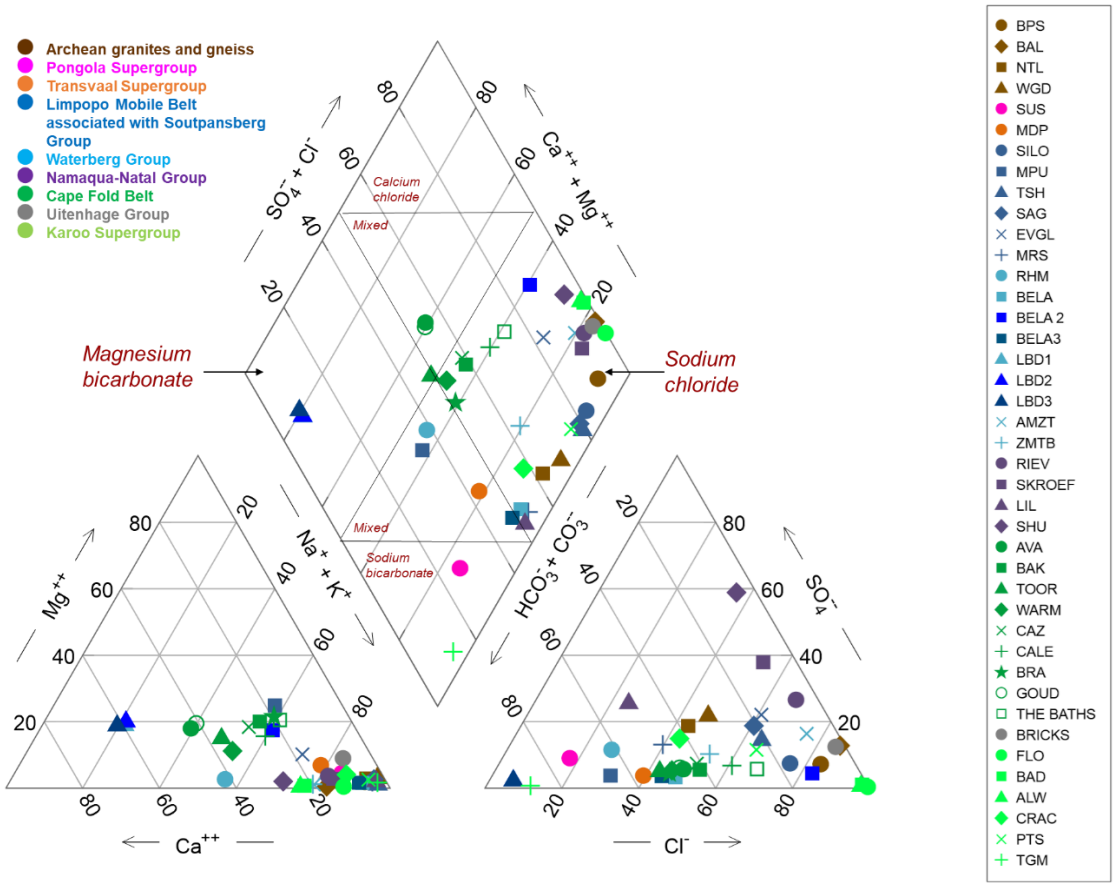

Figure 23: Piper diagram of the sampled geothermal waters in South Africa showing the cation and anion concentrations based on hydrochemical analyses (Piper, 1944; Bethke et al., 2022). The geothermal waters are colour coded per geological domain.

The main water types are Na-Cl, Na-HCO_3, Mg-HCO_3 and mixed waters. Most of the geothermal waters are characterized as Na-Cl-type water that occurs in most geological settings in South Africa (Figure 23). The geothermal waters that are dominated by Na-Cl are associated with the Archean granites and gneisses (Badplaas (BPS), Natal (NTL), Wagendrift (WGD) and Baleni (BAL)), Soutpansberg Group associated with the Limpopo Mobile Belt (Siloam (SILO), Tshipise (TSH), Sagole (SAG), Evangelina (EVGL) and Môreson (MRS)), Waterberg Group (Warmbaths (BELA2, BELA3), Zimthabi (ZMTB) and Amanzintaba (AMZT)), Namaqua-Natal Province (Riemvasmaak (RIEV), Skroef se Bad (SKROEF) and Shu Shu (SHU)), Cape Fold Belt (Baden Club (BAK), Warmwaterberg (WARM), Caledon (CALE), Calitzdorp (CAZ), Brandvlei (BRA) and THE BATHS)), Uitenhage Group (BRICKS) and Karoo Supergroup (Florisbad (FLO), Badsfontein (BAD), Aliwal (ALW), Cradock (CRAC) and Polile Tshisa (PTS)).

The geothermal waters sampled in the current study, that are characterised as Na-HCO_3-type water (Figure 23) are associated with the Pongola Supergroup (Sulphur Springs (SUS)) and Karoo Supergroup (Thangami TGM). Mg-HCO_3-type (Figure 23) are from the Waterberg Group (Loubad (LBD, LBD2 and LBD3)) and Cape Fold Belt (Toorwater (TOOR)). The geothermal waters sampled in this study that are characterised as mixed type (Figure 23) are associated with Transvaal Supergroup (Machadodorp (MDP)), Soutpansberg Group associated with the Limpopo Mobile Belt (Mphephu (MPU)), Waterberg Group (Rhemardo (RHM) and Warmbaths (BELA)), Namaqua-Natal Province (Lilani (LIL)) and Cape Fold Belt (Avalon (AVA) and Goudini (GOUD)).

To understand the ion exchange process in the geothermal waters, a plot of Ca+Mg vs SO_4+HCO_3 displays the distribution of geothermal waters between carbonate and silicate weathering. The carbonate weathering field occurs above the 1:1 equiline and silicate weathering below the 1:1 equiline in Figure 24. Most of the geothermal waters plot below the 1:1 equiline in the silicate weathering field.

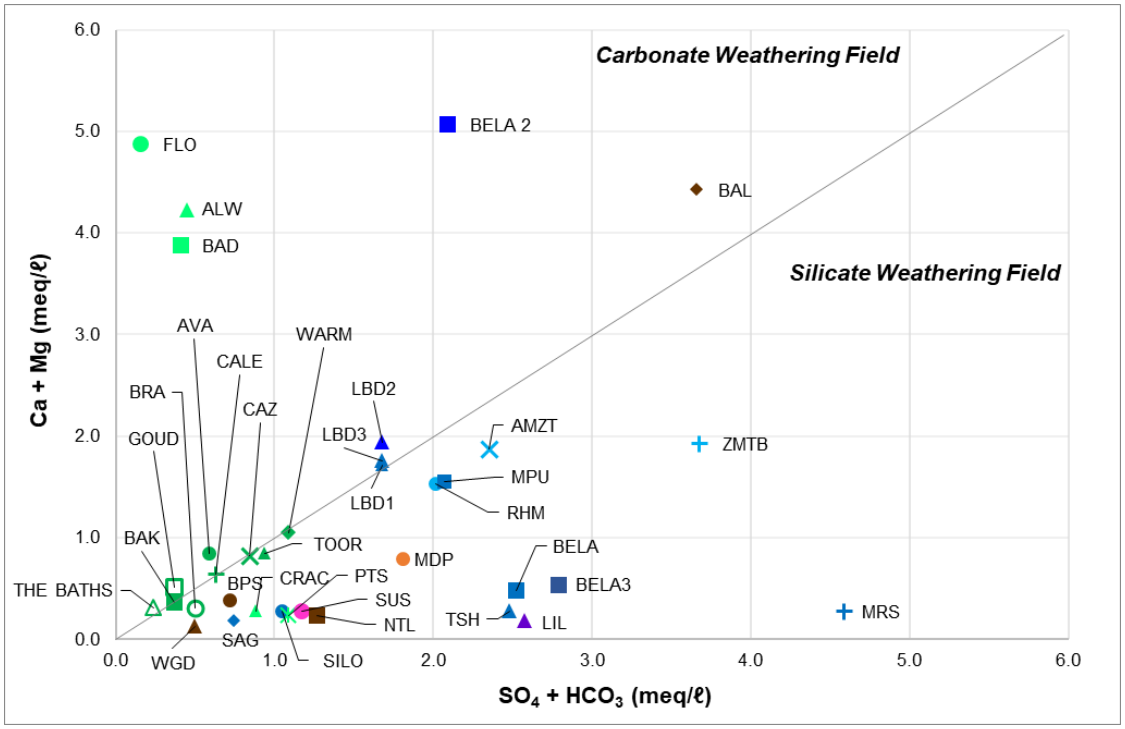

a)

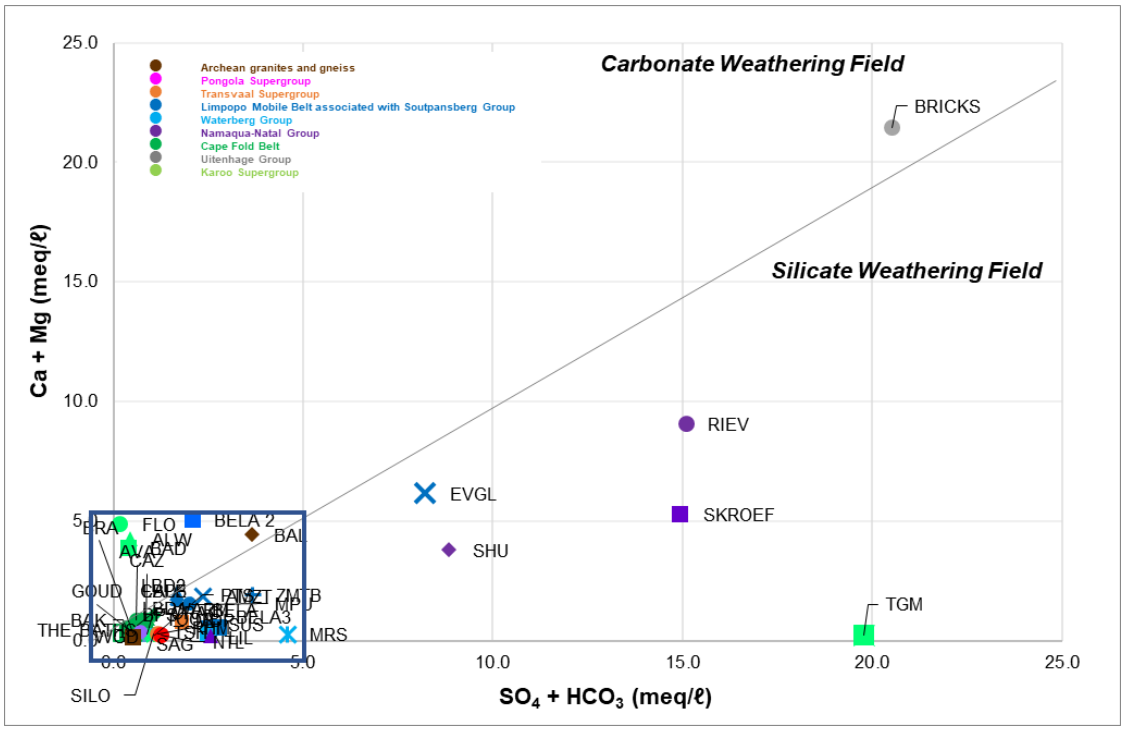

b)

Figure 24: Bivariate scatter plot displaying the relationship Ca+Mg and SO_4+HCO_3 in the sampled geothermal waters. The top plot (a) shows the zoomed area of the blue box from the bottom plot (b). The silicate and carbonate weathering are delineated by an equiline plotted that has a ratio of 1:1 to the ions. The geothermal waters are colour coded per geological domain.

Carbonate weathering taking place in the geothermal waters are associated with the Archean granites and gneisses (Baleni (BAL), Waterberg Group (Warmbaths (BELA2) and Loubad (LBD1,2,3), Cape Fold Belt (Avalon (AVA), THE BATHS and Goudini (GOUD), Uitenhage Group (BRICKS) and Karoo Supergroup ((Florisbad (FLO), Badsfontein (BAD) and Aliwal (ALW).

Silicate weathering taking place in the geothermal waters are associated with Archean granites and gneisses (Badplaas (BPS), Natal (NTL) and Wagendrift (WGD), Transvaal Supergroup (Machadodorp (MDP), Pongola Supergroup (Sulphur Springs (SUS), Soutpansberg Group associated with the Limpopo Mobile (Mphephu (MPU), Siloam (SILO), Tshipise (TSH), Sagole (SAG), Evangelina (EVGL) and Môreson (MRS), Waterberg Group (Rhemardo (RHM), Warmbaths (BELA1, BELA3), Amanzintaba (AMZT) and Zimthabi (ZMTB), Namaqua-Natal Province (Riemvasmaak (RIEV), Skroef se Bad (SKROEF), Lilani (LIL) and Shu Shu (SHU), Cape Fold Belt (Baden Club (BAK), Toorwater (TOOR), Warmwaterberg (WARM), Calitzdorp (CAZ), Caledon (CALE) and Brandvlei (BRA) and Karoo Supergroup (Cradock (CRAC), Polile Tshisa (PTS) and Thangami (TGM)).

To understand the ion exchange process in the geothermal waters, a plot of Ca+Mg vs Na+K (Figure 25) illustrates the distribution of geothermal waters between carbonate and silicate weathering. Figure 25 displays that most of the geothermal waters fall below the 1:1 equiline in the silicate weathering field.

a)

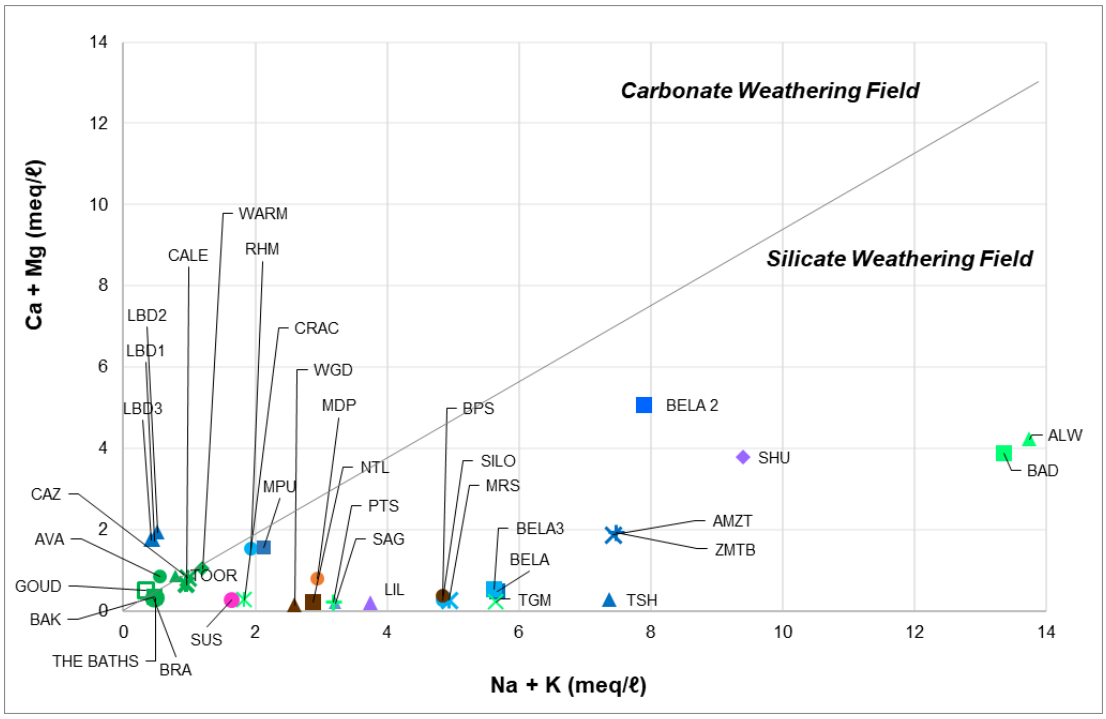

b)

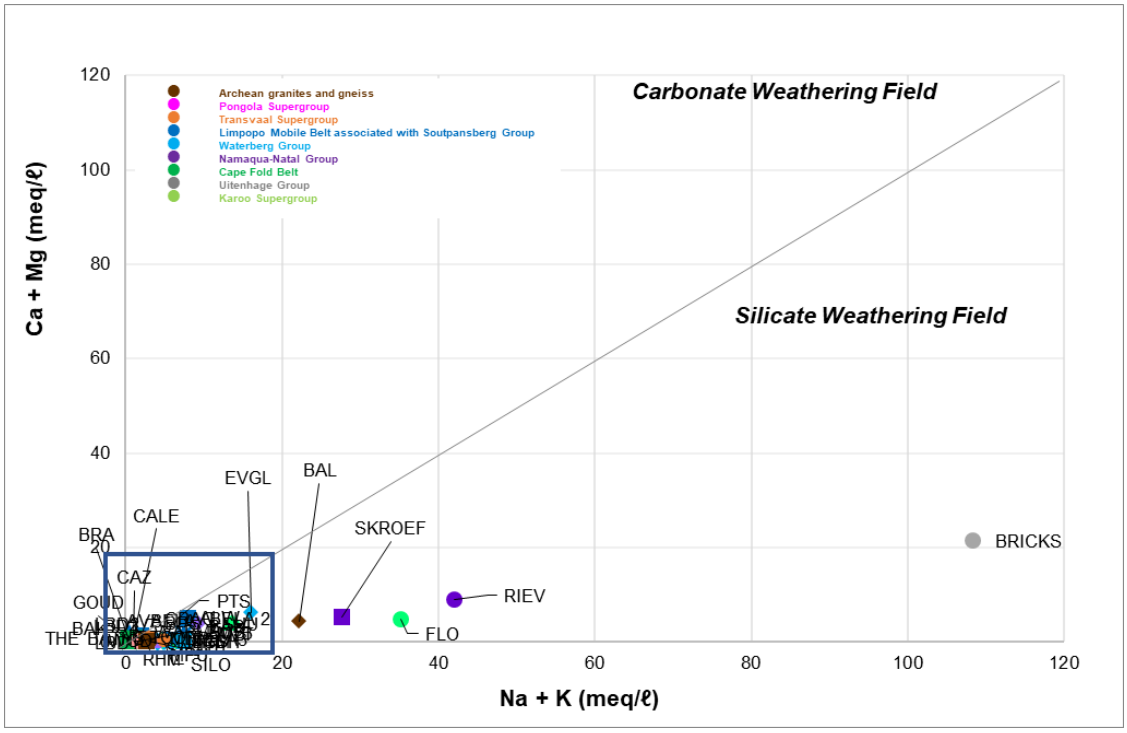

Figure 25: Bivariate scatter plot displaying the relationship Ca+Mg and Na+K (meq/l) in the sampled geothermal waters. The top plot (a) shows the zoomed area of the blue box from the bottom plot (b). The silicate and carbonate weathering fields are delineated by a line that has a ratio of 1:1 to the ions plotted. The geothermal waters are colour coded per geological domain.

Carbonate weathering occurring in the geothermal waters sampled are associated with Waterberg Group (Loubad (LBD)) and Cape Fold Belt (Avalon (AVA)). The remainder of the geothermal waters sampled exhibit silicate weathering.

In an endeavour to group the geothermal waters, a binary plot (Figure 26) with percentage of Na^+, K^+, Ca^{2+} and Mg^{2+} shows distinct groups of geothermal waters (Baioumy et al., 2015). The geothermal waters that are closely associated with the crustal signature (orange circle) or with seawater signature (blue circle). Geothermal waters that are partially or fully equilibrated plot close to the equilibration line.

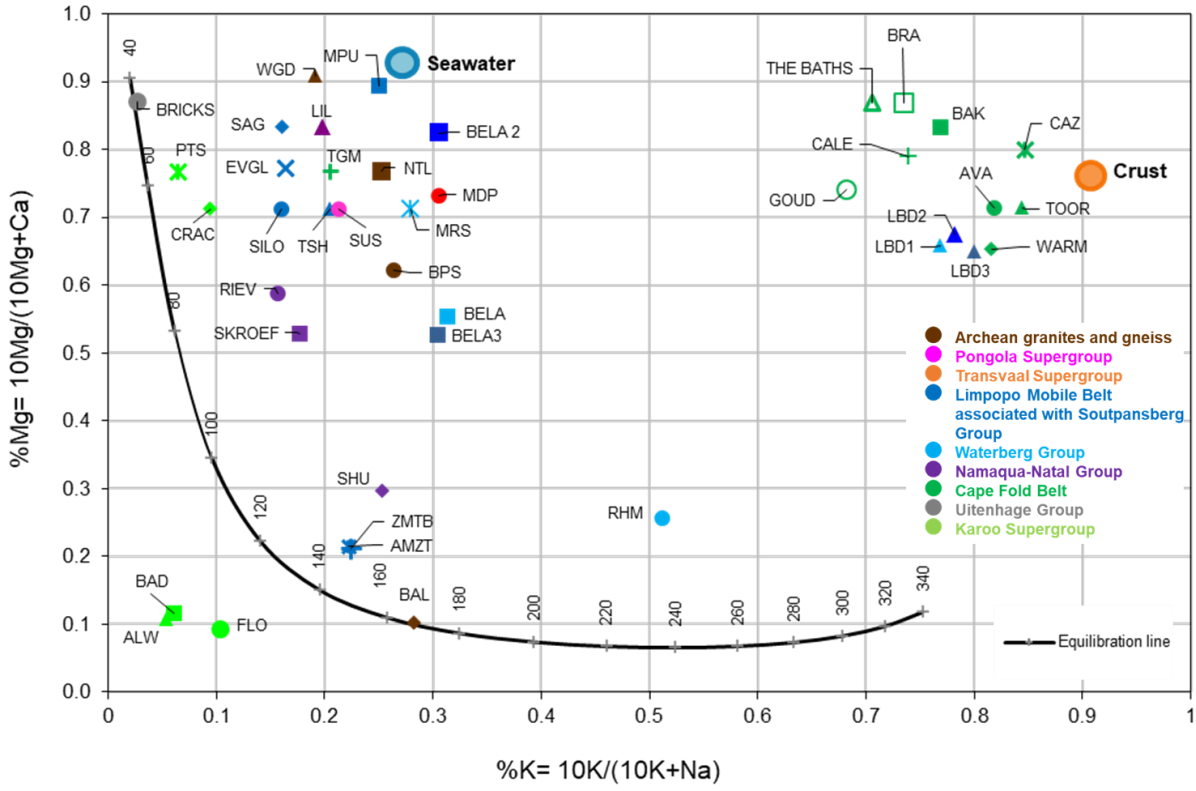

Figure 26: 10Mg/(Mg+Ca) versus 10K/(10K+Na) binary plot (Baioumy et al., 2015), of geothermal waters that were sampled for this study. The black line displays the equilibration line at various temperatures. The geothermal waters are colour coded per geological domain.

In the Karoo Supergroup geothermal waters (Florisbad (FLO), Badsfontein (BAD) and Aliwal (ALW) exhibit equilibrium between the host rock and geothermal water. The geothermal water associated with Archean granites and gneisses (Baleni (BAL)) and Uitenhage Group (BRICKS)) plots directly on the equilibrium line of ~169°C and ~44°C respectively. The geothermal waters associated with Cape Fold Belt (Avalon (AVA), Baden Club (BAK), Toorwater (TOOR), Warmwaterberg (WARM), Calitzdorp (CAZ),

Caledon (CALE) and Brandvlei (BRA), THE BATHS and Goudini (GOUD) have an affinity with the crustal signature exhibiting ratios of 0.9% K and 0.8% Mg on the binary plot.

Geothermal waters that plot closer to the seawater signature (0.3% K and 0.9% Mg) are associated with the Archean granites and gneisses (Badplaas (BPS), Natal (NTL) and Wagendrift (WGD)), Transvaal Supergroup (Machadodorp (MDP)), Pongola Supergroup (Sulphur Spring (SUS) and the Soutpansberg Group associated with the Limpopo Mobile Belt (Mphephu (MPU), Siloam (SILO), Tshipise (TSH), Sagole (SAG) and Evangelina (EVGL)), Waterberg Group (Warmbaths (BELA1,2,3), Namaqua-Natal Province (Riemvasmaak (RIEV), Skroef se Bad (SKROEF) and Lilani (LIL) and Karoo Supergroup (Thangami (TGM)). Some of the geothermal waters plot closer to the equilibrium line (no ion exchange) such as the geothermal waters associated with the Waterberg Group (Rhemardo (RHM), Amanzintaba (AMZT) and Zimthabi (ZMTB)), Namaqua-Natal Province (Shu Shu (SHU)) and Karoo Supergroup (Cradock (CRAC) and Polile Tshisa (PTS)). To further elaborate the grouping and enhance the understanding of the geothermal waters of South Africa a ternary diagram with Na^+, K^+, and Mg^{2+} illustrates half of the geothermal waters plot in the immature field (Figure 27) (Giggenbach, 1988 a, b).

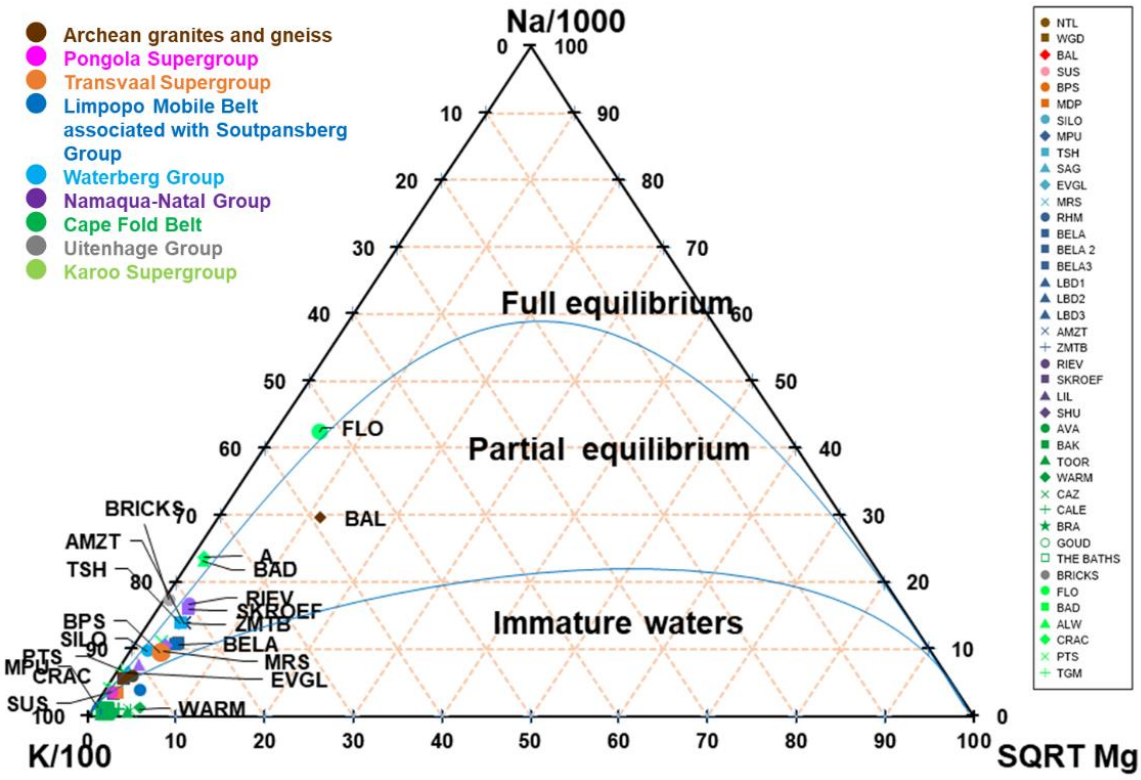

Figure 27: Ternary diagram of Na/1000, K/100 and square root of Mg ion analyses. The geothermal water ratios are plotted in the immature water field, partial equilibrium and full equilibrium fields as delineated. The geothermal waters are colour coded per geological domain.

The Karoo Supergroup geothermal waters (Florisbad (FLO), Badsfontein (BAD) and Aliwal (ALW)) exhibit equilibrium between the host rock and the geothermal waters (Figure 26 and Figure 27). The geothermal waters associated with Cape Fold Belt (Avalon (AVA), Baden Club (BAK), Toorwater (TOOR), Warmwaterberg (WARM), Calitzdorp (CAZ), Caledon (CALE) and Brandvlei (BRA), THE BATHS and Goudini (GOUD) plot in the immature waters region of Figure 27. Geothermal waters that plot in the partial equilibration are from the Archean granites and gneisses Badplaas (BPS), Natal (NTL) and Wagendrift (WGD), Transvaal Supergroup (Machadodorp (MDP), Pongola Supergroup (Sulphur Springs (SUS)), Soutpansberg Group associated with Limpopo Mobile Belt (Mphephu (MPU), (Siloam (SILO), Tshipise (TSH), Sagole (SAG), Evangelina (EVGL) and Môreson (MRS)), Waterberg Group (Rhemardo (RHM), Warmbaths (BELA2), Zimthabi (ZMTB) and Amanzintaba (AMZT)), Namaqua-Natal Province (Riemvasmaak (RIEV), Skroef se Bad (SKROEF) Shu Shu (SHU) and Lilani (LIL))), and Karoo Supergroup (Cradock (CRAC) and Polile

Tshisa (PTS) and Thangami (TGM)). Figure 28 summarises the geothermal waters hydrochemistry results and their associations with major geological structures in the form of maps.

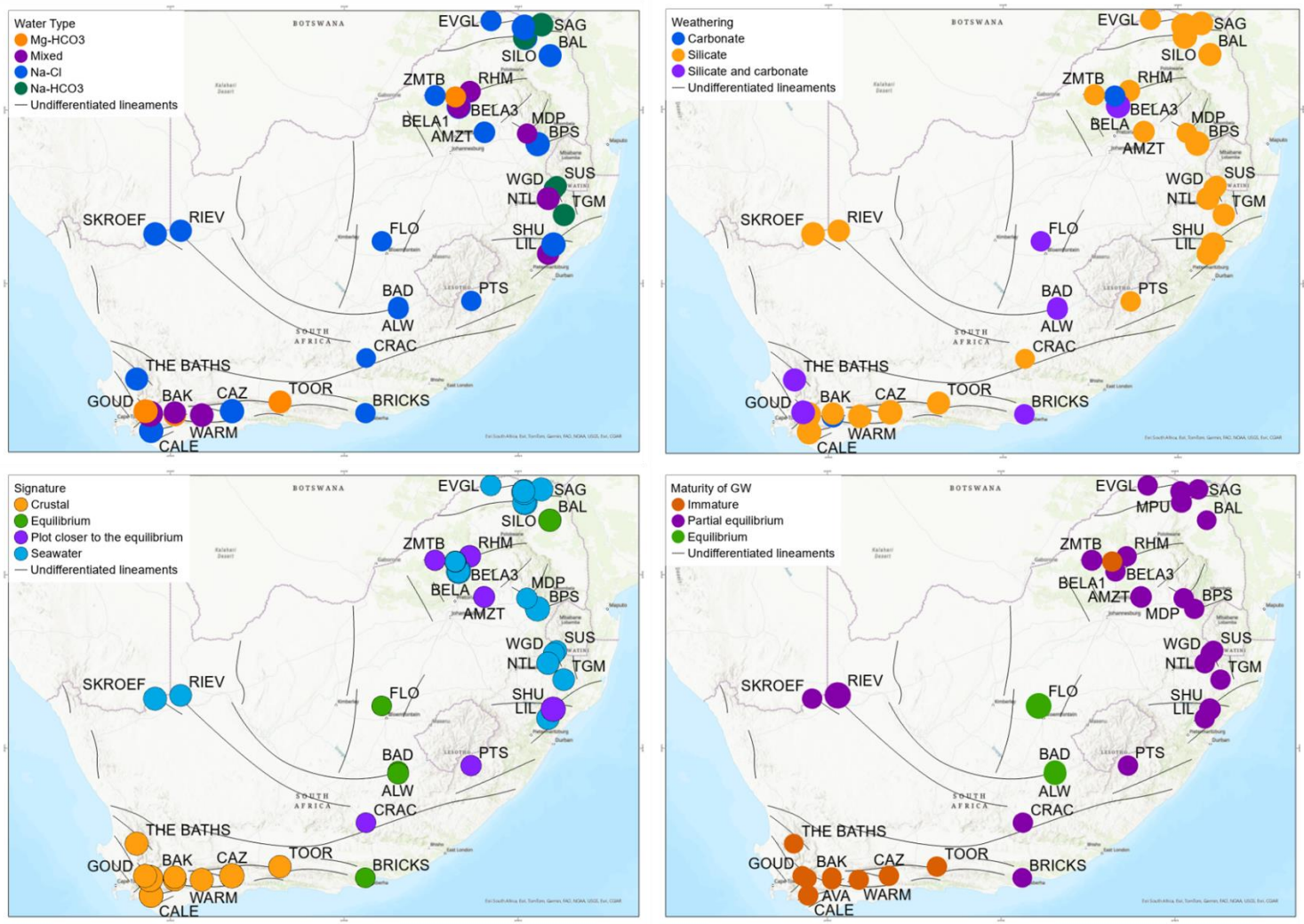

Figure 28: Maps illustrating the hydrochemistry results from the sampled geothermal waters together with the major structural features (produced in ArcGIS Pro).

5.2.3 Stable Isotopes: Oxygen 18 (δ18O) and deuterium (δD) results

To further characterise the geothermal waters, Figure 29 shows a comprehensive dataset for the stable δ18O and δD isotopic values. The data presented shows a large variation from -13.3‰ to -39.2‰ δD and from −3.46‰ to -7.28‰ δ18O. The Local Meteoric Water Line (LMWL) indicates the isotope ratio for global rainwater. A table of the tritium values is presented (Table 6) representing the age of the geothermal waters.

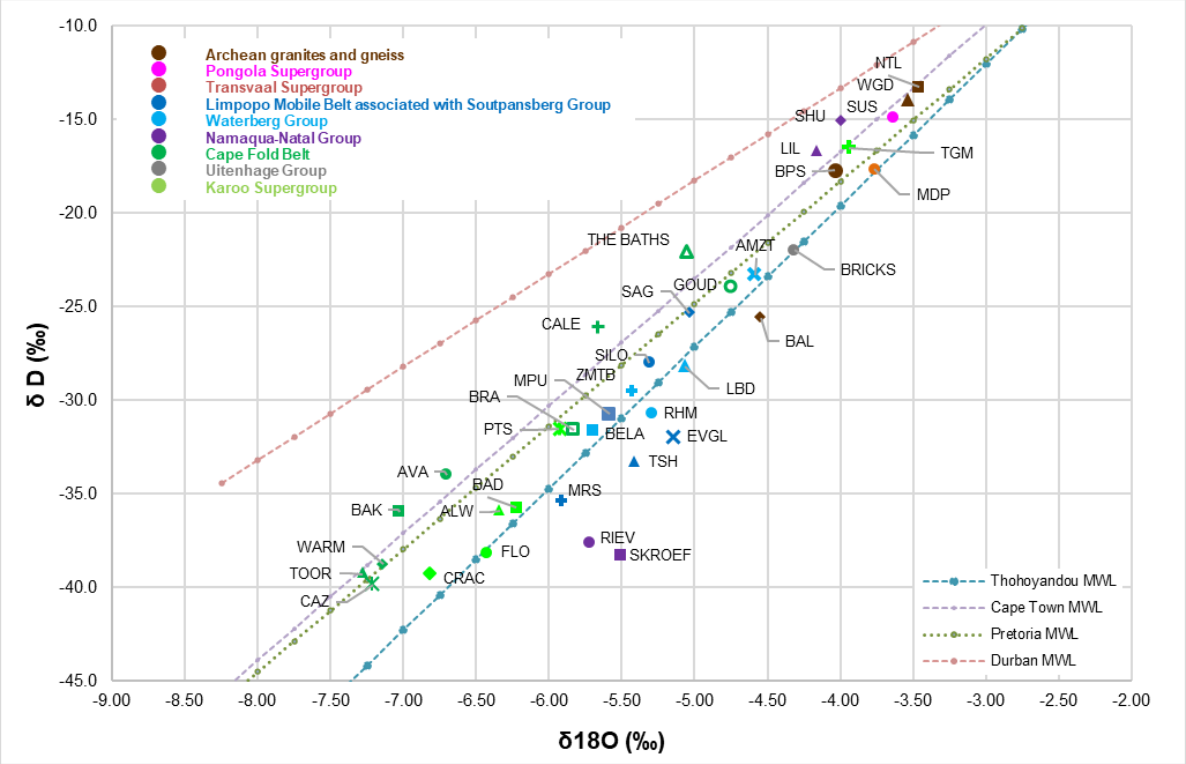

Figure 29: A plot of δD versus δ18O for the sampled geothermal waters, Local Meteoric Water Line (LMWL). The geothermal waters are colour coded per geological domain.

The results displayed are grouped according to the geological setting following the results from the hydrochemistry. In Figure 29 the geothermal waters enriched in δD and δ18O are associated with the Archean granites and gneisses (Badplaas (BPS), Natal (NTL) and Wagendrift (WGD))), Pongola Group (Sulphur Springs (SUS)), Natal Sector of the Namaqua-Natal Province (Shu Shu (SHU) and Lilani (LIL)) and Karoo Supergroup (Thangami (TGM)).

The geothermal waters of the Natal Sector (Shu Shu (SHU) and Lilani (LIL))from the Namaqua-Natal Province exhibit a negative shift from the Durban Meteoric Water Line (MWL). Two geothermal waters Riemvasmaak (RIEV) and Skroef se Bad (SKROEF) that occur along the Namaqua Sector of the Namaqua-Natal Province display depleted values of δ18O and δD. Along the Cape Fold Belt the geothermal waters (Toorwater (TOOR), Warmwaterberg (WARM), Calitzdorp (CAZ)) present depleted values in δD and δ18O approximately -38 ‰ and -7 ‰ respectively.

The geothermal waters associated with the Soutpansberg Group associated with the Limpopo Mobile Belt (Mphephu (MPU), (Siloam (SILO), Tshipise (TSH), Sagole (SAG), Evangelina (EVGL) and Môreson (MRS),) and the Waterberg Group (Rhemardo (RHM), Warmbaths (BELA), Loubad (LBD) and Zimthabi (ZMTB)) ,) exhibit a cluster with medium values of δD and δ18O. Amanzintaba (AMZT) is the most enriched with -4.59 δ18O and -23.3 δD values from the Waterberg Group while Môreson (MRS) (-5.91 δ18O and -35.4 δD) from the Soutpansberg Group associated with the Limpopo Mobile Belt is most depleted.

5.2.4 Tritium (^{3}H)

Table 6 tabulates the most comprehensive set of tritium data for the geothermal waters of South Africa as this type of analyses has not been contributed to any previously published work. With an analytical error of ±0.2 TU, overall, most of the geothermal waters exhibit low (0-0.5 TU) values. Four geothermal waters exhibit >0.5 TU values namely Natal (NTL), Evangelina (EVGL), Loubad (LBD) and Cradock (CRAC).

Table 6: Tritium values for the geothermal waters of South Africa with analytical error of 0.2 tritium unit (TU).

Geological Setting	Geothermal water sites	Abbreviation	Tritium units (TU)
Archean granites and gneisses	Badplaas	BPS	0.0
	Natal	NTL	0.6
	Wagendrift	WGD	0.0
	Baleni	BAL	0.3
Pongola Supergroup	Sulphur-Spring	SUS	0.2
Transvaal Supergroup	Machadodorp	MDP	0.0
Soutpansberg Group associated with Limpopo Mobile Belt	Siloam	SILO	0.4
	Mphephu	MPU	0.0
	Tshipise	TSH	0.1
	Sagole	SAG	0.3
	Evangelina	EVGL	0.8
	Môreson	MRS	0.5
Waterberg Group	Rhemardo	RHM	0.1
	Warmbath	BELA	0.2
	Loubad	LBD	0.8
	Zimthabi	ZMTB	0.2
	Amanzintaba	AMZT	0.0
Namaqua-Natal Province	Riemvasmaak	RIEV	0.1
	Skroef Se Bad	SKROEF	0.0
	Lilani	LIL	0.0
	Shu-Shu	SHU	0.0
Cape Fold Belt	Avalon	AVA	0.1
	Baden Club	BAK	0.1
	Toorwater	TOOR	0.0
	Warmwaterberg	WARM	0.0
	Calitzdorp	CAZ	0.1
	Caledon	CALE	0.0
	Brandvlei	BRA	0.0
	Goudini	GOUD	0.2
	The Baths	THE BATHS	0.1
Uitenhage Group	Bricks	BRICKS	0.3
Karoo Supergroup	Florisbad	FLO	0.0
	Badsfontein	BAD	0.2
	Aliwal	ALW	0.0
	Cradock	CRAC	0.8
	Polile Tshisa	PTS	0.0
	Thangami	TGM	0.0

5.3 Geothermometry

The solute based equations are presented below. The relationship between quartz and chalcedony geothermometers shows an exponential increase in Figure 30 with increasing temperature.

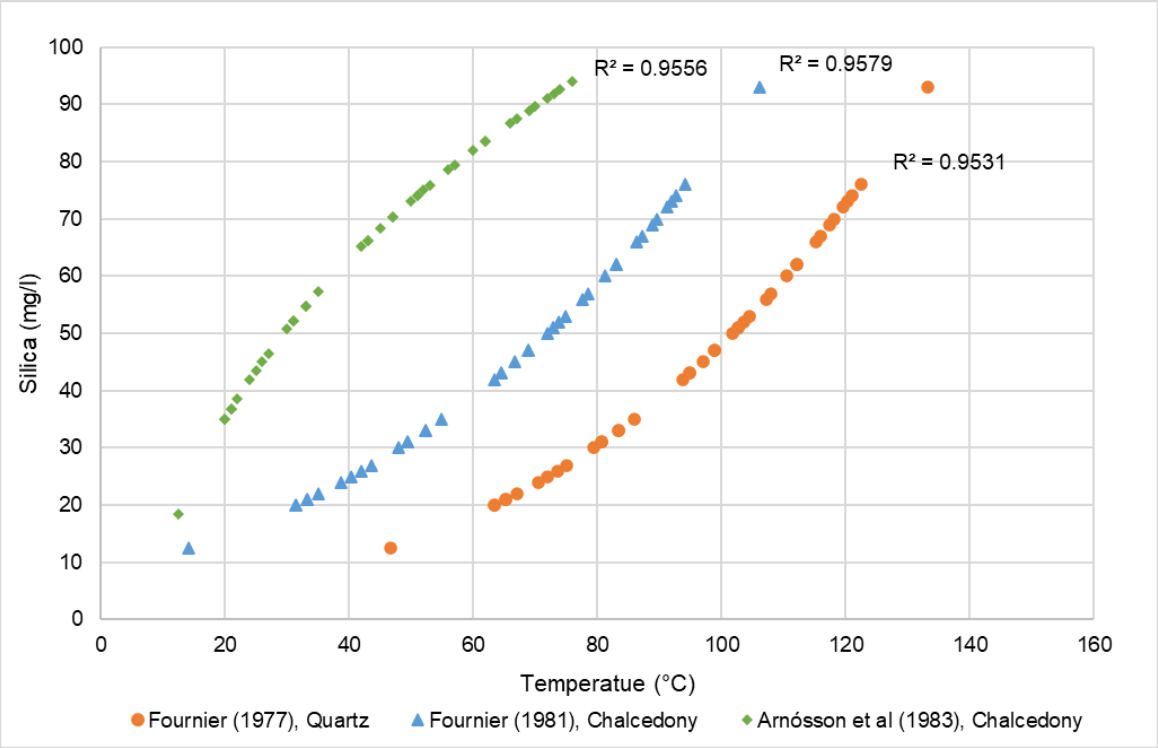

Figure 30: The equilibration graphs of quartz and chalcedony show exponential increase in silica ions (mg/l) and temperature (°C).

Geothermometry equations (see Table 3) were applied to the sampled geothermal waters, the results are tabulated in Appendix C and illustrated in Figure 31 Figure 33. Values from the silica geothermometers (Figure 31) range from -60°C BRICKS associated with Uitenhage Group to 239°C Môreson (MRS) associated with the Limpopo Mobile Belt. The hottest quartz geothermometry of 148°C is associated with the Limpopo Mobile Belt (Môreson (MRS)). The chalcedony and amorphous silica geothermometry results are lower than measured surface temperature (discussed further in Section 6.5). The quartz and quartz steam loss equations from Fournier (1977) compute similar resource temperatures and are higher than the measured surface temperatures of the geothermal waters. The highest silica based computed temperatures are displayed from Arnórsson (1985). Generally, the calculated trends are similar for all the geothermal waters sampled.

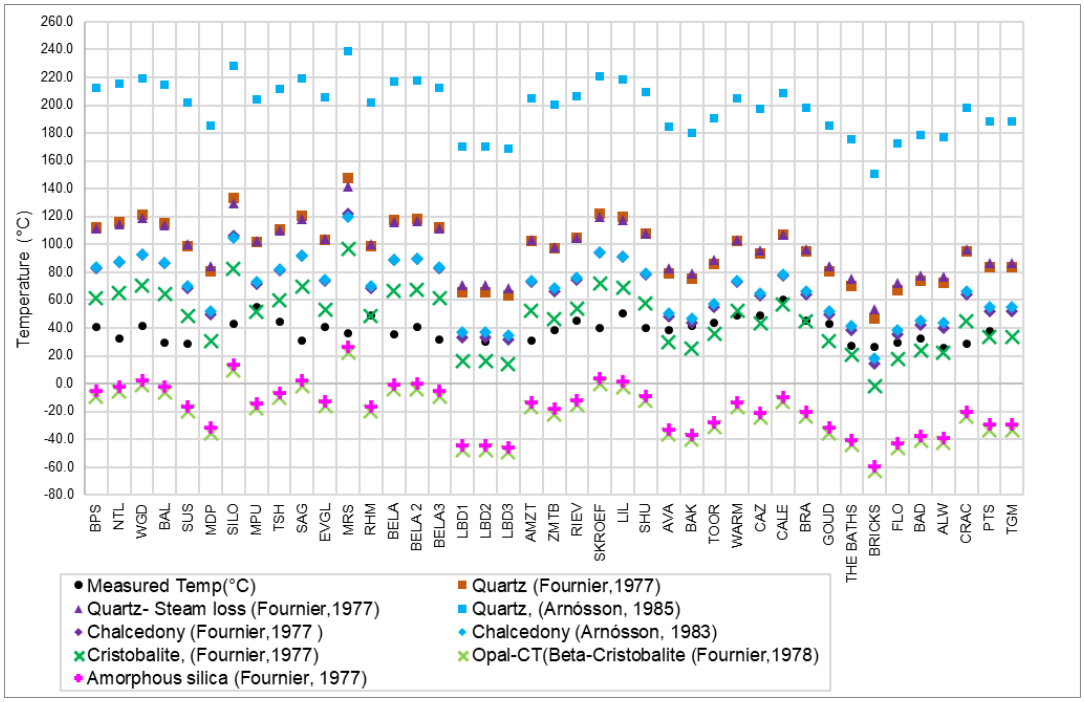

Figure 31: Computation comparison of the geothermometry (°C) representing various forms of silica.

By plotting the theoretical curves for the silica geothermometers and the sampled geothermal waters. The most suitable geothermometer is where the computed temperatures and the theoretical curves are closest together by considering the measured temperature of the geothermal waters at surface.

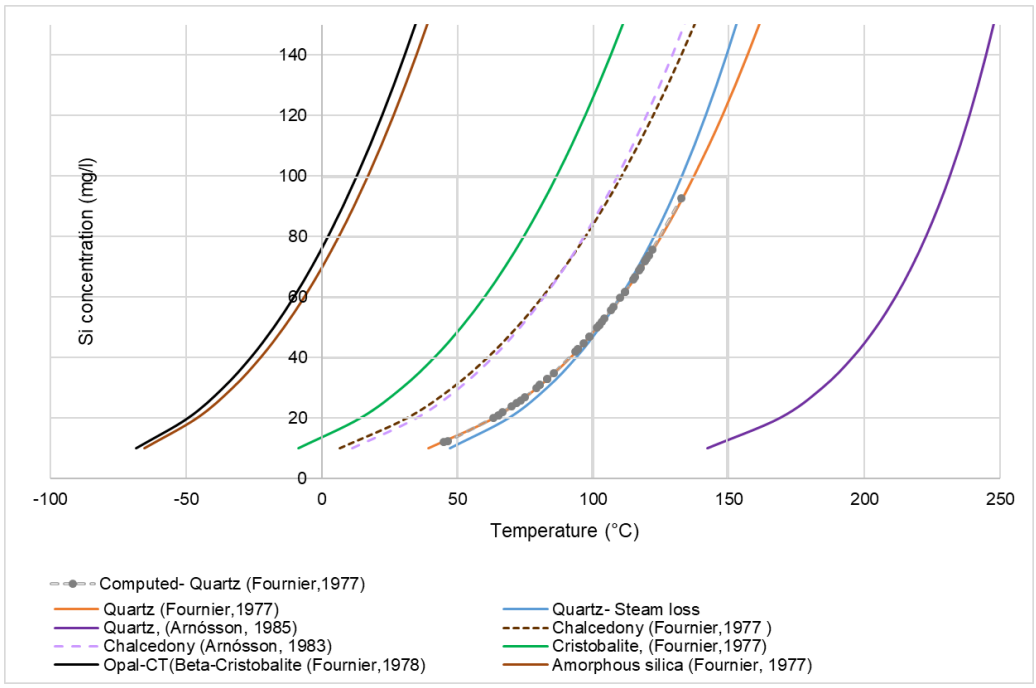

Figure 32: Theoretical curves for the silica geothermometry compared to the calculated quartz (Fournier, 1977) geothermometer of the sampled geothermal waters.

Figure 32 indicates that the quartz (Fournier, 1977) calculations lie on the same line as the theoretical line and are therefore taken as the best fit. Even though the reported range is different, experimental work shows that the silica geothermometer works best for subsurface temperatures above 150°C (Fournier, 1977).

Temperatures from the Na-K geothermometers (Figure 33) range from -32°C Polile Tshisa (PTS) to 511°C Calitzdorp (CAZ). The lower temperatures for the computed geothermometers are discussed further in Section 6.5. The Na-K geothermometer yields very hot temperatures compared to the silica and the K-Mg geothermometers. Calculating the resource temperature using the K-Mg geothermometer, Baleni (BAL) exhibits the hottest resource temperature of 113°C and Cradock (CRAC)) calculated to be the coldest geothermal water resource at 27°C.

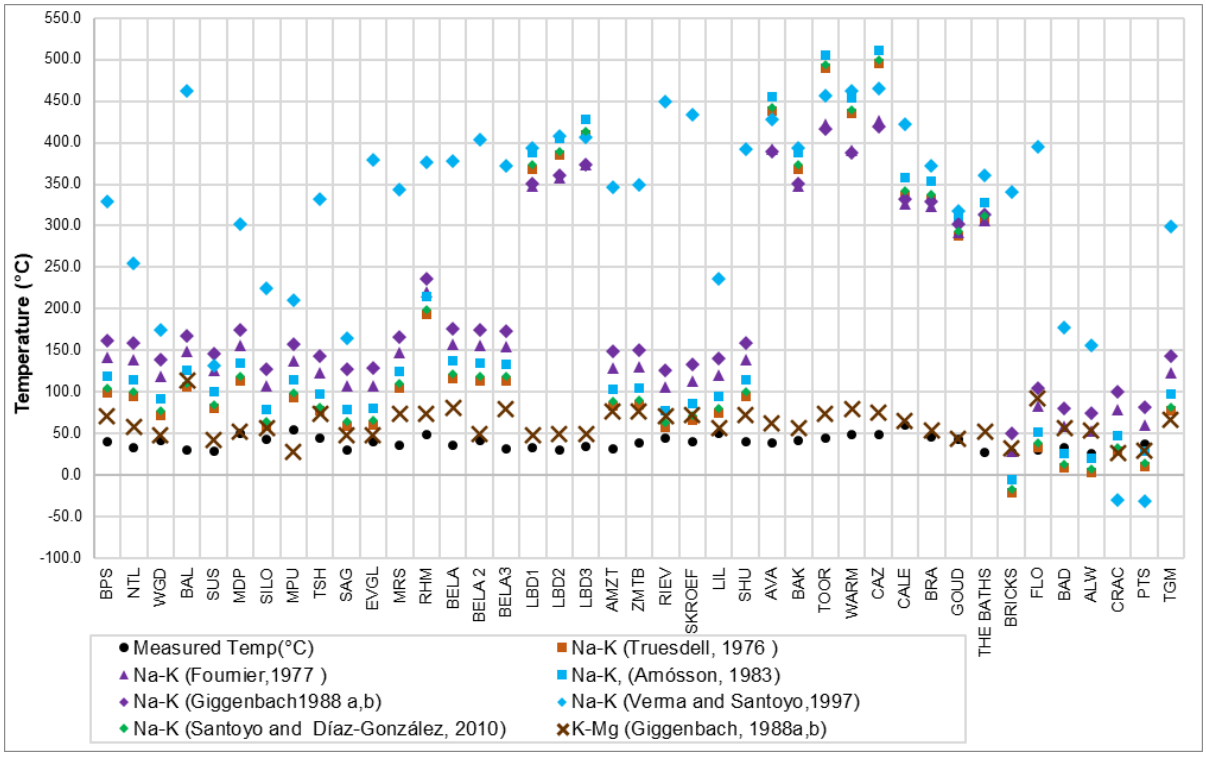

Figure 33: Computation comparison of the geothermometry (°C) utilising Na^{+}, K^{+} and Mg^{2+} concentrations.

5.4 Enthalpy

The enthalpy range is derived from the calculated temperatures of the potential geothermal resource. The calculated temperatures of the geothermal water samples vary where some are below the surface temperatures of the geothermal waters. Temperatures with similar ranges which are above surface temperatures are derived from quartz geothermometer by Fournier, (1977). The enthalpy of these temperatures is presented in Table 7. To heat the waters, the Henley Steam Table 1 (Appendix B) provided the enthalpy range from 188 to 632 kJ/kg (Henley et al., 1984).

The highest enthalpy is 624 kJ/kg from Môreson (MRS) with 148° C resource temperature located in the Soutpansberg Group associated with the Limpopo Mobile Belt and lowest is BRICKS with enthalpy of 197 kJ/kg and a resource temperature of 47°C. Medium enthalpy according to Sveinbjörnsson (2016) (Table 1) is between 419 to 852 kJ/kg, hence 20 out of 41 geothermal waters sampled exhibit enthalpy values high enough for power generation. These potential geothermal waters occur across South Africa.

Table 7: The enthalpy range (Figure 10) and calculated quartz geothermometry (°C) (Fournier, 1977).

Geological setting	Geothermal water sites	Abbreviated	Measured Temp. (°C)	Quartz geothermometry (°C) (Fournier, 1977)	Enthalpy (kJ/kg)
Archean granites and gneisses	Badplaas	BPS	49.4	112	468
	Natal	NTL	40.6	116	486
	Wagendrift	WGD	32.5	121	508
	Baleni	BAL	41.6	115	483
Pongola Supergroup	Sulphur-Spring	SUS	29.7	99	414
Transvaal Supergroup	Machadodorp	MDP	28.8	81	339
Soutpansberg Group associated with the Limpopo Mobile Belt	Siloam	SILO	50.6	133	559
	Mphephu	MPU	43.4	102	428
	Tshipise	TSH	54.9	111	466
	Sagole	SAG	44.7	120	504
	Evangelina	EVGL	30.7	104	436
	Môreson	MRS	40.4	148	624
Waterberg Group	Rhemardo	RHM	36.5	99	414
	Warmbath1	BELA	49.0	117	491
	Warmbath2	BELA 2	35.4	118	492
	Warmbath3	BELA3	40.9	112	470
	Loubad1	LBD1	32.1	65	272
	Loubad2	LBD2	32.9	65	272
	Loubad3	LBD3	30.2	63	264
	Amanzintaba	AMZT	34.2	97	406
	Zimthabi	ZMTB	31.0	103	432
Namaqua-Natal Province	Riemvasmaak	RIEV	38.4	105	444
	Skroef Se Bad	SKROEF	45.0	122	512
	Lilani	LIL	40.0	120	504
	Shu-Shu	SHU	50.5	108	453
Cape Fold Belt	Avalon	AVA	40.3	79	331
	Baden Club	BAK	38.5	75	314
	Toorwater	TOOR	41.8	86	360
	Warmwaterberg	WARM	44.0	103	432
	Calitzdorp	CAZ	49.0	94	394
	Caledon	CALE	48.8	107	449
	Brandvlei	BRA	60.5	95	398
	Goudini	GOUD	45.2	81	339
	The Baths	THE BATHS	43.0	70	293
Uitenhage Group	Bricks	BRICKS	27.0	47	197
Karoo Basin	Florisbad	FLO	26.8	67	280
	Badsfontein	BAD	29.4	74	310
	Aliwal	ALW	32.6	72	301
	Cradock	CRAC	25.4	95	398
	Polile Tshisa	PTS	29.1	83	348
	Thangami	TGM	37.5	83	348

5.5 Circulation depth estimations of geothermal waters with low to medium enthalpy range

To compute the circulation depths of the geothermal waters in the current study, Equation 18 (Section 4.5) was utilised. The variables in Equation 18 were the calculated temperatures (Table 7), the ambient temperature for each geothermal water site as sourced from The World Bank Group (2021) and the geothermal gradient from Dhansay et al. (2017) (Appendix D). The depths of the geothermal waters are presented in Figure 34 and Appendix E. Môreson (MRS) in the Limpopo Mobile Belt associated with the Soutpansberg Group is calculated to have the deepest reservoir ~2.7km with an enthalpy of 624 kJ/kg. It will take 0.91 km to reach the reservoir temperature of 63°C at BRICKS.

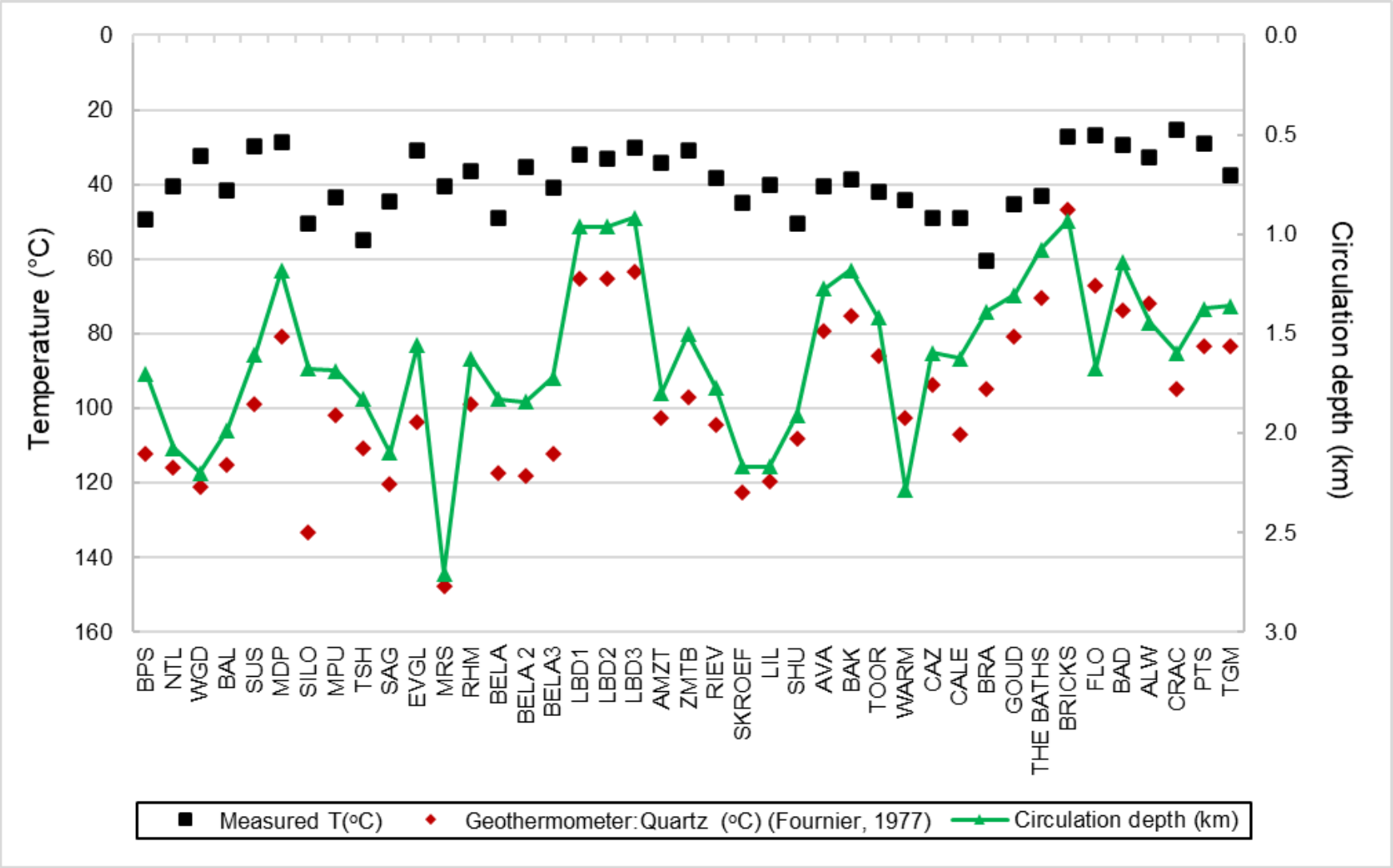

Figure 34: Circulation depth of the geothermal waters together with measured temperature of the geothermal waters at surface and quartz geothermometry temperatures (°C).

CHAPTER 6 DISCUSSION

The previous chapters described the association between productive geothermal energy, geological settings, investigation methods and tools applied while studying the geothermal waters. The results of the current investigation are also presented. In this chapter, the intention is to discuss these results obtained from the currently sampled geothermal waters. The geological settings and structural controls of the geothermal waters will be discussed (Figure 35). Thereafter the geothermal waters characteristics such as the chemistry, fluid mineral equilibria and isotopic classification will be discussed. These properties give insight into the source rock and water-rock interaction of changing conditions underground. The geothermal waters have been grouped based on their geological setting to the characteristics of the geothermal waters. Furthermore, the most suitable geothermal waters will be assessed for power generation.

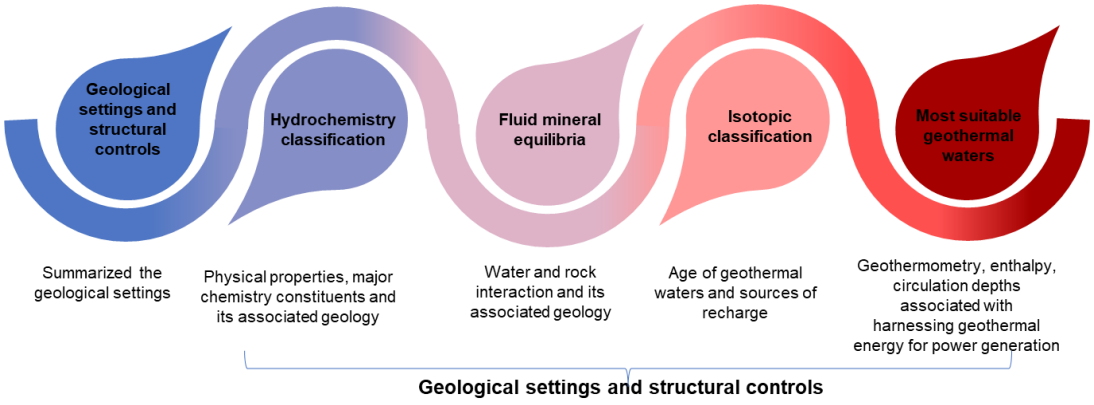

Figure 35: The current study process flow for the discussion of the results.

6.1 Geological settings

Geothermal waters in South Africa occur in various geological settings. These geological settings have common properties that have produced geothermal waters. These properties (See details in Section 2.2) include:

1) Heat source(s) capable of producing relatively high heat flow in the crust. Furthermore, in the Archean granites and gneisses which exhibit similar concentration of U=58-339ppm and Th=19.9-99ppm (Wang et al., 2020), compared to the central Kaapvaal Craton concentration of U=170-424ppm and Th=42-110ppm and may contribute to heating of geothermal waters.

(Baughman and Flowers, 2020). However, within the Waterberg Group the concentration is considerably higher of U=69-1574ppm and Th=26-1030ppm (Mtimkulu, 2009) which contribute extensively towards heating of the geothermal waters.

Other areas having lower radiogenic concentrations with lesser capability of generating geothermal waters include: Anhalt Suite (U=1-8ppm and Th=11-26ppm), the Groot Letaba Gneiss (U=<1-8ppm and Th=1-17ppm), the Limpopo Mobile Belt (U=2ppm and Th=14ppm) (Andreoli et al., 2011) and the Cape Granite Suite (U=5ppm and Th=18ppm) (García-Arias et al., 2024). Radiogenic heat from crystalline granite or basement heat is known as petrothermal heat.

A second heat source that contributes towards heating of ground water involves heat that flows from the mantle to the crust. Even though the uranium and thorium concentrations are low in the Limpopo Mobile Belt the heat source is located at a depth of 10 km, originating from the mantle (Khoza et al., 2013). Heat flows for the Limpopo Mobile Belt (as described in Section 2.2.2) is moderate at 55 mW m^{-2} while that of the Namaqua-Natal Province is 50 to 75 mW m^{-2} (Jones, 2017) yet one of the hottest geothermal waters Tshipise (TSH) with a temperature of 55°C, is located in the Limpopo Mobile Belt.

2) Thermal insulation to trap heat in the Earth's crust such as thick packages of sediments located in the Pongola Supergroup (~9100 m thick sequence) (Wilson et al., 2013), or the Waterberg Group which can be ~5 km thick in places (Dorland et al., 2006). Even a thinner package of 2.5 km thickness of the Uitenhage Trough (Makhubele and Bordy, 2021) could act as insulator for heat hosting BRICKS geothermal waters.
3) Fluid flow paths facilitate the geothermal waters ascension to surface such as the structures associated with orogenic belts that host 18 of the geothermal waters (Siloam (SILO), Mphephu (MPU), Tshipise (TSH), Sagole (SAG), Evangelina (EVG), Môreson (MRS), Riemvasmaak (RIEV), Skroef se Bad (SKROEF), Shu Shu (SHU), Lilani (LIL), Avalon (AVA), Baden Club (BAK), Toorwater (TOOR), Warmwaterberg (WARM), Calitzdorp (CAZ), Caledon (CALE), Brandvlei (BRA), Goudini (GOUD) and The Baths (THE BATHS)) (Figure 19). In addition, other geothermal waters such as Florisbad (FLO) is located on the Trompsberg Lineament, Badsfontein (BAD) located close to the

Doringberg Fault and Aliwal (ALW) is close to the Lilani Matingulu Fault (Figure 19). All three of these geothermal waters are in the Karoo Supergroup.

In sedimentary basins the permeability is influenced by either lithology (grain size and mineralogy) of the sediments or biofacies (fossil content) while faults and fractures are secondary mechanism in sedimentary basins for geothermal waters to ascend to the surface.

Consequently, the properties suitable for geothermal waters to occur can be summarised in Figure 36 representing three main geological settings: 1) basement/crystalline rock, 2) orogenic belts and associated structures and 3) intracratonic basins characterised by thick sedimentary packages that act as insulation of heat.

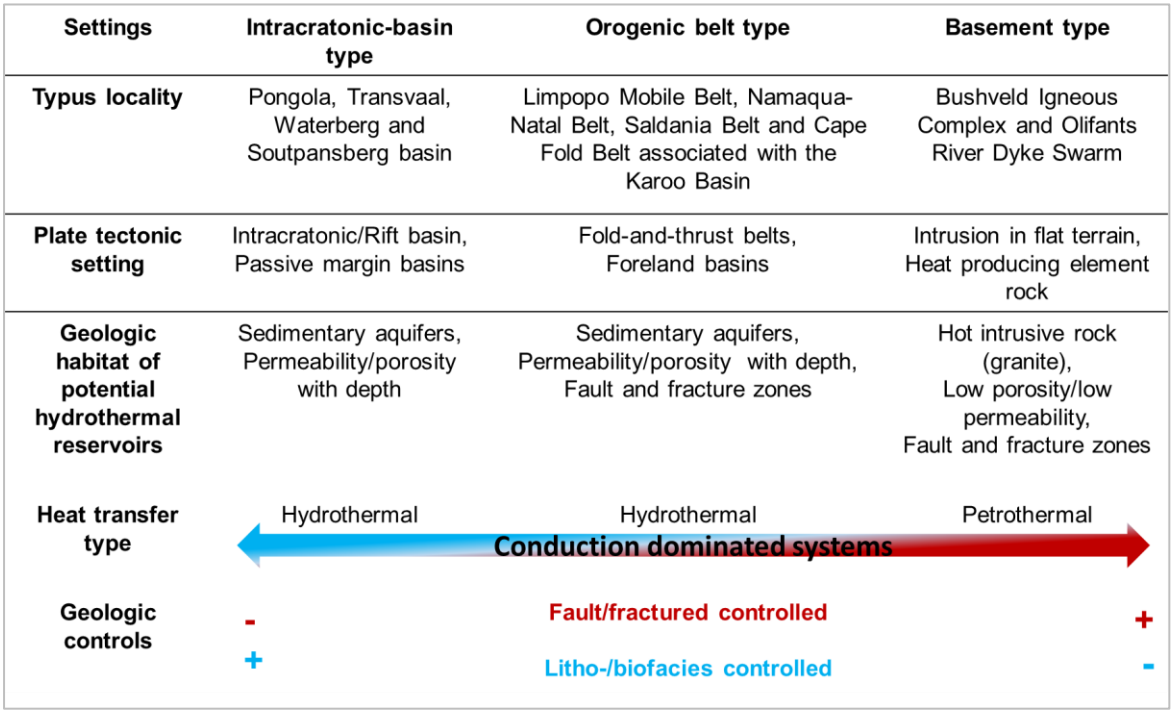

Figure 36: The various types of geological settings and heat transfer mechanism of the geothermal waters in South Africa (modified from Moeck, 2014).

The categorised geological settings highlight the controlling influences the South African geothermal waters. This could assist with exploration that is site specific for development of geothermal applications. By arranging the geological settings and their dominant geologic controls on the geothermal waters in South Africa existing geothermal developments can be compared with global developments (Moeck, 2014).

6.2 Hydrochemistry classification

6.2.1 Physical properties

This study presents updated analyses for forty-one geothermal waters the results of which are comparable to previous work (Chapter 3) conducted on the geothermal waters of South Africa.

The electrical conductivity of the geothermal waters is contributed to by all ions present in the geothermal waters (Stober and Bucher, 2013). Electrical conductivity results show that temperature does not correlate with a particular geological setting. However the geothermal waters that measured >1000 µS/cm and temperatures higher than 32°C are associated with the Waterberg Group (Zimthabi (ZMTB) and Amanzintaba (AMZT), Namaqua-Natal Province (Riemvasmaak (RIEV), Skroef se Bad (SKROEF) and Shu Shu (SHU)) and Cape Fold Belt (Warmwaterberg (WARM), thus having a positive correlation with temperature, implying the contribution of a Cl-dominated deep reservoir (JICA, 2014) (Figure 37).

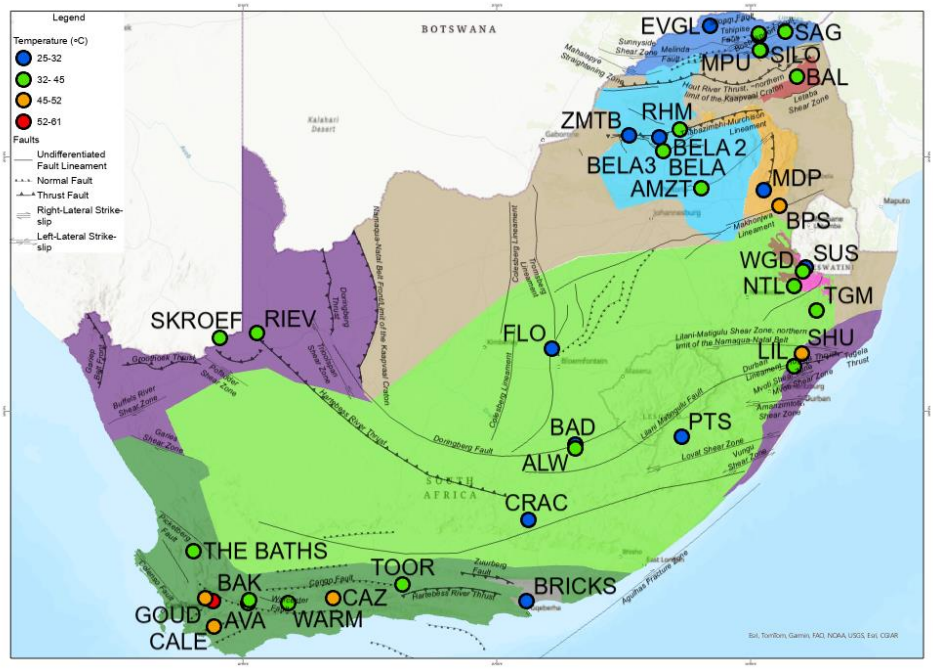

GeoWs Site	Abbreviation
Badplaas	BPS
Natal	NTL
Wagendrift	WGD
Baleni	BAL
Sulphur-Spring	SUS
Machadadorp	MDP
Siloam	SILO
Mphephu	MPU
Tshipise	TSH
Sagole	SAG
Evangelina	EVGL
Môreson	MRS
Rhemardo	RHM
Warmbath1	BELA
Warmbath2	BELA 2
Warmbath3	BELA3
Loubad1	LBD1
Loubad2	LBD2
Loubad3	LBD3
Amanzintaba	AMZT
Zimthabi	ZMTB
Riemvasmaak	RIEV
Skroef Se Bad	SKROEF
Lilani	LIL
Shu-Shu	SHU
Avalon Spring	AVA
Baden Club	BAK
Toorwater	TOOR
Warmwaterberg	WARM
Calitzdorp	CAZ
Caledon	CALE
Brandvlei	BRA
Goudini	GOUD
The Baths	THE BATHS
Bricks	BRICKS
Florisbad	FLO
Badsfontein	BAD
Aliwal	ALW
Cradock	CRAC
Polile Tshisa	PTS
Thangami	TGM

Figure 37: Geothermal water sites sampled including the geology and structure of the areas.

The geothermal waters that associated with the Karoo Supergroup (Florisbad (FLO), Badsfontein (BAD) and Aliwal (ALW)) display higher EC values (2000 – 4000 µS/cm) with lower temperatures (26-35°C) (Figure 20) are characteristic of HCO_3^- dominated waters. Furthermore, temperature generally having an inverse correlation with HCO_3^- implying that the geothermal waters are being heated conductively, meaning that there could be heat sources at depth (JICA, 2014).

Of interest is the electrical conductivity at Baleni (BAL) that measured 2 µS/cm which is low however as indicated by Murray et al. (2015) the groundwater in the Baleni area can range between 0 to 70 µS/cm, it could therefore be a possibility. In addition, estimating the electrical conductivity of the geothermal water by relative contribution of ions that could contribute to the electrical conductivity is dependent on the ionic molar conductivity. Some ions have major contributions to might have not been measured such as H^+, NH_4^+, Al^{3+} and organics (McCleskey et al., 2012). This can result in the electrical conductivity being underestimated.

According to Hubert and Wolkersdorfer (2015) to estimate the electrical conductivity from the ions a conversion factor is required. However, there are ionic variations in space and time, and it would be necessary to calculate a conversion factor for each site. Also, the conversion factor is taken at 25°C and hotter waters are not considered (Hubert and Wolkersdorfer, 2015).

The Pearson correlation coefficient displays the influence of physical properties on each other and on the ion content of the geothermal waters sampled. In Table 5 the correlation between temperature and both salinity and electrical conductivity (EC) are negative. This therefore suggest that temperature d of the geothermal water does not contribute to the salinity and EC of the geothermal waters. This is supported by the same inverse relationship of the EC and temperature in Figure 20, but the geothermal water associated with the Waterberg Group (Zimthabi (ZMTB) and Amanzintaba (AMZT)), Namaqua-Natal Province (Riemvasmaak (RIEV), Skroef se bad (SKROEF) and Shu Shu (SHU)) and Cape Fold Belt (Warmwaterberg (WARM)), have a positive correlation with temperature implying the contribution of a Cl-dominated deep reservoir (JICA, 2014).

The SO_4^{2-} correlates well with major ions Ca-SO_4 (r=0.82), Mg-SO_4 (r=0.72), Na-SO_4 (r=0.79), Cl-SO_4 (r=0.72) but correlates only moderately with K-SO_4 (r=0.55). This could account for many of the geothermal waters having a distinct sulphur odour. The dissolved sulphate could contribute to the odour as the hydrogen sulphide oxidises to sulphuric acid and pentathionic acid ($H_2S_5O_6$). Pentathionic acid could be the source of the antibacterial and antifungal activity of the geothermal water on the skin (Ármannsson, 2012; Giampaoli et al., 2012; Cruz Pauccara, 2018). Sulphuric acid dissolves primary minerals and leaches the elements such as K^+ and Na^+ contributing to the Na^+ signature in the geothermal waters. Additionally, the sources of sulphur could be from either sulphate such as soda alunite, anhydrite, alunite, and barite or sulphides e.g. chalcopyrite, galena, pyrrhotite, pyrite, sphalerite and galena (Ármannsson, 2012; Cruz Pauccara, 2018; Baba et al., 2019). Another, source of sulphides could be from resident fossil seawater at depth or when geothermal gases condensate in shallow ground waters rich in oxygen (Stober and Bucher, 2013; Aydin et al., 2020).

The presence of high SO_4^{2-} in Shu Shu (SHU) suggests that there could be magmatic influences or that the geothermal water traverse through marcasite and pyrite-bearing rocks during their ascension to the surface (Gevers, 1942; Olivier et al., 2008; Gravelét-Blondin, 2013). Furthermore, the presence of high SO_4^{2-} could be indicative of prolonged interaction times with the surrounding country rock. Furthermore, the oxidation of alkali and alkali earth sulphides (formed at depth where dissolved sulphuretted hydrogen and bases are present) at the surface (El-Sayed et al., 2012). The absence of Mg^{2+} in Shu Shu (SHU) can be attributed to adsorption of Mg^{2+} onto clay minerals (Gravelét-Blondin, 2013). At Shu Shu (SHU), the K^+ concentration is lower could be due to the retention of K^+ by absorption and base exchange in the clay products of weathering (Gevers, 1942).

6.2.2 Chemical properties

Based on the Piper diagram (Figure 23) most of the geothermal waters are classified as Na-Cl-type waters. Fewer sampled geothermal waters are characterised as Na-HCO_3, Mg- HCO_3 and a mixture of waters. This could suggest that the geothermal water chemistry has been affected by the local geology. In low enthalpy systems the chemistry is mainly lithology dependent. In contrast to high enthalpy geothermal

waters chemistry is different to the host rocks because of cation exchange and temperature dependent reactions between primary and secondary alteration minerals which significantly impact fluid chemistry (Battistel et al., 2016). Later, the discussion accounts for evidence of fluid mineral equilibria and structural pathways for the geothermal waters to surface.

6.2.2.1 Na-Cl-type waters

The Na-Cl concentrations in this study ranges between 0 to 10 meq/l Cl and 0 to 108 meq/l Na. Most of Na-Cl-type waters are from 21 sites namely: (Baleni (BAL),Badplaas (BPS), WARMBATHS (BELA1-2), Zimthabi (ZMTB), Amanzintaba (AMZT), Siloam (SILO), Tshipise (TSH), Evangelina (EVGL), Môreson (MRS), Riemvasmaak (RIEV), Skroef se Bad (SKROEF), Shu Shu (SHU), Caledon (CALE), Calitzdorp (CAZ), THE BATHS, Florisbad (FLO), Badsfontein (BAD), Aliwal (ALW), Polile Tshisa (PTS) and BRICKS) from all the geological settings (Figure 37).The Na-Cl could have been produced by water-rock interaction processers (Cruz Pauccara, 2018). The Na-Cl type water is a common water type for geothermal water systems (Arnórsson et al., 2007).

The elevated Na-Cl signatures may be linked to geothermal waters flowing through Na-bearing sequences (Stober and Bucher, 2013; Olivier and Jonker, 2013). Likewise, the Na contribution may be linked to the processers of ion exchange at depth, within clay rocks where Ca and Mg are replaced between the electrostatic surface ions and the geothermal water (Murray et al., 2015). Sources of Na^+ are linked to Cl^- where Cl^- can also occur on grain boundaries of silicate minerals (Craig, 1961). However, chlorine is one of the elements that is most conservative in a hydrothermal system, when compared to most dissolved elements as it is unlikely to alter significantly by interaction with surrounding environment. Chloride ion concentration will change only when water traverses through halite bearing rocks, or when water is boiled or evaporated. Most other elements can vary as they interact with the immediate environment (Murray et al. 2015).

Na-Cl-type water originates from marine and deep ancient groundwater environments such as central upflowing zones of liquid-dominated hydrothermal systems (Fournier 1982; Arnórsson et al., 2007). These can be found in most high temperature systems where mixing with the groundwater is a possibility (Cruz Pauccara**,** 2018). However,

Belhai et al. (2015) who reported on the geochemistry of the Northern Algerian geothermal system suggested that the higher Na-Cl concentrations were because of the mixing of geothermal waters with shallower salt water. This could account for the geochemical conditions observed at BRICKS. Gevers (1942) mentions that sodium chloride could originate from salt carried inland from the sea and precipitated from rain. Furthermore, the Na-Cl-type water may form through reactions between magmatic HCl and rock-forming minerals (Arnórsson et al., 2007).

Previous researchers (Olivier et al., 2008; Duah, 2010; Shabalala et al., 2015; Swana, 2016; Durowoju et al., 2018) also characterised Siloam (SILO), Tshipise (TSH), Warmbaths (BELA), Zimthabi (ZMTB), Caledon (CALE) and Aliwal (ALW) (Figure 37). as Na-Cl-type water. Stober and Bucher, (2013)and Olivier and Jonker, (2013) suggested that geothermal water flowing through gneisses could resemble seawater-type waters. This could be the case for the Na-Cl-type water typically associated with both the Waterberg and Soutpansberg Groups. Olivier et al. (2008) reported that Warmbaths (BELA) and Zimthabi (ZMTB), were also characterised as Na-Cl-type waters.

Olivier et al. (2010) reported Evangelina (EVGL) to be Cl^- rich however, Figure 22 shows a lower Cl^- concentration. As Evangelina is located in the Soutpansberg Group the main source of sodium in the geothermal waters could be from weathering of sodium minerals such as plagioclase. Results of hydrochemical parameters of geothermal springs within the Soutpansberg Group suggest that the thermal gradient, carbonate weathering, mineral dissolution, ion exchange, and evaporation are the main factors controlling geochemical processes resulting in the variation of the geothermal water chemistry (Durowoju et al., 2019).

Duah (2010) showed that Calitzdorp (CAZ) was characterised as mixed-type water, but in Figure 20 Calitzdorp (CAZ) exhibits Na-Cl-type water. The current study is 10 years after that of Duah (2010). The differences in chemistry of the geothermal waters could reflect an improvement in the method of analyses or that the geothermal water could be interacting with feldspar grains which could have contributed to these variations in results. It is also possible that there could have been mixing of sodium rich waters, or evaporation at surface which could have increased the concentration

of sodium (Durowoju et al., 2019)This study confirms that Caledon (CALE) is a Na-Cl-type water when compared to the findings of Duah (2010). Swana (2016), reported Aliwal (ALW) as Na-Cl-type water as well.

6.2.2.2 Na-HCO_3-type waters

The geothermal water sampled, that exhibit Na-HCO_3-type waters include Wagendrift (WGD), Sulphur Sprins (SUS), Sagole (SAG) and Thangami (TGM). Na-HCO_3 concentrations are between 1 meq/l and 19 meq/l with Na <0.1 meq/l.

Several factors are known to be associated with increased HCO_3^- content. For example, granites that have a relatively high sodium carbonate content compared to levels found in the atmosphere and soil (Ármannsson, 2012; Stober and Bucher, 2013), the solution of carbonate rocks (Mohammed and Garba Abba, 2015), or carbonate-rich steam condensing and mixing with water (Ármannsson, 2012; Stober & Bucher, 2013). The ion exchange property contributes to the affinity of geothermal water with seawater (Figure 26).

The water type at Wagendrift (WGD) may be associated with underlying lithologies comprising of granite. Sulphur Springs (SUS) is associated with underlying lithologies from the Pongola Supergroup (Figure 37). Furthermore, under high temperatures calcite could have precipitated along the flow path in the aquifer, or feldspars could have dissolved into the geothermal waters (Aydin et al., 2020). Similarly, Sagole (SAG) is associated with lithologies of the Limpopo Mobile Belt (Figure 37).associated with the Soutpansberg and Waterberg Groups as these are typically Na-Cl-HCO_3-type waters. Olivier and Jonker, (2013) summarised that the geothermal waters originating from basalts depict NaCl-HCO_3 type waters for geothermal water occurring in the Waterberg Group and the Soutpansberg Group.

Thangami (TGM) is associated with the volcanic rocks of the Karoo Supergroup (Figure 37) giving rise to Na-Cl-HCO_3 type waters (Sæmundsson, 1991; Olivier and Jonker, 2013).

6.2.2.3 Mg-HCO_3-type waters

The Mg concentrations in this study are between 0.1 meq/l and 0.4 meq/l. The Mg-HCO_3-type geothermal water signature is indicative of geothermal waters that occur deeper underground (JICA, 2014). Baba et al., (2019) elaborated on the reactions of Ca-Mg-HCO_3 waters as they circulated deeper in the crust, suggesting that there is an increase concentration of Na^+ and K^+ with deeper circulation. Additionally, the dissolution of carbonate rocks could contribute to the signature of the Mg-HCO^3-type waters (Aydin et al., 2020). The dominant anion HCO_3^- may be derived from the atmosphere, soil and solution of carbonate rocks (Mohammed & Garba Abba, 2015). Characteristically the Mg-HCO_3-type waters have minor amounts of SO_4^{2-} typically percolating through sandstone (Olivier et al., 2008).

Mg-HCO_3-type waters include those sampled at Loubad (LOU), Avalon (AVA), Toorwater (TOOR), and Goudini (GOUD). Lower concentrations of Na^+ and K^+ are observed in the Mg-HCO_3-type waters (Figure 23). Loubad (LBD) is associated with lithologies from the Waterberg Group and the Bushveld Igneous Complex (Figure 37) (Kent, 1946). It is believed that Mg-HCO_3-type waters are derived from feldspars whereas diabase intrusions could account for the supply of Mg^{2+} (Kent, 1946). Olivier and Jonker (2013) observed that Loubad (LBD) is characterised differently from the geothermal waters of the Waterberg region but are similar to Libertas with regards to anions composition. Unfortunately, Libertas was not sampled for the current study, given the inaccessibility to the geothermal water at the time of sampling.

Avalon (AVA), Toorwater (TOOR) and Goudini (GOUD) are associated with the Cape Fold Belt lithologies (Figure 37), where dolomite and diabase strata are likely to contribute to the increase in Mg^{2+} content (Mohammed & Garba Abba, 2015). These characteristics of Goudini (GOUD) differ from the findings of Duah's (2010) where he classified GOUD as mixed-type water. However, Olivier and Jonker (2013) affirmed the geothermal water chemistry for Avalon (AVA), Toorwater (TOOR) and Goudini (GOUD).

6.2.2.4 Mixed-type waters

Geothermal waters sampled that are characteristically mixed-types waters include Natal (NTL), Machadodorp (MDP), Mphephu (MPU), Rhemardo (RHM) and Warmbaths (BELA), Lilani (LIL), Warmwaterberg (WARM), Baden Club (BAK), Brandvlei (BRA) and Cradock (CRAC). Mixed-type waters represent mixtures of dominant ions with similar concentrations.

The mixed-type waters represent a variety of environments from deep ancient groundwaters, and deeper groundwater influenced by ion exchange to shallow fresh groundwaters (Fournier, 1982; Ármannsson, 2012). The variation in chemistry may be due to mixing of various waters or ongoing water-rock interactions.

Natal (NTL) is associated granite, Machadodorp (MDP) occurs within the Transvaal Supergroup, Mphephu (MPU), is associated with the Limpopo Mobile Belt, Rhemardo (RHM) and Warmbaths (BELA), are associated with lithologies from the Waterberg Group, Lilani (LIL) is associated with sequences from the Namaqua-Natal Province, Warmwaterberg (WARM), Baden Club (BAK), Brandvlei (BRA) and Cradock (CRAC) is associated with lithologies of the Cape Fold Belt (which is also associated with the Karoo Supergroup).

Duah (2010) and Swana (2016) also categorized Warmwaterberg (WARM), Baden Club (BAK), Brandvlei (BRA) and Cradock (CRAC) as mixed-type waters. In 2010, Olivier et al. reported that the Mphephu (MPU) geothermal waters to be enriched in Mg^{2+}, and Shabalala et al. (2015) confirmed Mphephu (MPU) waters as a Na-HCO_3 type water.

6.3 Fluid-mineral equilibria

The binary plots of silicate and carbonate weathering (Figure 24 and Figure 25) illustrates that the majority of the geothermal waters fall below the 1:1 equiline, indicating silicate weathering where ion exchange is the major process. Sodium and potassium ions dominate the water chemistry, indicating the reaction of feldspar minerals with carbonic acid in the presence of geothermal water. The geothermal waters that are above the 1:1 equiline exhibit carbonate weathering in which reverse ion exchange occurs as the dominant process taking place in the geothermal waters (Durowoju et al., 2019; Henry, 2020; Mahwa et al., 2023).

The Karoo Supergroup (Florisbad (FLO), Badsfontein (BAD) and Aliwal (ALW)) exhibit equilibrium between the host rock and the geothermal waters (Figure 26 and Figure 27). The Cape Fold Belt geothermal waters Avalon (AVA), Baden Club (BAK), Toorwater (TOOR), Warmwaterberg (WARM), Calitzdorp (CAZ), Caledon (CALE), BRANDVLEI (BRA), THE BATHS and Goudini (GOUD) plot in the immature waters field, supported by the crustal signature (Figure 26 and Figure 27). The ion concentration of the geothermal waters from the Cape Fold Belt (Baden Club (BAK), Warmwaterberg (WARM), and Brandvlei (BRA) displays characteristics of shallow groundwaters and products of dissolution of the average (immature) crustal rock (Figure 24, Figure 25 and Figure 27). Furthermore, immature waters acquire their salinity signatures through simple rock leaching or mixing (Giggenbach, 1988 a, b; Baioumy et al., 2015; Cruz Pauccara, 2018; Herzhegovina et al., 2020; Ayari et al., 2023). Geothermal waters that plot in the partial equilibration group have no distinct geological setting. Due to the leaching of aquifer material, the Na^{2+} concentration in groundwater can increase. Na^{2+} replaces Ca^{2+} and Mg^{2+} within clay rocks during ion exchange. Elevated concentrations and higher (Na+K)/ (Ca+Mg) ratio indicate geothermal waters that have been underground for extended periods (Baioumy et al., 2015; Baba et al., 2019). Olivier and Jonker (2013), reported similar water chemistry for the Cape Fold Belt geothermal waters.

Carbonate weathering and reverse ion exchange predominate geothermal waters from the Waterberg Group (Loubad (LBD)) and the Cape Fold Belt (Avalon (AVA)). Their (Loubad (LBD)) and Avalon (AVA))chemical signatures corresponds with plots in Figure 23-24.

Loubad (LBD) associated with the Waterberg Group also exhibits immature water in Figure 27., This differs from the other geothermal waters sampled associated within the Waterberg Group. Olivier et al., (2010) mentions that Loubad (LBD) shows reduced signs of dissolution, mixing and ion exchange compared to other geothermal waters from the Limpopo Mobile Belt associated with the Soutpansberg and Waterberg Group. The current study presents similar observations to those of Olivier et al., (2010) implying that the source and water-rock interactions are consistent over time.

Baleni (BAL) geothermal water is associated with the Archean granites and gneisses that plots on the partial equilibrium line in Figure 27 compared to Figure 26, where it has been equilibrated. Furthermore, Baleni (BAL) displays equal carbonate and silicate weathering in Figure 24 and Figure 25. Baleni is close to equilibrium, possibly due the geothermal waters are circulating faster through fractured aquifers (Uzelli et al., 2017).

BRICKS, Baleni (BAL), Florisbad (FLO), Aliwal (ALW) and Badsfontein (BAD) are in equilibrium (Figure 26), suggesting that there was little or no mixing with cold water and no dissolution (Giggenbach, 1988 a, b; Baioumy et al., 2015; Cruz Pauccara, 2018; Herzhegovina et al., 2020; Ayari et al., 2023). BRICKS and Baleni (BAL) display equal silicate and carbonate weathering (Figure 24 and Figure 25). BRICKS is associated with the Uitenhage Group, while Baleni (BAL) is associated with Archean granite and gneisses (Gevers, 1963). However, Figure 27 shows that both BRICKS and Baleni (BAL) display partial equilibrium. Cradock (CRAC) and Polile Tshisa (PTS) plot close to the equilibrium line (Figure 26), suggesting that the salinity is the results of simple rock leaching and is close to equilibration (Giggenbach, 1988 a, b; Cruz Pauccara, 2018; Herzhegovina et al., 2020; Ayari et al., 2023).

6.4 Isotopic classification

6.4.1 Stable Isotopes

The geothermal waters analysed have a slope of 7 (Figure 29), common for groundwater in South Africa (Murray et al. 2015). The δ18O values are affected by the surrounding rock as rock contains 50 wt.% O and minor amounts of H. The signature of δ18O will shift, as it is dependent on the O isotope fractionation factor between water and rock, as well as temperature and δ18O value of the rock. Geothermal waters enriched in δD and δ18O suggest an evaporation effect and a closer affinity with seawaters (Diamond and Harris, 2000; Geyh, 2000; Murray et al., 2015). The values for δD and δ18O are slightly below the local meteoric value, indicative of palaeowater origin (Geyh, 2000).

Nine geothermal waters (Avalon (AVA), Baden Club (BAK), Toorwater (TOOR), Warmwaterberg (WARM), Calitzdorp (CAZ), Florisbad (FLO), Badfontein (BAD), Aliwal (ALW) and Cradock (CRAC)) display depleted values of δD (-40‰ to -35‰) and δ18O (-7.5 to -5.5‰). These plot close to the Local Meteoric Water Lines of Cape Town, Thohoyandou and Pretoria exhibiting a lighter isotope signature(Figure 29). The lighter isotope signatures may indicate that the geothermal waters are from a deeper source (Diamond & Harris, 2000; Mazor, 2003) or that the geothermal waters have had a longer residence time for the fractionation of the stable isotopes that may have the same source affected by temperature (Geyh, 2000). Lastly, it could be that the rainwater is associated with depleted signatures that circulate through the source (Murray et al., 2015). Furthermore, these geothermal waters could occur at lower altitudes which tend to have depleted δD and $\delta^{18}O$ values, described as the altitude effect (Aydin et al., 2020).

In addition, generally heavy rainfall events will result in the infiltration of precipitation and subsequent depletion of the heavier isotopes. During heavy rainfall, the air gets filled with moisture, hence less enrichment (lighter isotopes) of raindrops occur. Heavy rainfall and isotope exchange might happen before the water reaches the ground (Geyh, 2000; Diamond, 2014). This interaction with CO_2 enriched in ^{16}O might explain the negative ^{18}O shift (Khosrawi, 1996).

Depleted signatures of δD and δ18O (-35‰ and -6.2‰ respectively) along the Cape Fold Belt (Toorwater (TOOR), Warmwaterberg (WARM) and Calitzdorp (CAZ) are characteristic of deep groundwater (palaeowater) that could have mixed with the geothermal waters (Geyh, 2000; Murray et al., 2015). The geothermal waters associated with the Cape Fold Belt displays immature, crustal signatures although there is a distinct difference in δD and δ18O ratios. Of interest is that Goudini (GOUD) and Avalon (AVA) sites which occur close to each other but exhibit different isotope signatures. Different isotope signatures could mean that geothermal waters have different sources, as the Colenso Fault separates Goudini (GOUD) from Avalon (AVA). The Colenso Fault is a prominent northwest–southeast-trending fault, a ~550 Ma shear zone associated with granitoids (Kisters et al., 2002). The Colenso Fault divides geothermal waters with enriched δD and δ18O ratios to the west and depleted δD and δ18O ratios to the east. Furthermore, geothermal waters more enriched in δD and

δ18O occur on the Kaapvaal Craton. Exceptions are Shu Shu (SHU) and Lilani (LIL) from the Namaqua-Natal Province, which exhibit enriched δD and δ18O signatures.

The analyses reported by Mazor and Verhagen, (1983) and Diamond and Harris, (2000) are seventeen years apart, with different measured values (Figure 38). The difference in values could be due to the improvement in technology for analysing isotopes. However, isotope changes occur concurrently for instance, a shift in the deuterium values would be a mirrored by a shift in ^{18}O values (Mazor & Verhagen, 1983). In Figure 38, the trend of concurrent shift of δD and δ18O is absent. In addition, the analyses reported in this study are a further twenty-four years apart from those reported in Diamond and Harris's (2000) research.

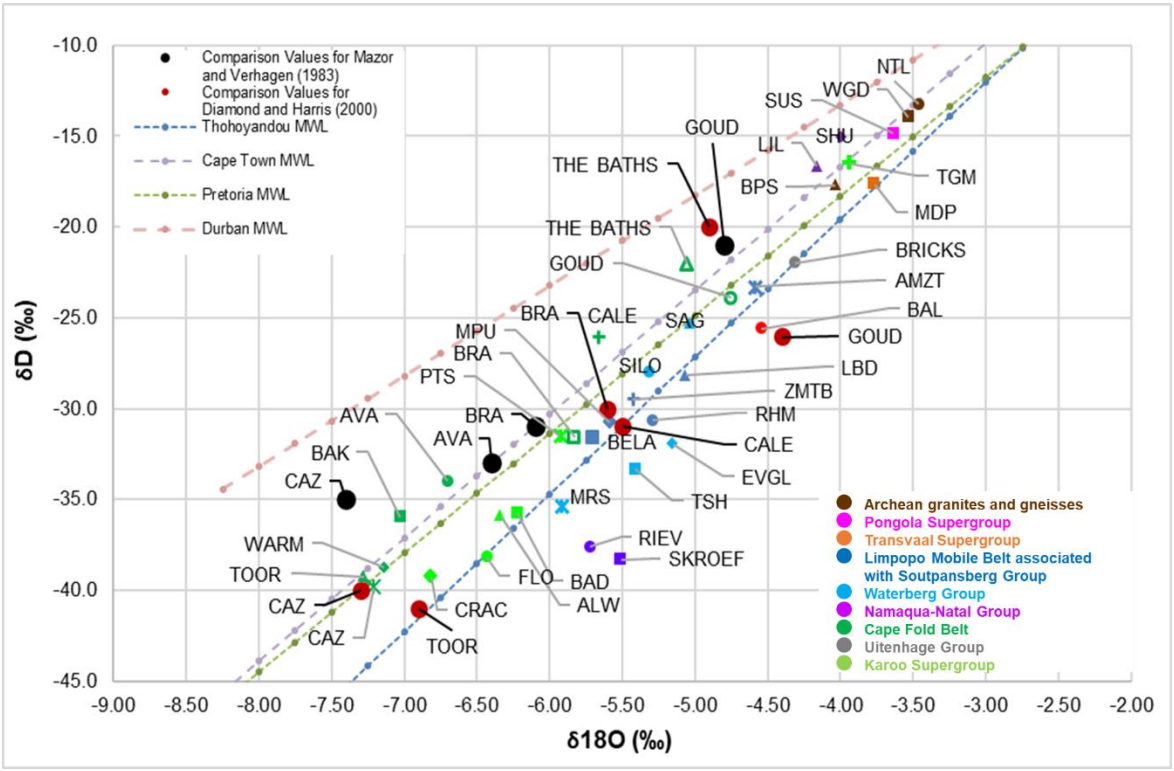

Figure 38: A plot of δD versus δ18O for the South African geothermal waters and the Local Meteoric Water Line (LMWL). Previous isotope analyses plotted in red (Diamond and Harris, 2000) and black (Mazor and Verhagen, 1983). Colour coded per geological domain.

The older analyses of Mazor and Verhagen (1983) and Diamond and Harris (2000) show an affinity with the meteoric line. Results from Diamond and Harris (2000) display two distinct groups. The first group enriched in δD and δ18O (Caledon (CALE), Brandvlei (BRA), Goudini (GOUD) and THE BATHS) occur in the mountains but closer

to the coastline (Figure 29). The second group Avalon (AVA), Toorwater (TOOR), Baden Club (BAK), Warmwaterberg (WARM) and Calitzdorp (CAZ), depleted in δD and δ18O are situated in the mountains but are further inland (Figure 29). Diamond and Harris (2000) in their research concluded that the geothermal water isotope ratios are significantly lower than ambient rainfall where recharge takes place at higher elevations .

Olivier and Jonker (2013) further elaborated on enriched values of δD and δ18O for Siloam (SILO), Tshipise (TSH), Mphephu (MPU), Evangelina (EVGL), Môreson(MRS), Rhemardo (RHM), Loubad (LBD), Warmbaths (BELA) and Zimthabi (ZMTB) from the Soutpansberg Group (associated with Limpopo Mobile Belt) and the Waterberg Group. The sites enriched in δD and δ18O either have similar sources or are of meteoric origin. For example, Rhemardo (RHM), Warmbaths (BELA) and Zimthabi (ZMTB) occur close to Thabazimbi–Murchison Lineament (Figure 37) which could link the sources of the geothermal waters. The Thabazimbi–Murchison Lineament is a ~2.96 Ga old major tectonic fault extending ~500 km in an NNE–SSW direction and situated on the northern boundary of the Kaapvaal Craton (Jansen, 1982; Johnson et al., 2006). Siloam (SILO), Tshipise (TSH) and Môreson(MRS), occur within an extensive network of faults in the Tshipise Straightening Zone (Dhansay et al., 2016).

Badplaas (BPS), Natal (NTL), Wagendrift (WGD), Sulphur Springs (SUS), Machadodorp (MDP), Lilani (LIL), Shu Shu (SHU) and Thangami (TGM) display enriched values for δD (-40‰ to -35‰) and δ18O (-4.0 to -3.5‰). The enriched values of δD and δ18O may have been affected by evaporation or have a close affinity with sea waters where connate waters have influenced the source in faulted regions (Geyh, 2000; Murray et al., 2015).

6.4.2 Radiogenic isotope tritium

The low (0-0.5 TU) and negligible TU values are indicative of deep and older water and have a pre-1952 age (Mazor, 2003; Murray et al., 2015) suggesting that most of the geothermal waters in South Africa pre-date 1952. It is suggested that the geothermal waters with little but measurable tritium (0.5-10.0 TU) is a mixture of pre- and post- 1952 water (Mazor, 2003). The geothermal waters that exhibit a mixture of

pre- and post-1952 water is associated with Archean granites and gneisses (Natal (NTL) = 0.6), Soutpansberg Group associated with Limpopo Mobile Belt (Evangelina (EVGL) = 0.8), Waterberg Group (Loubad (LBD) = 0.8) and the Karoo Supergroup (Cradock (CRAC) = 0.8). These geothermal waters exhibit signatures of waters more than 70 years old mixed with younger waters (Gökgöz, 1998; Mazor, 2003).

6.5 Most suitable geothermal waters

The quartz geothermometer predicted temperatures determined in this study are below 150°C. It is sometimes found that silica contents reflect equilibrium with chalcedony (Arnórsson, 1983) rather than the quartz geothermometer (Fournier, 1977). The chalcedony geothermometry is based on albite-microcline, albite-adularia or Na-K montmorillonite and water. The geothermometry assumes that the reaction takes longer to reach equilibrium at a given temperature than the common based geothermometers. This gives calculated temperatures that are comparatively higher as the geothermal waters originates in the deeper part of the system where geothermal waters residence times are longer (Arnórsson, 1983). The geothermometry values for some geothermal waters are below the surface temperature signifying lower concentrations of the specific ions in the geothermal waters. Lower concentrations of ions could indicate that the time for water-rock interaction is low, and/or that the concentrations of the ions in the rocks are lower and could not contribute to the chemical signature.

One of the aims of this study is to classify the geothermal waters into low-medium enthalpy sources as illustrated in Table 1 and Figure 10. There are 20 potential geothermal waters that may be harnessed for power generation as shown in Figure 39 and Appendix F. The remainder of the geothermal waters may be utilised for recreational activities, aquaculture, agriculture, space heating and food processing (Figure 10).

The calculated potential geothermal waters for power generation are associated with Archean granites and gneisses (Badplaas (BPS), Baleni (BAL), Natal (NTL), Wagendrift (WGD)), Limpopo Mobile Belt associated with the Soutpansberg and

Waterberg Group (Siloam (SILO), Mphephu (MPU), Tshipise (TSH), Sagole (SAG), Evangelina (EVGL), Môreson(MRS), Warmbaths (BELA1-3) and Zimthabi (ZMTB)), Namaqua Natal Province (Riemvasmaak (RIEV), Skroef se Bad (SKROEF), Lilani (LIL) and Shu Shu (SHU)), and Cape Fold Belt (Caledon (CALE), Warmwaterberg (WARM)) (Figure 39). The common theme amongst these potential geothermal waters is that they all occur on or close to major structural zones with high heat flow (Figure 39).

Môreson (MRS) exhibits the highest enthalpy of 624 kJ/kg, for a resource temperature of 148°C and circulation depth of 2.7 km that is associated with the Soutpansberg Group and the Limpopo Mobile Belt. Môreson (MRS) is characterised as Na-Cl-type water (Figure 23). Warmwaterberg (WARM) associated with the Cape Fold Belt exhibits the lowest enthalpy of ~432 kJ/kg, for a reservoir temperature of ~102°C and circulation depth of 2.3 km. Môreson (MRS)and Warmwaterberg (WARM) exhibit silicate weathering but occur in different geological settings.

All the geothermal waters associated with Archean granites and gneisses indicate the potential of low-medium enthalpy owing to their higher temperatures due to the decay of radioactive elements that occur in the granites and gneisses. The same can be predicted for the geothermal waters associated with the Namaqua-Natal Province as all these geothermal waters are associated with granites or intrusion lithologies (see section 5.1).

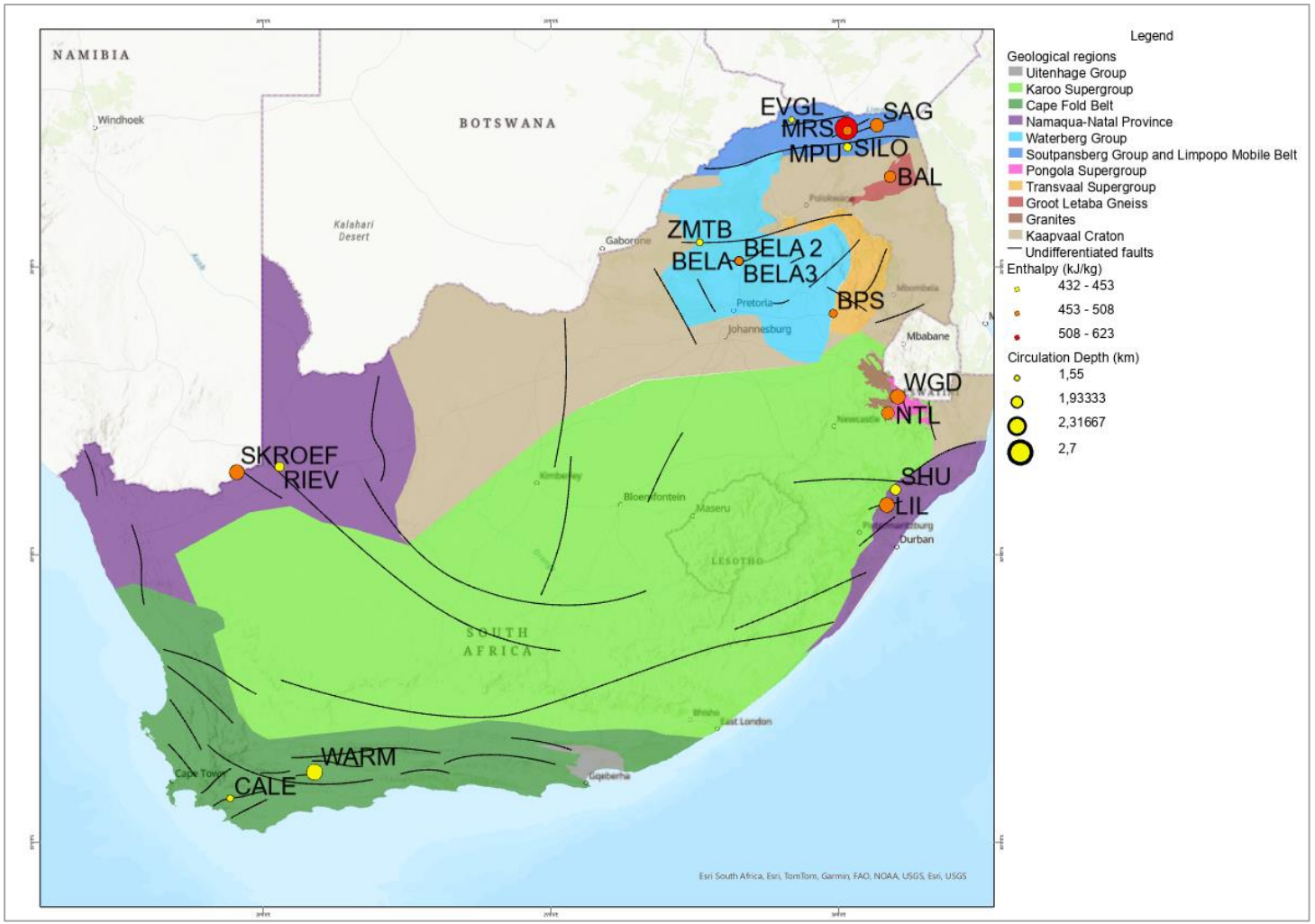

Figure 39: Overview of the major geological domains and tectonic structures across South Africa. The locations of the various potential geothermal waters for harnessing geothermal energy are marked on the map with enthalpy ranges denoted by circle size and calculated circulation depth of the geothermal waters. Produced in ArcGIS Pro and modified from Dhansay et al. (2017).

The 20 potential geothermal waters that could be harnessed for power generation will need boreholes to be drilled to at least 1 km to reach the geothermal resource. To optimise these geothermal resources, a cascading model, could be viable (details in Section 2.3) (Rybach, 1981; Rubio-Maya et al., 2015; Wallis et al., 2018; Jolie et al., 2021) similar to that of Onyango and Varet (2014) (Figure 40).

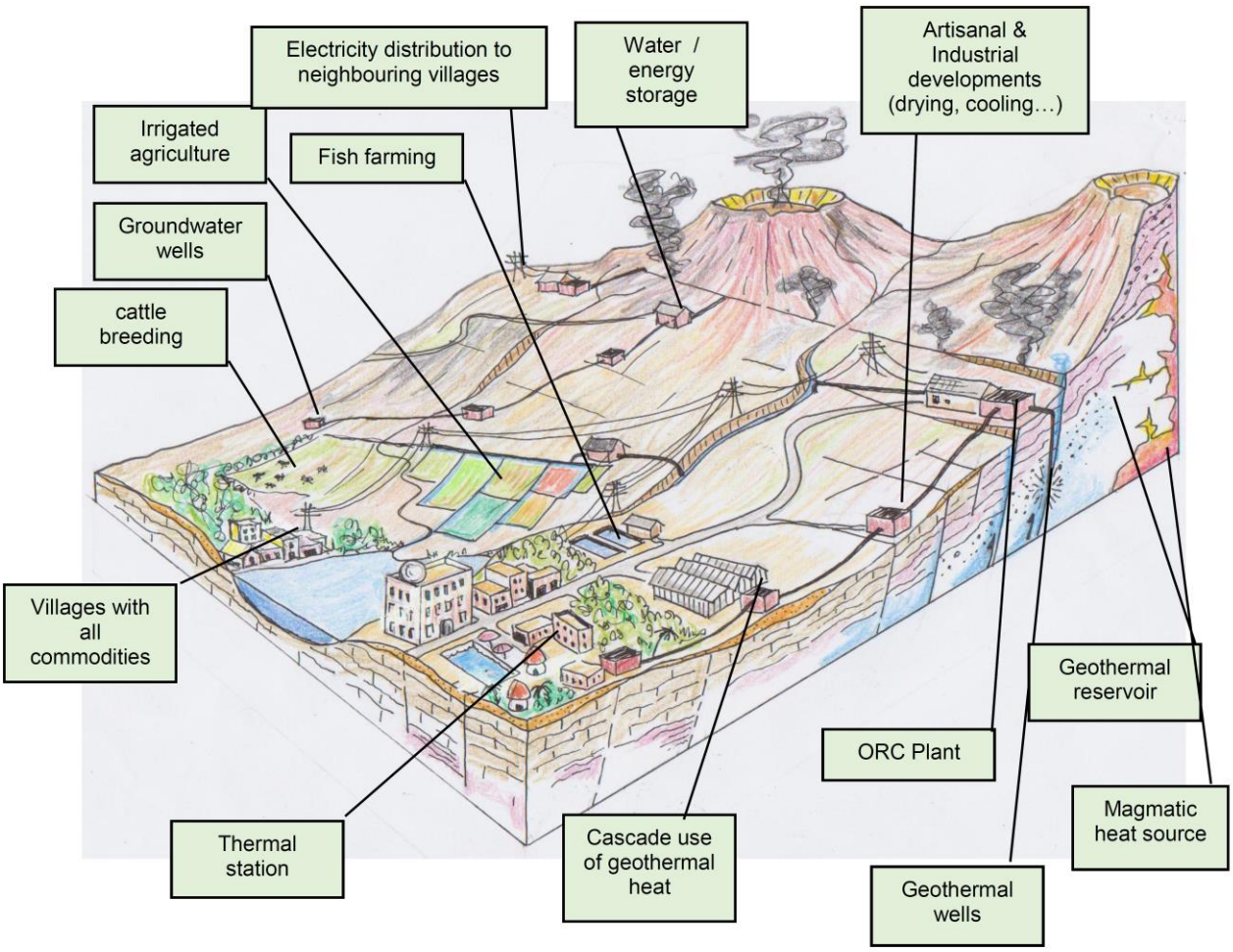

Figure 40: Schematic diagram of a conceptual model for harnessing geothermal energy in a cascading manner (Onyango and Varet, 2014).

CHAPTER 7 CONCLUSION AND RECOMMENDATIONS

This chapter provides a summary of the materials, methods, results and discussion from Chapters 4-6. The aims and objectives of this study are reevaluated. Including the contributions of this study, its impact and recommendations of the development of geothermal energy in South Africa.

7.1 Re-evaluation of the aims and objectives

This study set out to characterise the geothermal waters of South Africa based on their physical and hydrochemical properties. Such properties would then be used to predict the type of recharge, resource temperatures and the depth of the geothermal waters. The main purpose of the current study was to determine the enthalpy range of the geothermal waters that could be potentially harness for power generation.

Previously an updated characterisation of the geothermal waters did not exist as a single source (Jonker, 2016). This gap has now been closed by undertaking a detailed desktop study of the geology of the 41 geothermal waters sites. In addition, these geothermal waters across South Africa were sampled and analysed for their physical (temperature, pH, EC and salinity) and chemical properties (HCO^{3-}, Cl^{-}, SO_4^{2-}, F^{-}, Na^{+}, K^{+}, Ca^{2+}, Mg^{2+}, Fe^{2+} and [SiO2 (OH)2]$^{2+}$), stable isotopes (δ18O and δD) and radiogenic tritium. This current-day results are compared with those of previous years to understand the chemical changes of the geothermal waters.

Prior to this study it was difficult to categorise the geothermal waters in South Africa as the previous studies focussed either on individual geothermal waters or on a group. of geothermal waters. In the current study, all the geothermal water occurrences have been grouped according to three main geological settings: 1) basement/crystalline rock type settings, 2) intracratonic basins and 3) orogenic belts (Figure 36). Figure 36 incorporates the geological habitat for potential hydrothermal reservoirs, heat transfer type and the geologic controls for all sites. This lays the foundation for future research into exploration for and development of geothermal energy in the country.

This study has identified that the geothermal waters) exhibit different physicochemical characteristics dependent on their immediate geology (Kent, 1949; Drogue et al., 2000; Tassi et al., 2006; Mohamed & Ehara, 2009; Baioumy et al., 2015; Yan et al., 2017; Zhenhua et al., 2018; Aydin et al., 2020; Chimeddorj et al., 2021; Temizel et al., 2021; Yu et al., 2022; Kiełczawa, 2023; Mahwa et al., 2023; Yin et al., 2023). This research has also identified that the geothermal water exhibit temperature range of 25 to 61°C, pH of 4 to 9 and electrical conductivity measurements of 2 to 4930 µS/cm.

The results of this investigation have identified four geothermal water types in South Africa: Na-Cl, Na-HCO_3, Na-HCO_3 and mixed-type. This is similar to findings of earlier studies (Figure 23). An implication of the types of water showed there are different water-rock interactions that have taken place between the geothermal waters and various host rocks.

Most of the geothermal waters were classified as Na-Cl-type water irrespective of their various geological settings. Such water types are regarded as being immature to partially equilibrated and are associated with seawater signatures (Figure 28). Only five geothermal waters (Baleni (BAL), Florisbad (FLO), Badsfontein (BAD), Aliwal (ALW) and BRICKS) appear to be in equilibrium. This study has found that generally geothermal water originates from marine and deep ancient groundwater environments such as central upflowing zones of liquid-dominated hydrothermal systems, with deeper groundwater influenced by both ion exchange and mixing with shallow fresh groundwaters.

The stable isotope signatures confirm that the geothermal waters are of meteoric origin as the analyses have a close affinity to the Local Meteoric Water Line in the various regions (Figure 29). Further investigation highlighted that the structural features (faults, joints, fractures) separate the geothermal waters laterally and that these structures may serve to link the geothermal water sources. However, there are exceptions e.g. geothermal waters more enriched in δ18O and δD occur on the Kaapvaal Craton except for Shu Shu (SHU) and Lilani (LIL) from the Namaqua-Natal Province. The attempt to cluster the physical and chemical results into a particular geological setting proved fruitless.

Further to characterising the geothermal waters the overarching aim was to investigate the geothermal waters for their suitability to harness geothermal energy for power generation, based on their viable enthalpy ranges. Different geothermometers produced a range of potential temperatures for the geothermal resource. However, the quartz geothermometer (Fournier, 1977) is most viable for predicting the temperature of the geothermal resources. The cation geothermometers calculated very high temperatures of ~550°C and/or temperatures below the measured surface temperatures of the geothermal waters. By utilising the calculated quartz geothermometer, enthalpy range (low-medium) and geothermal gradient, revealed 20 geothermal waters that have the potential to harness geothermal energy for power generation.

The 20 geothermal waters enthalpy range between 432 and 624kJ/kg and their calculated geothermal resource temperatures measured between 107°C and 148°C where the geothermal water circulation depths are between 1.6 km and 2.7 km. Although this study presents an updated comprehensive dataset of the geothermal waters of South Africa, further research is necessary before actual harnessing of geothermal energy is possible.

7.2 Contributions and impact

It is envisioned that the results of this research will facilitate a better understanding of potential geothermal energy sources in South Africa. The updated characterisation of the geothermal waters showed that low-medium enthalpy geothermal waters exist in South Africa. As technology advances, it may well be possible to harness geothermal energy at lower enthalpy ranges such as those found in South African. This could result in geothermal waters posing a potential energy source to South Africa's energy needs and would require a huge investment for energy generation. This research could impact the future Integrated Resource Plan where geothermal energy could be added to this plan. Currently, the South African government is in the process of amending the Electricity Regulation Bill to allow independent power producers to supply energy to customers using the existing power infrastructure (Electricity Regulation Amendment Bill, 2023), that could enable independent developers of geothermal energy to add to the power grid.

7.3 Recommendations

Further analyses such as seasonal sampling and carbon dating of the geothermal waters will assist in understanding variations in recharge rates, temperature ranges and mixing models for energy production. To increase confidence levels in this dataset, the five highest enthalpy geothermal waters undertake a detailed understanding of surface geological settings will assist in improving the geothermal system classification for use in decision making at the pre-drilling phase of exploration. In addition, downhole geophysics and temperature data for boreholes drilled in recent years will add to the geothermal gradient map and inform further exploration into suitable geothermal water sources. Geophysical surveys will assist with locating geothermal waters sources at depth (confirming the geothermometry datasets) together with their conduits, enabling a pre-feasibility study and constraining the geothermal source for energy production. These datasets can provide reliable cataloguing data applicable to site-specific field developments.

REFERENCES

1. Akinbami, O. M., Oke, S. R. and Bodunrin, M. O., 2021. The state of renewable energy development in South Africa: An overview. Alexandria Engineering Journal, 60, 5077-5093.
2. Anderson, D. N. and Lund, J. W (Editors), 1980. Direct utilization of geothermal energy: A layman's guide. Geothermal Resources Council special report No. 8, United States, 97pp.
3. Andreoli, M. A., Brandl, G., Coetzee, H., Kramers, J. D. and Mouri, H., 2011. Intracrustal radioactivity as an important heat source for Neoarchean metamorphism in the Central Zone of the Limpopo Complex. Geological Society of America Memoirs, 207, 143-161.
4. Arnórsson, S., 1983. Chemical equilibria in Icelandic geothermal systems-implications for chemical geothermometry investigations. Geothermics, 12, 119-128.
5. Arnórsson, S., 1985. The use of mixing models and chemical geothermometers for estimating underground temperatures in geothermal systems. Journal of Volcanology and Geothermal Research, 23, 299-335.
6. Arnórsson, S., Stefánsson, A. and Bjarnason, J. Ö., 2007. Fluid-fluid interactions in geothermal systems. Reviews in Mineralogy and Geochemistry, 65, 259-312.
7. Ármannsson, H., 2012. Geochemical aspects of geothermal utilization. In: A. Sayigh (Editor), Comprehensive Renewable Energy. Elsevier, Oxford, 7, 95-168.
8. Ayari, J., Barbieri, M., Boschetti, T., Barhoumi, A., Sellami, A., Braham, A., Manai, F., Dhaha, F. and Charef, A., 2023. Major-and trace-element geochemistry of geothermal water from the Nappe Zone, Northern Tunisia: Implications for mineral prospecting and health risk assessment. Environments, 10, 26pp.
9. Aydin, H., Karakuş, H. and Mutlu, H., 2020. Hydrogeochemistry of geothermal waters in eastern Turkey: Geochemical and isotopic constraints on water-rock interaction. Journal of Volcanology and Geothermal Research, 390, 106708.

10. Baba, A., Şaroğlu, F., Akkuş, I., Özel, N., Yeşilnacar, M.İ., Nalbantçılar, M.T., Demir, M.M., Gökçen, G., Arslan, Ş., Dursun, N. and Uzelli, T., 2019. Geological and hydrogeochemical properties of geothermal systems in the southeastern region of Turkey. Geothermics, 78, 255-271.

11. Baioumy, H., Nawawi, M., Wagner, K. and Arifin, M.H., 2015. Geochemistry and geothermometry of non-volcanic hot springs in West Malaysia. Journal of Volcanology and Geothermal Research, 290, 12-22.

12. Baiyegunhi, C., Mupandawana, N. W., Oloniniyi, T.L. and Gwavava, O., 2014. Characterization of Aliwal North hot spring in the Eastern Cape Province of South Africa, using magnetic, electromagnetic and radiometric methods. Journal of Engineering, 4, 43-58.

13. Baughman, J. S. and Flowers, R. M., 2020. Mesoproterozoic burial of the Kaapvaal Craton, southern Africa during Rodinia supercontinent assembly from (U-Th)/He thermochronology. Earth and Planetary Science Letters, 531, 1-13.

14. Battistel, M., Hurwitz, S., Evans, W. C. and Barbieri, M., 2016. The chemistry and isotopic composition of waters in the low-enthalpy geothermal system of Cimino-Vico Volcanic District, Italy. Journal of Volcanology and Geothermal Research, 328, 222-229.

15. Belhai, M., Fujimitsu, Y., Bouchareb-Haouchine, F.Z. and Nishijima, J., 2015. Geology, geothermometry, isotopes and gas chemistry of the Northern Algerian geothermal system. Geology, 19, 25.

16. Beardsmore, G. R. and Cull, C. P., 2001. Crustal heat flow: a guide to measurement and modelling. Cambridge University Press, Cambridge, 324pp.

17. Bertani, R. 2016. Geothermal power generation in the world 2010–2014 update report. Geothermics, 60, 31-43.

18. Bethke, C. M., Farrell, B. and Melika, S., 2022. The geochemist's workbench. Release 17 ed. Aqueous Solutions LLC, Champaign, Illinois, 226pp.

19. Bird, P., Ben-Avraham, Z., Schubert, G., Andreoli, M. and Viola, G., 2006. Patterns of stress and strain rate in southern Africa. Journal of Geophysical Research, 111, 1-14.

20. Boden, D. R., 2017. Geologic fundamentals of Geothermal Energy. Taylor and Francis Group, CRC Press, Boca Raton, London, New York, 381pp.

21. Boekstein, M. S., 1998. Hot spring holidays: Visitors' guide to hot springs and mineral spa resorts in southern Africa. Mark Boekstein, Cape Town, 51pp.

22. Boekstein, M. S., 2012. Revitalising the healing tradition: Health tourism potential of thermal springs in the Western Cape. Unpublished PhD thesis, Cape Peninsula University of Technology. Cape Town, South Africa, 182pp.[Online] Available at https://etd.cput.ac.za/handle/20.500.11838/1623.

23. Boshoff, R., 2008. The Neoarchaean to Palaeoproterozoic evolution of the polymetamorphic Central Zone of the Limpopo high-grade terrain in South Africa. Unpublished PhD thesis. University of Johannesburg, Johannesburg, South Africa, 216pp.

24. Boslaugh, S. and Watters, P.A., 2008. Statistics in a nutshell: A desktop quick reference (2nd Edition). O'Reilly Media. Sebastopol, USA, 452pp.

25. Brandl, G., 1981. The geology of the Mesina area. Explanation of the sheet 2230. Geological Survey of South Africa, Pretoria, South Africa, 35pp.

26. Burgassi, P. D., 1999. Historical outline of geothermal technology in the Larderello region to the middle of the 20th century. In: R. Cataldi, S.F. Hodgson, and J.W. Lund (Editors), Stories from a heated Earth: Our geothermal heritage. Geothermal Resources Council and International Geothermal Association, California, USA, 195-219.

27. Callaghan, C. C., Eriksson, P. G. and Snyman, C.P., 1991. The sedimentology of the Waterberg Group in the Transvaal, South Africa: an overview. Journal of African Earth Sciences (and the Middle East), 13, 121-139.

28. Cave, L. and Clarke, S., 2003. A feasibility study on the use of chemical geothermometers for tracing deep groundwater flow. Water Research Commission report no. 1331/1/03. Water Research Commission. Pretoria, South Africa, 53pp.

29. Chand, K. and Kumar, R., 2014. Geothermal energy – An alternative source of clean and sustainable energy in India. World Focus Indo centric Foreign Affairs Monthly Journal, 50, 71-82.

30. Chimeddorj, B., Munkhbat, D., Altanbaatar, B., Dolgorjav, O. and Oyuntsetseg, B., 2021. Hydrogeochemical characteristics and geothermometry of hot springs in the Altai region, Mongolia. Geochemistry: Exploration, Environment, Analysis, 21, geochem2021-016.
31. Chiasson, A. D., 2016. Geothermal heat pump and heat engine systems: Theory and practice. John Wiley and Sons, Ltd. New Jersey, USA, 496pp.
32. Clemens, J. D. and Stevens, G., 2021. S-to I-to A-type magmatic cycles in granitic terranes are not globally recurring progressions. The cases of the Cape Granite Suite of Southern Africa and central Victoria in southeastern Australia. South African Journal of Geology, 124, 565-574.
33. Coward, M. P., 1976. A discussion on natural strain and geological structure-Archaean deformation patterns in Southern Africa. Philosophical Transactions of the Royal Society of London. Series A, Mathematical and Physical Sciences, 283, 313-331.
34. Craig, H., 1961. Isotopic variations in meteoric waters. Science, 133, 1702-1703.
35. Cruz Pauccara, V., 2018. Chemical and isotopic composition of hot spring waters in the Tacna region, Southern Peru. Ingemmet: 16pp.
36. CSIR., 2022. CSIR. [Online] Available at https://www.csir.co.za/sites/default/files/Documents/Loadshedding%20plot.pdf. Accessed 19 March 2024.
37. Department of Mineral Resources and Energy., 2019. Integrated Resource Plan 2019. Department of Mineral Resources and Energy, Pretoria, South Africa, 98pp.
38. Department of Mineral Resources and Energy., 2021. Annual Performance Plan 2020/21. Department of Mineral Resources and Energy, Pretoria, South Africa, 138pp.
39. De Wit, M.J., de Ronde, C.E., Tredoux, M., Roering, C., Hart, R.J., Armstrong, R.A., Green, R.W., Peberdy, E. and Hart, R.A., 1992. Formation of an Archaean continent. Nature, 357, 553-562.
40. De Wit, M., Furnes, H., MacLennan, S., Doucouré, M., Schoene, B., Weckmann, U., Martinez, U. and Bowring, S., 2018. Paleoarchean bedrock

lithologies across the Makhonjwa Mountains of South Africa and Swaziland linked to geochemical, magnetic and tectonic data reveal early plate tectonic genes flanking subduction margins. Geoscience Frontiers, 9, 603-665.

41. Dhansay, T., 2012. Evaluation for harnessing low-enthalpy geothermal energy in South Africa based on a model pilot plant in the Limpopo Mobile Belt. Unpublished MSc thesis, Nelson Mandela Metropolitan University, Gqerberha, South Africa, 134pp.

42. Dhansay, T., Brandl, G. and De Wit, M. J., 2016. Fractal geometry of the fault network across the Soutpanberg Mountains, Limpopo, South Africa. South African Journal of Geology, 119, 235-242.

43. Dhansay, T., Musekiwa, C., Ntholi, T., Chevallier, L., Cole, D. and De Wit, M. J., 2017. South Africa's geothermal energy hotspots inferred from subsurface temperature and geology. South African Journal of Science, 113, 1-7.

44. Diamond, R. E., 2014. Stable isotope hydrology of the Table Mountain group. Unpublished PhD. thesis, University of Cape Town, Cape Town, South Africa, 206pp.

45. Diamond, R. E. and Harris, C., 2000. Oxygen and hydrogen isotope geochemistry of thermal springs of the Western Cape, South Africa: recharge at high altitude? Journal of African Earth Sciences, 31, 467-481.

46. Diamond, R. E. and Harris, C., 2019. Stable isotope constraints on hydrostratigraphy and aquifer connectivity in the Table Mountain Group. South African Journal of Geology, 122, 317-330.

47. Dorland, H. C., Beukes, N.J., Gutzmer, J., Evans, D. A. D. and Armstrong, R.A., 2006. Precise SHRIMP U-Pb zircon age constraints on the lower Waterberg and Soutpansberg Groups, South Africa. South African Journal of Geology, 109, 139-156.

48. Douglas, R. M., 2001. The quality of the Florisbad spring-water in relation to the quality of the groundwater and the effects of rainfall. Water SA, 27, 39-48.

49. Drogue, C., Cat, N. N., and Dazy, J., 2000. Geological factors affecting the chemical characteristics of the thermal waters of the carbonate karstified aquifers of Northern Vietnam. Hydrology and Earth System Sciences, 4, 332-340.

50. Duah, A. A., 2010. Sustainable utilisation of Table Mountain Group aquifers. Unpublished PhD. thesis, University of Cape Town, Cape Town, South Africa, 167pp.
51. Durowoju, O. S., 2015. Trace element concentrations in geothermal springs and their impact on soil and vegetation in Siloam and Tshipise. Unpublished MSc thesis, University of Venda, Thohoyandou , South Africa, 116pp.
52. Durowoju, O.S., Odiyo, J. O. and Ekosse, G.E., 2016. Horizontal variation in trace elements and soil characteristics at Siloam and Tshipise geothermal springs, Limpopo Province, South Africa. Water SA, 42, 694-702.
53. Durowoju, O.S., Odiyo, J. O. and Ekosse, G.I., 2018. Geochemistry of Siloam and Tshipise geothermal springs, Limpopo province, South Africa. American Journal of Environmental Sciences, 14, 63-76.
54. Durowoju, O. S., Butler, M., Ekosse, G. I. E. and Odiyo, J. O., 2019. Hydrochemical processes and isotopic study of geothermal springs within Soutpansberg, Limpopo Province, South Africa. Applied Sciences, 9, 18.
55. Eglington, B. M., 2006. Evolution of the Namaqua-Natal Belt, Southern Africa–A geochronological and isotope geochemical review. Journal of African Earth Sciences, 46, 93-111.
56. Electricity Regulation Amendment Bill., 2023. Parliament: Minister of Mineral Resources and Energy, B23-2023. Pretoria, South Africa, 31pp.
57. Ellis, A. J., 1979. Chemical geothermometry in geothermal systems. Chemical Geology, 25, 219-226.
58. El-Sayed, M. H., Abo El-Fadl, M. M. and Shawky, H. A., 2012. Impact of hydrochemical Processes on Groundwater Quality, Wadi Feiran, South Sinai, Egypt. Australian Journal of Basic and Applied Sciences, 6, 638-654.
59. ENGINE Coordination Action., 2008. Best practice handbook for the development of unconventional geothermal resources with a focus on enhanced geothermal system. Collection Actes/Proceedings, BRGM Editions, Orleans, 97pp. [Online] Available at: http://engine.brgm.fr/Documents/ENGINE_BestPracticeHandbook.pdf
60. Feng, J. L., Lin, Y. C., Gao, S. P. and Zhang, J. F., 2012. Enrichment of trace elements in ferromanganese concretions from terra rossa and their potential desorption. Geochemical Journal, 46, 151-161.

61. Fourie, C. J. S. and Johnson, D., 2017. Analysis of the geothermal structures of Aliwal North, South Africa. Power Generation Africa Conference, Johannesburg, South Africa.
62. Fournier, R. O., 1977. Chemical geothermometers and mixing models for geothermal systems. Geothermics, 5, 41–50.
63. Fournier, R. O., 1982. Geochemistry in geothermal exploration and production. Proceedings of Pacific Geothermal Conference 1982 incorporating the 4th New Zealand Geothermal Workshop. Auckland, New Zealand, 1, 209-216.
64. Fournier, R. O. and Potter, R. W. II., 1982. A revised and expanded quartz geothermometer. Bulletin Geothermal Resource Council Bulletin, 11, 3-9.
65. García-Arias, M., Camera, M. M., Dahlquist, J. A., Gao, P., Couzinié, S. and Díez-Montes, A., 2024. The tectonic significance of peri-Gondwanan Late Neoproterozoic-Early Palaeozoic felsic peraluminous magmatism. Earth-Science Reviews, 104803.
66. Gehringer, M. and Loksha, V., 2012. Geothermal Handbook: Planning and financing power generation. Energy Sector Management Assistance Program; The World Bank, Washington, 150pp.
67. Geng, H., Brandl, G., Sun, M., Wong, J. and Kröner, A., 2014. Zircon ages defining deposition of the Palaeoproterozoic Soutpansberg Group and further evidence for Eoarchaean crust in South Africa. Precambrian Research, 249, 247-262.
68. Gevers, T. W., 1942. The hot springs in the Tugela River near Kranskop, Natal. South African Journal of Geology, 45, 65-74.
69. Gevers, T. W., 1963. Thermal springs at Lilani, Natal, and their geologic setting. South African Journal of Geology, 66, 129-156.
70. Geyh, M., 2000. Environmental isotopes in the hydrological cycle: Principles and applications. UNESCO and IAEA, Paris, 196pp.
71. Giampaoli, S., Valeriani, F., Gianfranceschi, G., Vitali, M., Delfini, M., Festa, M.R., Bottari, E. and Spica, V.R., 2013. Hydrogen sulfide in thermal spring waters and its action on bacteria of human origin. Microchemical Journal, 108, 210-214.
72. Giggenbach, W. F., 1986. Graphical techniques for the evaluation of water/rock equilibration conditions by use of Na, K, Mg and Ca contents of discharge

waters. Proceedings of the 8th New Zealand Geothermal Workshop, New Zealand, 37-44.

73. Giggenbach, W. F., 1988 a, b. Geothermal solute equilibria. Derivation of Na–K–Mg–Ca geoindicators. Geochimica et cosmochimica acta, 52, 2749-2765.
74. Gokcen, G., Ozturk, H. K. and Hepbasli, A., 2004. Overview of Kizildere geothermal power plant in Turkey. Energy conversion and management, 45, 83-98.
75. Gravelét-Blondin, K. R., 2013. A geological and hydrogeological study of the Shu Shu thermal springs, KwaZulu-Natal. Unpublished MSc thesis, University of KwaZulu-Natal, Durban, South Africa, 170pp.
76. Gudmundsson, J. S., Freeston, D. H. and Lienau, P. J., 1985. The Lindal diagram. Geothermal Research Council Transactions, 9, 15-19.
77. Gökgöz, A., 1998. Geochemistry of the Kizildere-Tekkehamam-Buldan-Pamukkale geothermal fields, Turkey. Geothermal training programme, United Nations University, Iceland, 5, 115-156.
78. Güleç, N., 2005. Applications of geothermometry, geothermal geochemistry and some new geothermal approaches. In: M. Y. Savaşçın and O. Mertoğlu, (Editors), Reviewed course book of International Summer School on Geothermal Geochemistry, Dokuz Eylül Üniversity, Ankara, 85–103.
79. Hansma, J., Tohver, E., Schrank, C., Jourdan, F. and Adams, D., 2016. The timing of the Cape Orogeny: New 40Ar/39Ar age constraints on deformation and cooling of the Cape Fold Belt, South Africa. Gondwana Research, 32, 122-137.
80. Harvey, C. C., Beardsmore, G. R., Moeck, I. and Rueter, H., 2016. Geothermal Exploration: Global Strategies and Applications. International Geothermal Association Academy, Bochum, Germany, 196pp.
81. Hattingh, J. and Goedhart, M. L., 1997. Neotectonic control on drainage evolution in the Algoa Basin, southeastern Cape Province. South African Journal of Geology, 100, 43-52.
82. Henley, R. W., Truesdell, A.H., Barton, P. B. and Whitney, J. A., 1984. Fluid-mineral equilibria in hydrothermal systems. In: Reviews Economic Geology, Society of Economic Geologists, Yale, 267pp.

83. Henry, S., 2020. The hydrochemical and isotopic characterization of groundwater in southern Mozambique. Unpublished MSc thesis, University of Cape Town, Cape Town, South Africa, 77pp.
84. Herzhegovina, H. H., Abdurrachman, M., Hafidh, M. and Divi, M., 2020. Geochemical Exploration of Geothermal Manifestations: Study case of Bajawa Volcanic Complex, Flores Island, East Nusa Tenggara Province. IOP Conference Series: Earth and Environmental Science, 589, 012006.
85. Hicks, N. and Gold, D. J. C., 2020. Lithostratigraphy of the Sinqeni Formation, Pongola Supergroup, South Africa. South African Journal of Geology, 123, 399-420.
86. Hoffmann, J. R. H., 1979. Die chemiese samestelling van warmwaterbronne in Suid- en Suidwes-Afrika, CSI report no. WAT 56A. Council for Scientific and Industrial Research, Pretoria, 21pp.
87. Hongmei, W., Lidai, Z. H. O. U. and Yu, G., 2006. Application of cation temperature scale in medium-low temperature geothermal resource. Journal of Heilongjiang Institute of Science and Technology, 16, 27-30.
88. Hoole, R. J., 2000. The development of Lilani Hot Springs: an analysis of socio-economic and environmental impacts. Unpublished MSc thesis, University of Natal, Pietermaritzburg, South Africa, 165pp.
89. Hubert, E. and Wolkersdorfer, C., 2015. Establishing a conversion factor between electrical conductivity and total dissolved solids in South African mine waters. Water SA, 41, 490-500.
90. Huttrer, G. W., 2021. Geothermal power generation in the world 2015-2020 Update report. Proceedings World Geothermal Congress 2020+1, Reykjavík Iceland.
91. Idrissi, O., Orucu, Y., Hallgrimsdottir, E., Mateos Merino, A. and Akin, S., 2021. Understanding CO_2 emissions from geothermal power generation in Turkey. World Bank Publications Report, LiveWire. 10pp.
92. IGA Service GmbH, 2014. Best practices guide for geothermal exploration (2nd Edition). Bochum University of Applied Sciences, Bochum, Germany, 194pp.
93. Jansen, H., 1982. The geology of the Waterberg basins in the Transvaal, Republic of South Africa. Memoir Geological Survey of South Africa, Pretoria, 71, 98pp.

94. JICA., 2014. Data collection survey on geothermal energy development in the East Africa final report (Uganda). Japan International Cooperation Agency West, Japan engineering consultants, Inc. Mitsubishi materials techno cooperation, Japan, 53-70pp.
95. Joao, S. A., Salie, K., Jackson, T. K., Guwa, O. and Wilson, L., 2022. The utilisation of geothermal water for Tilapia aquaculture to promote food security and skills development at the Brandvlei correctional services centre, Water Research Commission report no. TT 892/22. Water Research Commission, Pretoria, 66pp.
96. Johnson, M. R., Anhaeusser, C. R. and Thomas, R. J., 2006. The Geology of South Africa. Geological Society of South Africa and Council for Geoscience, Johannesburg and Pretoria, 691pp.
97. Johnston, S. T., 2000. The Cape Fold Belt and syntaxis and the rotated Falkland Islands: dextral transpressional tectonics along the southwest margin of Gondwana. Journal of African Earth Sciences, 31, 51-63.
98. Jolie, E., Scott, S., Faulds, J., Chambefort, I., Axelsson, G., Gutiérrez-Negrín, L. C., Regenspurg, S., Ziegler, M., Ayling, B., Richter, A. and Zemedkun, M. T., 2021. Geological controls on geothermal resources for power generation. Nature Reviews Earth and Environment, 2, 324-339.
99. Jones, M. Q. W., 1988. Heat flow in the Witwatersrand Basin and environs and its significance for the South African shield geotherm and lithosphere thickness. Journal of Geophysical Research: Solid Earth, 93, 3243-3260.
100. Jones, M. Q. W., 2017. Anomalous geothermal gradients and heat flow in the Limpopo Province, South Africa: Implications for geothermal energy exploration. South African Journal of Geology, 120, 231-240.
101. Jones, M. Q. W. and Scheiber-Enslin, S. E., 2022. Heat flow in the Main Karoo Basin, South Africa. South African Journal of Geology, 125, 345-360.
102. Jonker, C. Z., 2016. Balneological classification of South African thermal springs. Unpublished PhD thesis, University of South Africa, Pretoria, 451pp.
103. Kaczmarczyk, M., Tomaszewska, B. and Operacz, A., 2020. Sustainable utilization of low enthalpy geothermal resources to electricity generation through a cascade system. Energies, 13, 2495.

104. Kai, B., Xiaojun, N., Weimin, W., Xiaojun, W., Yu, P. and Panchal, B., 2020. Application of geothermal thermometric scale in the study of deep reservoir temperature. Energy Exploration and Exploitation, 38, 2618-2630.
105. Kenan, A. O. and Chirenje, E., 2016. Uranium in South Africa: Exploration and supply capacity. Natural Resources and Conservation, 4, 25-33.
106. Kent, L. E., 1946. The warm springs at Loubad, near Nylstroom, Transvaal. Transactions of the Royal Society of South Africa, 31, 151-168.
107. Kent, L. E., 1949. The thermal waters of the union of South Africa and Southwest Africa. South African Journal of Geology, 52, 231-264.
108. Kent, L. E., 1962a. Warm and cold springs on Richmond, Pilgrims Rest District, Transvaal. Annals of the Geological Survey of South Africa. Government Printer, Pretoria, 1, 175-182.
109. Kent, L. E., 1962b. Die Warmbrom Klein-Tshipise in Noord-Transvaal. Annals of the Geological Survey of South Africa. Government Printer, Pretoria, 1, 169-173.
110. Kent, L. E., 1979. Buffelskloof warm spring, Eastern Transvaal. Annals of the Geological Survey of South Africa. Government Printer, Pretoria, 13, 139-150.
111. Kent, L. E., 1980. The warm springs near Burgersfort, Eastern Transvaal. Annals of the Geological Survey of South Africa, 14, 105-115.
112. Kent, L. E., 1980. Warm springs near Hazyview, Eastern Transvaal. Annals of the Geological Survey of South Africa, Pretoria, 14, 33-42.
113. Kent, L. E., 1981. The thermal springs of south-eastern Transvaal and northern Natal. Annals of the Geological Survey of South Africa, 15, 51-67.
114. Kent, L. E., 1986. The thermal saline springs of north-eastern Transvaal. Annals of the Geological Survey of South Africa, 20, 141-154.
115. Kent, L. E. and Groeneveld, D., 1962b. Warm and cold springs on Richmond, Pilgrim's Rest district, Transvaal. Transvaal and northern Natal. Annals of the Geological Survey of South Africa, 1, 75-182.
116. Kent, L. E., Groeneveld, D. and Temperley, B.N., 1966. Thermal springs and groundwater of the Badfontein Valley, Eastern Transvaal. Annals of the Geological Survey of South Africa, 5, 29-151.

117. Kent, L. E. and Haughton, S.H., 1942. The Letaba hot spring. Transactions of the Royal Society of South Africa, 29, 35-47.

118. Kent, L.E. and Russell, H.D., 1949. The warm spring on Buffelshoek, near Thabazimbi, Transvaal. Transactions of the Royal Society of South Africa, 32, 161-175.

119. Kerjha, 2021. Kerjha, Headlines. [Online] Available at: https://kerjha.com/memetik-ragam-manfaat-energi-panas-bumi/. Accessed 05 August 2021.

120. Khosrawi, K., 1966. Geochemistry of geothermal springs in the Sabalan area, Azarbydjan-Iran. Geothermal training programme, United Nations University. Reykjavík, Iceland, 135-158.

121. Khoza, D. T., Jones, A. G., Muller, M. R., Evans, R. L., Webb, S. J. and Miensopust, M. P., 2013. Tectonic model of the Limpopo belt: Constraints from magnetotelluric data. Precambrian Research, 226, 143-156.

122. Kiełczawa, B., 2023. Determination of reservoir temperatures of low-enthalpy geothermal systems in the Sudetes (SW Poland) using multicomponent geothermometers. Water, 15, 422.

123. Kisters, A. F., Belcher, R.W., Scheepers, R., Rozendaal, A., Jordaan, L. S. and Armstrong, R.A., 2002. Timing and kinematics of the Colenso Fault: The Early Paleozoic shift from collisional to extensional tectonics in the Pan-African Saldania Belt, South Africa. South African Journal of Geology, 105, 257-270.

124. Kramers, J.D., McCourt, S., Roering, C., Smit, C.A. and Van Reenen, D.D., 2011. Tectonic models proposed for the Limpopo complex: Mutual compatibilities and constraints. Memoir of the Geological Society of America, 207, 311-324.

125. Linol, B., Dhansay, T., De Wit, M. and De Wit, M., 2021. The Cape Fold Belt and Karoo Basin of South Africa. In: D. Alderton and S.A. Elias (Editors). Encyclopedia of Geology, (2nd Edition). Elsevier, United Kingdom, 220–243.

126. Linol, B. and De Wit, M. J., 2016. Origin and evolution of the Cape Mountains and Karoo Basin. In: Regional Geology Reviews. Springer International Publishing, Switzerland, 45-54.

127. Lopez, S., Hamm, V., Le Brun, M., Schaper, L., Boissier, F., Cotiche, C. and Giuglaris, E., 2010. 40 years of Dogger aquifer management in Ile-de-France, Paris Basin, France. Geothermics, 39, 339-356.

128. Lund, J. W. and Toth, A. N., 2020. Direct utilization of geothermal energy 2020 Worldwide Review. Proceedings World Geothermal Congress 2020+1, Reykjavík, Iceland, 1-39.
129. Madi, K., Nyabeze, P., Gwavava, O., Sekiba, M. and Zhao, B., 2014. Uranium, thorium and potassium occurrences in the vicinity of hot springs in the northern neotectonic belt in the Eastern Cape Province, South Africa. Journal of Radioanalytical and Nuclear Chemistry, 301, 351-363.
130. Mahwa, J., Ping, J., Leng, W., Zhao, J. and Liu, J., 2023. Tectonics and hydrogeochemical features of geothermal waters in Tangyin Rift SE Taihang Mountain. Geothermics, 109, 102657.
131. Makhubele, M. H., and Bordy, E. M., 2021. Sequence stratigraphy in the Algoa and Gamtoos basins (South Africa): a shoreline's journey since the Middle Mesozoic. Geo-Marine Letters, 41, 52.
132. Masindi, K. and Abiye, T., 2018. Assessment of natural and anthropogenic influences on regional groundwater chemistry in a highly industrialized and urbanized region: a case study of the Vaal River Basin, South Africa. Environmental Earth Sciences, 77, 1-14.
133. Matsumura, R., 2014. The petrogenesis of the Nelshoogte pluton: The youngest and most compositionally variable TTG pluton in the Barberton Granite-Greenstone Terrain. Unpublished MSc thesis, Stellenbosch University, Stellenbosch, South Africa, 108pp.
134. Mazor, E., 2003. Chemical and isotopic groundwater hydrology. Marcel Dekker Incorporation, New York, 453pp.
135. Mazor, E. and Verhagen, B. T., 1983. Dissolved ions, stable and radioactive isotopes and noble gases in thermal waters of South Africa. Journal of Hydrology, 63, 315-329.
136. McCleskey, R. B., Nordstrom, D. K. and Ryan, J. N., 2012. Comparison of electrical conductivity calculation methods for natural waters. Limnology and Oceanography: Methods, 10, 952-967.
137. Michel, R. L., 2004. Tritium hydrology of the Mississippi River basin. Hydrological Processes, 18, 1255-1269.
138. Misra, S., Reinhardt, J. and Wilson, A. H., 2017. Petrochemical evolution of the White Mfolozi Granite pluton: evidence for a late Palaeoarchaean A-type granite from the SE Kaapvaal Craton, South Africa. Lithos, 286, 480-501.

139. Mlaba, K., 2021. Global citizen-News. [Online] Available at: https://www.globalcitizen.org/en/content/cop26-south-africa-funding-coal-power/. Accessed 05 November 2021.

140. Moeck, I.S., 2014. Catalog of geothermal play types based on geologic controls. Renewable and Sustainable Energy Reviews, 37, 867-882.

141. Mohamed, A. Z. and Ehara, S., 2009. Heat flow and geothermal resources in Egypt. Journal of the Geothermal Research Society of Japan, 31, 155-166.

142. Mohammed, D. and Garba Abba, H., 2015. Graphical techniques of presentation of hydro-chemical data. Journal of Environmental Earth Sciences, 5, 65-76.

143. Mook, W. G., 2000. Volume I, Introduction theory methods review. In: W. G. Mook (Editor), Environmental isotopes in the hydrological cycle: Principles and applications. UNESCO, Paris, 280pp.

144. Moore, J. M., Tsikos, H. and Polteau, S., 2001. Deconstructing the Transvaal Supergroup, South Africa: Implications for Palaeoproterozoic palaeoclimate models. Journal of African Earth Sciences, 33, 437-444.

145. Moyen, J. F., McCoy-West, A. J., Bruand, E., Millet, M. A., Nebel, O., Cawood, P. A., Saji, N., Ladwig, A., Klaver, M. and Elburg, M., 2024. Felsic crust development in the Kaapvaal Craton, South Africa: A reference sample collection to investigate a billion years of geological history. Earth-Science Reviews, 250, 1-35.

146. Mtimkulu, M. N., 2009. A provisional basinal study of the Waterberg-Karoo, South Africa. Unpublished MSc thesis. University of Pretoria, Pretoria, 133pp.

147. Mukasa, S. B., Wilson, A. H. and Young, K. R., 2013. Geochronological constraints on the magmatic and tectonic development of the Pongola Supergroup (Central Region), South Africa. Precambrian Research, 224, 268-286.

148. Murray, R., Swana, K., Miller, J., Talma, S., Tredoux, G., Vengosh, A. and Darrah, T., 2015. The use of chemistry, isotopes and gases as indicators of deeper circulating groundwater in the Main Karoo Basin. Water Research

Commission report no. 2254/1/15. Water Research Commission, Pretoria, 215pp.

149. Nemzer, M., Page, D.S. and Carter, A.K., 2005. Energy for Keeps: Electricity from Renewable Energy: An Illustrated Guide for Everyone who Uses Electricity. Energy Education Group, California, USA, 29-38.

150. Okoroafor, E. R., Smith, C. M., Ochie, K. I., Nwosu, C. J., Gudmundsdottir, H. and Aljubran, M., 2022. Machine learning in subsurface geothermal energy: Two decades in review. Geothermics, 102,102401.

151. Olivier, J. and Jonker, N., 2013. Optimal utilisation of thermal

152. springs in South Africa. Research Commission report no. TT577. Water Research Commission, Pretoria, 144pp.

153. Olivier, J., Van Niekerk, H. J. and Van der Walt, I. J., 2008. Physical and chemical characteristics of thermal springs in the Waterberg area in Limpopo Province, South Africa. Water SA, 34, 163-174.

154. Olivier, J., Venter, J. S. and Van Niekerk, H. J., 2010. Physical and chemical characteristics of thermal springs in Limpopo Province, South Africa. Proceedings World Geothermal Congress-2010. Bali, Indonesia, 1482.

155. Olivier, J., Venter, J. S. and Jonker, C. Z., 2011. Thermal and chemical characteristics of hot water springs in the northern part of the Limpopo Province, South Africa. Water SA, 37, 427-436.

156. Omenda, P. A. and Karingithi, C. W., 1993. Hydrothermal model of Ebburru geothermal field, Kenya. Geothermal Resources Council Transactions, 17, 155-160.

157. Omenda, P., Ofwona, C., Mangi, P. and Mwangi, M., 2020. Country update report for Kenya 2020. 8th African Rift Geothermal Conference Proceedings, Nairobi, Kenya.

158. Onyango, S. and Varet, J., 2014. For a new social gender-based approach to local geothermal development. Arusha. 5th African Rift Geothermal Conference Proceedings, Arusha, Tanzania.

159. Osman, A. I., Hefny, M., Abdel Maksoud, M. I. A., Elgarahy, A. M. and Rooney, D. W., 2021. Recent advances in carbon capture storage and utilisation technologies: a review. Environmental Chemistry Letters, 19, 97-849.

160. Pang, Z. H. and Reed, M., 1998. Theoretical chemical thermometry on geothermal waters: problems and methods. Geochimica et Cosmochimica Acta, 62, 1083-1091.

161. Paiz Ramirez, C. D., 2021. The San Michkael Project, an example of multiple direct uses of low to medium enthalpy geothermal source for developing countries. Proceedings World Geothermal Congress 2020+1. Reykjavík, Iceland.

162. Pankhurst, R. J., Rapela, C. W., Fanning, C. M. and Márquez, M., 2006. Gondwanide continental collision and the origin of Patagonia. Earth-Science Reviews, 76, 235-257.

163. Paton, D. A., MacDonald, D. I. M. and Underhill, J. R., 2006. Applicability of thin or thick skinned structural models in a region of multiple inversion episodes; southern South Africa. Journal of Structural Geology, 28, 1933-1947.

164. Piper A. M., 1944. A graphical procedure in the geochemical interpretation of water analyses. Eos Transactions American Geophysical Union, 25, 914-923.

165. Poujol, M., Robb, L. J., Anhaeusser, C. R. and Gericke, B. 2003. A review of the geochronological constraints on the evolution of the Kaapvaal Craton, South Africa. Precambrian research, 127, 181-213.

166. Rattanawong, T., Bissen, R., Kumpairoh, W. and Chawchai, S., 2020. Geochemical Characteristics of three hot springs from Western Thailand. Applied Environmental Research, 42, 101-113.

167. Reczko, B. F. F., 1994. The geochemistry of the sedimentary rocks of the Pretoria Group, Transvaal Sequence. Unpublished PhD thesis, University of Pretoria, Pretoria, South Africa, 385pp.

168. Riley, T. R., Leat, P. T., Curtis, M. L., Millar, I. L., Duncan, R. A. and Fazel, A., 2005. Early–Middle Jurassic dolerite dykes from Western Dronning Maud Land (Antarctica): identifying mantle sources in the Karoo large igneous province. Journal of Petrology, 46, 1489-1524.

169. Rindl, M. R., 1916. The medicinal springs of South Africa. South African Journal of Science, 13, 528-552.

170. Rindl, M. R., 1918. The medicinal springs of South Africa (Supplement). South African Journal of Science, 15, 217-225.

171. Rindl, M. R., 1928. The medicinal springs of South Africa (Supplement). South African Journal of Science, 25, 116-126.

172. Rindl, M. R., 1930. International standard measurements in hydrology and a provisional register of medicinal waters of South Africa based on these standards. South African Journal of Science, 27, 213-226.

173. Rindl, M. R., 1931. The medicinal springs of South Africa (Supplement). South African Journal of Science, 28, 119-130.

174. Rindl, M. R., 1932. The medicinal springs of South Africa (Supplement). South African Journal of Science, 29, 278-280.

175. Rindl, M. R., 1934. The medicinal springs of South Africa (Supplement). South African Journal of Science, 31, 173-176.

176. Rindl, M. R., 1937. The medicinal springs of South Africa (Supplement). South African Journal of Science, 33, 254-257.

177. Rindl, M. R., 1940. The medicinal springs of South Africa (Supplement). South African Journal of Science, 13, 433-434.

178. Robb, L.J., Mayer, F.M., Hawkesworth, C.J. and Gardiner, N.J., 2021. Petrogenesis of Archean granites in the Barberton region of South Africa as a guide to early crustal evolution. South African Journal of Geology, 124,111-140.

179. Rosenberg, M.D., Bignall, G. and Rae, A.J., 2009. The geological framework of the Wairakei–Tauhara geothermal system, New Zealand. Geothermics, 38, 72-84.

180. Rubio-Maya, C., Diaz, V.A., Martínez, E.P. and Belman-Flores, J. M. (2015). Cascade utilization of low and medium enthalpy geothermal resources - A review. Renewable and Sustainable Energy Reviews, 52, 689-716.

181. Rybach, L., 1981. Geothermal systems, conductive heat flow, geothermal anomalies. In: L. Rybach and L. J. P. Muffler (Editors). Geothermal Systems: Principles and case histories. John Wiley and Sons, Chichester, UK, 3-31.

182. Santoyo, E. and Díaz-González, L., 2010. A new improved proposal of the Na/K geothermometer to estimate deep equilibrium temperatures and their uncertainties in geothermal systems. Proceedings World Geothermal Congress-2010. Bali, Indonesia, 25-29.

183. Schmitz, M. D., Bowring, S.A., De Wit, M.J. and Gartz, V., 2004. Subduction and terrane collision stabilize the western Kaapvaal craton tectosphere 2.9 billion years ago. Earth and Planetary Science Letters, 222, 363-376.

184. Schoeller, H., 1963. La classification géochemique des eaux. Hydrological Sciences Journal, 8, 16-24.

185. Scott, S. W., Covell, C., Júlíusson, E., Valfells, Á., Newson, J., Hrafnkelsson, B., Pálsson, H. and Gudjónsdóttir, M., 2019. A probabilistic geologic model of the Krafla geothermal system constrained by gravimetric data. Geothermal Energy, 7, 1-30.

186. Serpen, U. and DiPippo, R., 2022. Turkey - A geothermal success story: A retrospective and prospective assessment. Geothermics, 101, 102370.

187. Shabalala, A., Nyabeze, P.K., Mankayi, Z. and Olivier, J., 2015. An analysis of the groundwater chemistry of thermal springs in the Soutpansberg Basin in South Africa: Recent data. South African Journal of Geology, 118, 83-90.

188. Shestakova, A., Guseva, N., Kopylova, Y., Khvaschevskaya, A., Polya, D.A. and Tokarev, I., 2018. Geothermometry and isotope geochemistry of CO_2-rich thermal waters in Choygan, East Tuva, Russia. Water, 10, 729.

189. Stedman, R. L. and Hunter, D. R., 1990. Note on the Archaean geology, southeast of Paulpietersburg, northern Natal. South African Journal of Geology, 93, 857-863

190. Stefánsson, A., Driesner, T. and Bénézeth, P., 2013. Thermodynamics of geothermal fluids. Reviews in Mineralogy and Geochemistry, 76, 1-4.

191. Stettler, E.H., De Beer, J.H. and Blom, M.P., 1989. Crustal domains in the northern Kaapvaal Craton as defined by magnetic lineaments. Precambrian Research, 45, 263-276.

192. Stober, I. and Bucher, K., 2013. Geothermal Energy: From theoretical models to exploration and development. Springer, Heidelberg, Berlin, 1-64.

193. Sveinbjörnsson, B. M., 2016. Medium enthalpy geothermal systems in Iceland, thermal and electric potential. Iceland Geosurvey. Reykjavík, Iceland, 123pp.

194. Swana, K., 2016. Application of hydrochemistry and residence time constraints to distinguish groundwater systems in the Karoo Basin prior to shale-gas exploration. Unpublished MSc thesis. Stellenbosch University, South Africa, 111pp.

195. Sæmundsson, K., 1991. The geology of the Krafla system. In: A. Gardarsson and Á. Einarsson (Editors). The Natural History of Mývatn (in Icelandic). Hidíslenska náttúrufrædifélag, Reykjavík, Iceland, 25-95.

196. Tassi, F., Vaselli, O., Moratti, G., Piccardi, L., Minissale, A., Poreda, R., Delgado Huertas, A., Bendkik, A., Chenakeb, M. and Tedesco, D., 2006. Fluid geochemistry versus tectonic setting: the case study of Morocco. Geological Society Special Publications. London, 262, 131-145.

197. Temizel, E. H., Gültekin, F., Ersoy, A. F. and Gülbay, R. K., 2021. Multi-isotopic (O, H, C, S, Sr, B, Li) characterization of waters in a low-enthalpy geothermal system in Havza (Samsun), Turkey. Geothermics, 97, 102240.

198. Temperley, B. N., 1964. Thermal springs on Frischgewaag 236 near Paulpietersburg, Natal. Annals of the Geological Survey of South Africa, 3, 129pp.

199. Temperley, B. N., 1975. The Welgevonden Fault aquifer of the Central Traansvaal and it's thermal water: Groundwater Series No. 2, Geological Survey of South Africa, Pretoria, 22pp.

200. The World Bank Group, 2021. Climate change knowledge portal. [Online] Available at: https://climateknowledgeportal.worldbank.org/country/south-africa/climate-data-historical.Accessed on 24 January 2024.

201. Thomas, R. J., 1989. A tale of two tectonic terranes. South African Journal of Geology, 92, 306-321.

202. Thomas, R. J., Agenbacht, A. L. D., Cornell, D.H. and Moore, J.M., 1994. The Kibaran of Southern Africa: Tectonic evolution and metallogeny. Ore Geology Reviews, 9, 131-160.

203. Truesdell, A. H., 1976. Summary of section III-geochemical techniques in exploration. Proceedings 2nd UN Symposium on the development and use of geothermal resources, 1, 1iii-1xxix.

204. Tshibalo, A. E., Olivier, J. and Nyabeze, P. K., 2015. South Africa Geothermal Country Update (2010-2014). Proceedings of the World Geothermal Congress-2015, Melbourne, Australia.

205. Tshibalo, A. E., Olivier, J. and Venter, J., 2010. South Africa Geothermal Country Update (2005-2009). Proceedings World Geothermal Congress-2010. Bali, Indonesia.

206. Tshibalo, A. E. and Tekere, M., 2015. An evaluation of the potential Spirulina production at selected thermal springs in Limpopo, South Africa. Proceedings of the World Geothermal Congress-2015, Melbourne, Australia.

207. Türkiye Sınai Kalkınma Bankası A. Ş., 2023. Energy Outlook 2023. Türkiye Sınai Kalkınma Bankası A. Ş, Türkiye, 40pp.

208. Uzelli, T., Baba, A., Mungan, G. G., Dirik, R. K. and Sözbilir, H., 2017. Conceptual model of the Gülbahçe geothermal system, Western Anatolia, Turkey: Based on structural and hydrogeochemical data. Geothermics, 68, 67-85.

209. Van Niekerk, H. S., Elburg, M. A., Andersen, T. and Armstrong, R. A. 2022. Provenance of metasedimentary rocks of the Kheis Terrane and Kakamas Domain: support for accretionary tectonics during the development of the western Namaqua-Natal Metamorphic Province. South African Journal of Geology, 125, 61-78.

210. Verma, S. P. and Santoyo, E., 1997. New improved equations for NaK, NaLi and SiO_2 geothermometers by outlier detection and rejection. Journal of Volcanology and Geothermal Research, 79, 9-23.

211. Viola, G., Andreoli, M., Ben-Avraham, Z., Stengel, I. and Reshef, M., 2005. Offshore mud volcanoes and onland faulting in southwestern Africa: Neotectonic implications and constraints on the regional stress field. Earth and Planetary Science Letters, 231, 147-160.

212. Von Backström, J. W., 1957. The Riemvasmaak thermal spring, Gordonia District, Cape Province, Report No. GH1025. Geology Water Affairs, Pretoria, 6pp.

213. Von Backström J. W., 1962. Thermal springs on Driefontein 317 KR north of Naboomspruit, Potgietersrus District, Transvaal. Annals of the Geological Survey of South Africa, 1, 183-187.

214. Wallis, I. C., Rowland, J. V. and Demsey, D., 2018. The relationship between geothermal fluid flow and geologic context: A global review. Geothermal Resources Council Transactions, 42, 1-19.

215. Wang, H., Yang, J. H., Kröner, A., Zhu, Y. S., Wei, Q. D., Li, R. and Xu, L., 2020. Extensive magmatism and metamorphism at ca. 3.2 Ga in the eastern Kaapvaal Craton. Precambrian Research, 351, 105952.

216. Waring, G. A., 1965. Africa. In: R.R. Blankenship and R. Bentall (Editors). Thermal springs of the United States and other countries of the world: A summary. US Government Printing Office, Washington, 139-165.

217. Weaver, J. M. C., Talma, A. S. and Cavé, L. C., 1999. Geochemistry and isotopes for resource evaluation in the fractured rock aquifers of the Table Mountain Group, Water Research Commission report no. 481/1/99. Water Research Commission, Pretoria, 298pp.

218. Weaver, J. M. C., Cavé, L. and Talma, A. S., 2007. Groundwater Sampling: A comprehensive guide for sampling methods (2nd Edition). Water Research Commission report no. TT 303/07. Water Research Commission, Pretoria, 168pp.

219. Western Cape Branch of the Geological Survey of South Africa, 2013. Brandvlei hot springs. Council for Geoscience, Pretoria, 6pp.

220. Wilson, A., Groenewald, B. and Palmer, C., 2013. Volcanic and volcaniclastic rocks of the Mesoarchaean Pongola Supergroup in South Africa and Swaziland: distribution, physical characteristics, stratigraphy and correlations. South African Journal of Geology, 116(1), 119-168.

221. Xasa, F., 2021. Parliamentary Monitoring Group. [Online] Available at: https://pmg.org.za/committee-meeting/32417/. Accessed on 25 January 2022.

222. Yan, B., Qiu, S., Liu, Z., and Changlai, X., 2017. Characteristics of the geothermal water in Changbai Mountain volcanic region, northeast of China. Arabian Journal of Geosciences, 10, 1-13.

223. Yu, M., Wang, G., Ma, F., Zhang, W., Lin, W., Zhu, X. and Zhang, H., 2022. Geochemical characteristics of geothermal fluids of a deep ancient buried hill in the Xiong'an new area of China. Water, 14, 3182.

224. Zheng, B., Xu, J., Ni, T. and Li, M., 2015. Geothermal energy utilization trends from a technological paradigm perspective. Renewable Energy, 77, 430-441.

225. Zhenhua, R., Xun, Z., Miaolin, Y., Xiaocui, W., Yuhui, Z., Xiaolu, L. and Ye, S., 2018. Hydrochemical characteristics and formation of the Madeng hot spring in Yunnan, China. Geofluids, 2018, 2368246.

Appendix A: A comprehensive list of the analyses of geothermal waters from Kent (1949); Waring (1965) and Olivier and Jonker (2013).

Kent (1949) compilation of physicochemical analyses.

Ob_ID	Geothermal water sites	Temp. (°C)	Flow (cm^3/day)	TDS ppm at 110°C	Classification	Geological Structure determining origin	Date of Observed temperature and flow rate	Person observed temperature of the geothermal water site
12	Welgevonden	44	57	0		Diabase dyke along post Karroo (post-Permian) fault in Rooiberg felsites.	1938	Backström,J.W
6	Badplaats	50	817	335	D	Fracture in Archean granite	1948	Baths Superintendent
20	Lilani	39	0	0	D(S)	Fracture zone in Archean gneisses and amphibolites	1916	Du Toit, A.L
43	Etmembeni	28	0	0	0	Dolerite sill in Ecca series (Permian) shale	1931	Du Toit, A.L
3	Tugela Valley	52-53	00	0	A (SO4)	Fault in Archean Amphibolites and gneiss	1942	Grevers, T.W
13	Souting	43.9	136	0	A	Fault in Archean granite	1945	Grevers, T.W
14	Mphefu	42.8	0	0	E	Pre-Karoo (pre-Carboniferous) fault	1939	Kent, L.E
16	Tugela	42.8	12	1518	A	Joints in Archean gneiss	1948	Kent, L.E
17	Letaba	41	413		A	Dolerite dyke in Archean gneissic granite	1942	Kent, L.E
19	Goudini	40.1	0	0	E	Middle cretaceous graben in Cape system	1945	Kent, L.E
26	Loubad	31	1870	194	E	Artesian basin in Waterberg System	1940	Kent, L.E
27	Gamka valley	32.8	297	150	E(Fe)	Middle cretaceous fault in Table Mountain Series	1947	Kent, L.E
29	Grovesbac	32.8	0	0	0	Fissures in Bushveld granite	1942	Kent, L.E
30	Evangelina	32.5	0	0	A	Diabase dyke in Archean granite	1941	Kent, L.E
32	Cradock	30	83		D(S)	Dolerite dyke in Beaufort series sediments	1946	Kent, L.E
33	Buffelshoek	30.6	77	459	D	Diabase dyke as barrier on artesian slope of Bushveld granite	1944	Kent, L.E
37	Vetfontein	29.5	0	0	0	Post Karroo fault	1945	Kent, L.E
38	Knega Drift	29.3	0	0	0	Dolerite dyke in Beaufort series	1947	Kent, L.E
39	Riffontein	28.9	36	794	A-B	Fault in Rooiberg series (pre-Cambrian)	1942	Kent, L.E
41	Fort Beaufort	27	79	528	D(S)	Fissure in Beaufort series	1947	Kent, L.E
42	Stinkfontein	28.7	34	0	D(S)	Major joint in syncline of lower Beaufort sediments	1949	Kent, L.E
1	Brandvlei	64.2	11022	0	E	Middle Cretaceous fault in the Cape System	1947	Kent,L.E
5	Olifants Valley	50-51	655	156	E (Fe)	Middle cretaceous fault in Cape system	1947	Kent,L.E
8	Warmwaterberg	45.6	789	190	E (Fe)	Fault at nose of anticline of Table Mountain series	1947	Kent,L.E
11	Toverwater	44.3	980	0	E(Fe)	Middle cretaceous fault in Cape system	1946	Kent,L.E
44	Grasrand	26	16	0	0	Joints in lower Beaufort sediments	1949	Kent, L.E
25	Aliwal North	36.9	3813	0	A	Dolerite dyke in Beaufort series (L.Triassic)	1927	Lewis, S.V.R
31	Sulphur Springs	31	544	0	E(S)		1946	Marais, J.K
18	Black Umfolosi	41	0	0	B(S)	Fissure in Dwyka Tillite overlying Archean rocks	1898	Molengraaff, G
28	Malmesbury	32.9	816	0	A(S)	Fracture zone in Cape granite		Municipality
10	Natal Spa	44.4	294	0	D		1936	Owners
4	Warmbaths	51.9	726	397	D	Post Karroo fault in Bushveld granite	1931	Rindl,M
7	Caledon	49	817	0	E (Fe)	Middle Cretaceous fault in the Cape System	1931	Rindl,M
15	Die Bad	42.7	0	0	0	Barrier spring on west limb of syncline in Cape system	1916	Rindl,M
36	Winburg	29.5	18	0	A		1918	Rindl,M
40	Machadodorp	28	204	0	D		1916	Rindl,M
23	Skuitdrif Oos	38	0	0		Fracture zone in Archean granite	1943	Visser, D.J.L
34	Rooiwal	30	254	0	D	Dolerite dyke in Beaufort series	1947	Visser, D.J.L

Ob_ID	Geothermal water sites	Temp. (°C)	Flow (cm^3/day)	TDS ppm at 110°C	Classification	Geological Structure determining origin	Date of Observed temperature and flow rate	Person observed temperature of the geothermal water site
35	Badsfontein	28	231	0	B	Dolerite dyke in Beaufort series	1947	Visser, D.J.L
24	Gordonia	37.7	0	0	0	Fault in Archean gneiss	1948	Visser, H.N
9	Warmbad Noord	44.4	68	0	-	Fracture zone in Archean granodiorite	1943	Visser, J.L
2	Chipise	57.2	454	0	D,B	Intersection of two post Permian faults in Upper Karroo	1948	Visser,H.N
21	Die Oog	39.5	145	0	E	Diabase dyke along post Karroo (post-Permian) fault in Rooiberg felsites.	1938	von Backstrom, J.W
22	Vischgat	39.5	91	0		Post Karroo fault in Bushveld granite	0	0

Classification of geothermal waters:

A- Highly mineralized Chloride-sulphate waters, Total solids >1000 mgm/l, Cl>27 %, SO_4> 5 %
B- Slightly saline Chloride-sulphate waters, Total solids >300<500 mgm/l, Cl>27 %, SO_4< 3 %
C- Temporary hard Carbonate waters, Total solids <800 mgm/l, pH>7.6
D- Alkaline soda Carbonate waters, Total solids <1000 mgm/l, Na_2CO_3 or $NaHCO_3$> 15 %, Permanent hardness, nil
E- "Pure" Waters, Total solids <150 mgm/l, pH<7.1

Waring (1965) compilation of physicochemical analyses. 0 denotes no value report.

Ob_ID	Geothermal water sites	Temp. (°C)	Flow (imperial gallons/day)	Total dissolved solids (ppm)	Principal chemical constituents	Associated rocks
1	Paddysland	26	0	939	Ca, Mg, Na, HCO_3, Cl	Archean gneiss
2_1	Tugela Spring	42.8	2650	1517	Na, SO_4, Cl	0
2_2	Tugela Flowing well	48.9	15600	0	Na, SO_4, Cl	0
3	Evangelina	32.5	0	1355	Na, SO_4, Cl	Diabase dyke in Archean gneiss
4	Stindal	Warm	0	0	0	0
5	Icon	Warm	0	0	0	0
6	Vetfontein	29.5	0	0	0	Karroo beds_Permain through Jurassic
7	No name	Warm	0	0	0	0
8	Sulphur	Warm	0	0	0	0
9	Windhoek	Warm	0	0	0	0
10	Masequa	Warm	0	0	0	0
11	Gordonia	37.7	0	0	0	Faulted Archean gneiss
12	Klein Chipise	Hot	0	0	0	0
13	Chipise	57;65	100 000	502	Na, HCO_3, Cl	Faulted upper Karroo beds
14	Mpefu	42.8;43.7	0	low		Faulted pre-Carboniferous strata
15	Souting, near west bank of Kelin Letaba River	43.9	3000	high	$CaCO_3$=30,$CaSO_4$=218,NaCl=1270,SiO_2=71,Ca=30,Na=301,SO_4=64,Cl=139	Faulted Archean granite
16_1	Letaba 0.5 mile south of Groot Letaba River spring	40;42	91000	966	0	Dolerite dyke in granite
16_2	Letaba 0.5 mile south of Groot Letaba River flowing well	Warm	12000	0	0	0
17	Buffelshoek farm between Thabazimbi and Rooiberg	30.6	17000	459	0	Diabase dyke in Bushveld granite_Precambrain
18	Loubad_18 miles W-NW of Nylstroom	27-34	414300	188	0	Diabase dyke in Bushveld granite_Precambrain
19	Welgevonden	44	12500	0	0	Faulted Rooiberg felsite_Precambrian
20	Die Oog	39.5	32000	257	Na, HCO_3, Cl	Faulted Rooiberg felsite_Precambrian
21	Vischgat	39.5	20000	0	0	Faulted Bushveld granite
22	Adriaanskop	Warm	0	0	0	0
23	Warmbaths	51.9	160000	408	Na, HCO_3	Faulted Bushveld granite
24	Riffontein	28.3-29	8000	702	Na=235, HCO_3=238, Cl=248	Faulted Rooiberg series
25	Kameelpoort	Warm	0	0	0	0

Ob_ID	Geothermal water sites	Temp. (°C)	Flow (imperial gallons/day)	Total dissolved solids (ppm)	Principal chemical constituents	Associated rocks
26	Goederde	Warm	0	0	0	Bushveld granite
27	Grovesbad	32.8	0	0	0	Bushveld granite
28	Buffelsvlei	Hot	0	0	0	0
29	De Bad	Warm	0	0	0	Pretoria Series_Precambrian
30	Hartebeestspruit	Warm	0	0	0	Pretoria Series_Precambrian
31	Badfontein	Warm	0	0	0	Pretoria Series_Precambrian
32	Machadodorp	27.5-28.5	45000	214	Na, HCO_3	Pretoria Series_Precambrian
33	Badplaats	50	180000	409	Na, HCO_3, much free H_2S	Fractured Archean granite
34	Sulphur near Ermlo	31	120000	130	0	Pongola system_Proterozoic
35	Warm Bad	40;42.5	0	0	0	0
36	Overwacht	Warm	0	0	0	0
37	Natal	44.4	64800	273	Na, HCO_3	Archean granite
38	Black Umfolosi	41	0	0	0	Dwyka tillite Carboniferous
39	Entembeni	28	0	0	0	Dolerite sill in Ecca Shale_Permain
40	In Tugela gorge, 12 miles N-NE of Kranskop	52-53	0	1021	Ca=83, Na_=231, HCO_3=31, SO_4=368, H_2SiO_3=73	Faulted Archean gneiss
41	Lilani, 20 miles from Greytown	38-40	0	Moderately high	Na, HCO3, free H2S	Faulted Archean gneiss
42	Tierbank	Warm	0	0	0	0
43	Wolvepan	28.8	60000	0	0	Ventersdorp Series_Precambrian
44	Jonkersrust	34	48000	3536	0	Ventersdorp Lava
45	Vermenlenskraal	32.7	48000	0	0	Ventersdorp Lava
46	Baden-Baden_Gannafontein	24	480000	0	0	Ecca series_Lermian
47	Florisbad_Rietfontein	28-30	0	2189	0	Ecca series_Lermian
48	Vlakkraal	Warm	0	0	0	0
49	Winburg	29.5	4000	High	Na,SO_4,Cl	Beaufort Series_Lower Triassic
50	Trompsberg	37.2	24000	8463	0	Norite_pre-Karroo
51	Warmbad Noord	44.4	15000	0	0	Fractured Archean granodiorite
52	Skuitsdrif Oos	38	0	0	0	Fractured Archean granite
53	Riemvastmaak	Hot	0	0	0	0
54	Rooiwal	30	56000	Moderately high	Na, HCO_3	Dolerite dyke in Beaufort series_Lower Triassic
55	Badsfontein	25.5-30	51000	0	0	Dolerite dyke in Beaufort series_Lower Triassic
56	Aliwal North	36.9	840600	High	NA, SO_4, Cl, gas of 94% N_2	Dolerite dyke in Beaufort series_Lower Triassic
57	Badtsfontein	Warm	0	0	0	0
58	Kenega Drift	29.3	0	0	0	Dolerite dyke in Beaufort series_Lower Triassic
59	Inungi	25	0	Moderately high	0	Beaufort series_Lower Triassic
60	Die Bad	42.2,43.2	0	0	Table Mountain Sandstone, Devonian	2 springs, baths
61	No name	Warm	0	0	0	0
62	Malmesbury	32	180000	1186	Fractured Cape granite, Devonian	Water is Sulphurous, used for bathing
63	Goudini_Goudine,Jourdeans Bath near DuToit's Kloof	40.1	0	low	Table Mountain Sandstone, Devonian	Baths,
64	Brandvlei_Brand Vley, Brandvalleis	64.2	2430000	5	Faulted Table Mountain Sandstone, Devonian	Water used for bathing,

Ob_ID	Geothermal water sites	Temp. (°C)	Flow (imperial gallons/day)	Total dissolved solids (ppm)	Principal chemical constituents	Associated rocks
65	Caledon	35-42	180000	190	Faulted Table Mountain Sandstone, Devonian	Several springs issuing from iron-manganese mound: water contains considerable Fe. Much C)2, Sanatorium,
66	Baden	Hot	0	0	Faulted Table Mountain Sandstone, Devonian	0
67	Montagu	44.6	0	0	Faulted Table Mountain Sandstone, Devonian	Gass is 88% N2. Sanatorium,
68	No name	Warm	0	0	Faulted Table Mountain Sandstone, Devonian	0
69_1	Warmwaterberg:Spring	45.6	174000	205	Faulted Table Mountain Sandstone, Devonian	Water contains considerable Fe,
69_2	Warmwaterberg: Flowing well	28	31000	0	Faulted Table Mountain Sandstone, Devonian	100 foot deep
70	Gamka Valley	32.3-33.2	65500	low	Faulted Table Mountain Sandstone, Devonian	Water contains considerable Fe, used for bathing
71	Olifants Valley	50-51	144500	197	0	Several springs and wells. Water contains considerable Fe, used for bathing,
72	Stinkfontein	28.7	7500	806	Lower Beaufort series, Triassic	0
73	Kruidfontein	Warm	0	0	0	Pumped well
74	Toverwater_Agter de berg, War bath, Hottentor Holland's Bath, YserBaad_sout of Zwartebergen	44.3	21600	Low	0	Faulted Table Mountain Sandstone_Devonian
75	Grasrand	26	3600	0	0	Lower Beaufort series_Triassic
76	Near Cradock ford of the Fish River	29-31.3	18300	181	Na, HCO3, free H_2S	Dolerite dykes in Lower Beaufort series
77	Tarka Bridge	26-27	0	0	0	0
78	Moerlust	Warm	0	0	0	0
79	Fort Beaufort	27-29	17300	520	Na, HCO3, free H_2S	Lower Beaufort series_Triassic
80	Amanzi_Balmoral	Warm	0	0	0	0
81	Amanzi	Warm	0	0	0	0
82	Zwartkops_4 miles from Port Elizabeth	53.6	25000	365	Na, Cl	Cape System_Devonian

Olivier and Jonker (2013) compilation of physicochemical analyses. Ion analyses is in mg/l.

Ob_ID	Geothermal Water	Temp. (°C)	pH	Total dissolved solids (mg/l)	Electrical Conductivity (µS/cm)	Bicarbonate	Cl	SO_4	F	NO_3	NO_2	Na	K	Ca	Mg
1	Tshipise	57.9	9	436	79.7	116	156	47.5	5	0	0	152	4	5	0
2	Sagole	46.3	9	207	35.4	83	43	17.2	1	0	0	66	1	2	0
3	Evangelina	35.13	7	1323	216	225	507	210.2	4	9	0	355	6	78	27
4	Moreson	44	8	335	56.5	55	87	46	3	12	0	84	3	5	0
5	Mphephu	43.5	8	187	35.2	114	35	8.8	3	1	0	42	1	11	8
6	Siloam	66.1	9	192	32.5	89	44	9.6	6	0	0	61	3	6	0
7	Warmbad	51.97	8	369	69	98	88	12.1	19	0		126	4	10	2
8	Rhemardo	42	7	208	42	122	27	11.8	6	1	0	35	4	23	2
9	Soutini	43.9	7	-	273	34	680	170.3	2		0	486	15	86	5
10	Die Oog	38.83	7	235	34	115	26	10.4	6	1	0	42	4	25	2
11	Vischgat	40.05	7	324	55.5	145	34	97.1	6	1	0	58	6	37	2

Ob_ID	Geothermal Water	Temp. (°C)	pH	Total dissolved solids (mg/l)	Electrical Conductivity (µS/cm)	Bicarbonate	Cl	SO_4	F	NO_3	NO_2	Na	K	Ca	Mg
12	Loubad	30	7	164	25	142	3	2.2	1	0	0	8	3	29	6
13	Buffelshoek	30.05	7	450	-	214	139	35.1	7	0		152	6	27	5
14	Minvamadi	33.4	7	113	21.3	81	19	2.5	0	8	0	11	1	9	13
15	Eiland source	40.77	8	1026	194	70	546	76.7	3	1	0	352	15	34	2
16	Lekkerrus	49	7	162	20	105	7	8	7	0	0	22	5	19	9
17	Libertas	45	7	156	23.7	118	8	7.6	5	0	0	22	3	24	2
18	Brandvlei	63.05	7	48	8.9	19	14	2	0	1	0	10	2	4	2
19	Citrusdal	46.1	6	75	9.1	10	16	2	0	1	0	8	2	2	2
20	Caledon	49	7	116	23.3	38	33	5	0	0	0	18	5	8	3
21	Toverwater	45.15	7	113	20.9	59	25	4	0	0	0	13	7	11	3
22	Goudini	43.05	7	63	10.6	21	10	2	0	0	0	9	2	9	3
23	Calitzdorp	51	7	134	26	47	32	6	0	0	0	16	9	10	4
24	Montagu	42.5	7	84	12.9	-	15	6	4	1	10	3	1	7	3
25	Aliwal	35.13	9	1255	195.3	22	608	6	4	0	0	331	2	84	0
26	Cradock	29.1	8	214	37.2	22	46	17	5	1	0	43	1	10	3
27	Fish Eagle Spa	35.7	9	1294	196	16	853	10	4	1	0	335	3	76	0
28	Badsfontein	30.4	7	1093	190.5	17	684	4	4	0	0	316	2	72	0
29	Florisbad	27.8	8	2109	357.5	23	1264	89	5	3	0	681	10	96	1
30	Baden Baden	20.7	8	2183	322	39	1375	4	7	3	0	728	7	37	1
31	Riemvasmaak	33	8	3254	508	254	1145	612	4	6	0	913	17	142	19
32	Natal	43.2	8	229	34.7	84	42	18	7	0	0	67	4	6	1
33	Lilani	39.5	9	280	44.3	117	29	41	9	1	0	81	3	5	3
34	Thangami	38.5	9	398	63	143	42	28	10	0	0	112	4	6	2
35	Shu-Shu	50	9	724	111.5	118	93	52	8	0	0	145	6	8	5
36	Warmbaths	-	10	195	31	110	16	10	8	0	0	64	4	9	5
37	Birlanyoni	-	8	217	34	66	47	24	20	3	1	69	6	6	5
38	Badplaas	50.67	9	384	60.5	44	131	16	7	0	-	111	4	6	1
39	Grovesbad	32.8	-	-	-	-	-	-	-	-	-	-	-	-	-
40	Machadodorp	28	8	395	40.3	55	52	3	3	-	-	60	2	11	3
41	Falcon Glen	42	8	232	35.7	-	12	0	2	-	-	64	-	-	-
42	Amanzimtaba	32.5	8	699	106	58	298	69	7	3	0	140	5	28	1
43	Sulphur Springs	-	9	152	22	64	17	20	13	0	0	35	3	7	6
44	Swazi	42	9	-	-	-	6	4	6	-	-	26	1	4	0

Appendix B: Steam tables- Thermodynamic data for water at saturated vapor pressures and temperatures (adopted from Henley et al., 1984).

Temp. (°C)	Enthalpy liquid (kJ/kg)	Temp. (°C)	Enthalpy liquid (kJ/kg)	Temp. (°C)	Enthalpy liquid (kJ/kg)	Temp. (°C)	Enthalpy liquid (kJ/kg)
47	196.8	73	305.5	99	414.8	125	525.0
48	200.9	74	309.7	100	419.0	126	529.2
49	205.1	75	313.9	101	423.3	127	533.5
50	209.3	76	318.1	102	427.5	128	537.8
51	213.5	77	322.3	103	431.7	129	542.0
52	217.7	78	326.5	104	435.9	130	546.3
53	221.9	79	330.7	105	440.1	131	550.6
54	226.0	80	334.9	106	444.4	132	554.9
55	230.2	81	339.1	107	448.6	133	559.1
56	234.4	82	343.3	108	452.8	134	563.4
57	238.6	83	347.5	109	457.1	135	567.7
58	242.8	84	351.7	110	461.3	136	572.0
59	246.9	85	355.9	111	465.5	137	576.3
60	251.1	86	360.1	112	469.8	138	580.5
61	255.3	87	364.3	113	474.1	139	584.8
62	259.5	88	368.5	114	478.3	140	589.1
63	263.7	89	372.7	115	482.5	141	593.4
64	267.9	90	376.9	116	486.7	142	597.7
65	272.0	91	381.1	117	491.0	143	602.0
66	276.2	92	385.3	118	495.2	144	606.3
67	280.4	93	389.5	119	499.5	145	610.6
68	284.6	94	393.7	120	503.7	146	614.9
69	288.8	95	398.0	121	508.0	147	619.2
70	293.0	96	402.2	122	512.2	148	623.6
71	297.2	97	406.4	123	516.5	149	627.9
72	301.4	98	410.6	124	520.7	150	632.2

Appendix C: Geothermometry (°C) for geothermal waters for current study.

Geothermometry temperatures (°C) for quartz, chalcedony, cristobalite, amorphous silica geothermometers.

Geothermal water sites	Measured Temp. (°C)	Quartz (Fournier, 1977) (°C)	Quartz-Steam loss (Fournier, 1977) (°C)	Quartz, (Arnórsson, 1985) (°C)	Chalcedony (Fournier, 1977) (°C)	Chalcedony (Arnórsson, 1983) (°C)	Cristobalite, (Fournier, 1977) (°C)	Opal-CT(Beta-Cristobalite (Fournier, 1977) (°C)	Amorphous silica (Fournier, 1977) (°C)
BPS	49.4	112	111	213	83	84	62	-9	-5
NTL	40.6	116	115	216	87	87	65	-6	-2
WGD	32.5	121	119	220	93	93	70	-1	3
BAL	41.6	115	114	215	86	87	65	-6	-2
SUS	29.7	99	100	202	69	70	49	-20	-16
MDP	28.8	81	84	186	49	52	31	-35	-32
SILO	50.6	133	129	229	106	105	83	9	13
MPU	43.4	102	103	204	72	73	51	-18	-14
TSH	54.9	111	110	211	81	82	60	-10	-7
SAG	44.7	120	118	219	92	92	70	-2	2
EVGL	30.7	104	104	206	74	75	53	-16	-12
MRS	40.4	148	141	239	122	120	97	22	26
RHM	36.5	99	100	202	69	70	49	-20	-16
BELA	49	117	116	217	89	89	67	-4	-1
BELA 2	35.4	118	117	217	90	90	68	-4	0
BELA3	40.9	112	111	213	83	84	62	-9	-5
LBD1	32.1	65	71	171	33	37	16	-48	-45
LBD2	32.9	65	71	171	33	37	16	-48	-45
LBD3	30.2	63	69	169	31	35	14	-49	-46
ZMTB	34.2	97	98	200	67	68	47	-22	-18
AMZT	31	103	103	205	73	74	52	-17	-13
RIEV	38.4	105	105	207	75	76	54	-15	-12

Geothermal water sites	Measured Temp. (°C)	Quartz (Fournier, 1977) (°C)	Quartz-Steam loss (Fournier, 1977) (°C)	Quartz, (Arnórsson, 1985) (°C)	Chalcedony (Fournier, 1977) (°C)	Chalcedony (Arnórsson, 1983) (°C)	Cristobalite, (Fournier, 1977) (°C)	Opal-CT(Beta-Cristobalite (Fournier, 1977) (°C)	Amorphous silica (Fournier, 1977) (°C)
SKROEF	45	122	120	221	94	94	72	0	4
LIL	40	120	118	218	91	91	69	-2	1
SHU	50.5	108	108	209	79	79	58	-12	-9
AVA	40.3	79	83	184	48	51	30	-36	-33
BAK	38.5	75	79	180	44	47	25	-40	-36
TOOR	41.8	86	89	190	55	57	36	-31	-28
WARM	44	103	103	205	73	74	52	-17	-13
CAZ	49	94	96	197	63	65	44	-24	-21
CALE	48.8	107	107	209	78	79	57	-13	-9
BRA	60.5	95	97	198	64	66	45	-24	-20
GOUD	45.2	81	84	186	49	52	31	-35	-32
THE BATHS	43.0	70	75	176	39	42	21	-44	-40
BRICKS	27.0	47	54	151	14	18	-2	-63	-60
FLO	26.8	67	72	172	35	39	18	-46	-43
BAD	29.4	74	78	179	42	45	24	-41	-38
ALW	32.6	72	77	177	40	43	23	-42	-39
CRAC	25.4	95	97	198	64	66	45	-24	-20
PTS	29.1	83	87	188	52	55	33	-33	-30
TGM	37.5	83	87	188	52	55	33	-33	-30

Geothermometry temperatures (°C) for Na, K and Mg geothermometers.

Geothermal water sites	Measured Temp(°C)	Na-K (Truesdell, 1976) (°C)	Na-K (Fournier,1977) (°C)	Na-K, (Arnósson, 1983) (°C)	Na-K (Giggenbach1988 a,b) (°C)	Na-K (Verma and Santoyo,1997) (°C)	Na-K (Santoyo and Díaz-González, 2010) (°C)	K-Mg (Giggenbach, 1988a,b) (°C)
BPS	49.4	98	142	119	162	330	104	71
NTL	40.6	95	139	115	159	255	100	58
WGD	32.5	72	119	92	139	174	77	49
BAL	41.6	105	148	126	168	462	111	113
SUS	29.7	80	126	100	146	132	85	42
MDP	28.8	113	155	134	174	302	119	52
SILO	50.6	59	107	79	128	225	64	57
MPU	43.4	94	138	114	158	210	99	28
TSH	54.9	77	123	97	143	331	82	73
SAG	44.7	59	107	79	128	164	65	49
EVGL	30.7	60	108	80	129	379	65	48
MRS	40.4	104	147	125	167	343	110	73
RHM	36.5	193	221	215	236	377	199	74
BELA	49.0	116	158	137	177	379	122	81
BELA 2	35.4	114	156	134	175	404	119	50
BELA3	40.9	113	155	134	174	372	118	79
LBD1	32.1	368	348	388	351	394	374	48
LBD2	32.9	385	359	405	361	408	390	50
LBD3	30.2	409	374	428	374	406	414	49
AMZT	34.2	83	129	104	149	347	89	76
ZMTB	31.0	84	130	104	150	350	90	76
RIEV	38.4	57	105	77	126	450	63	71
SKROEF	45.0	66	113	86	134	434	71	73
LIL	40.0	74	121	94	141	236	80	57

Geothermal water sites	Measured Temp(°C)	Na-K (Truesdell, 1976) (°C)	Na-K (Fournier,1977) (°C)	Na-K, (Arnósson, 1983) (°C)	Na-K (Giggenbach1988 a,b) (°C)	Na-K (Verma and Santoyo,1997) (°C)	Na-K (Santoyo and Díaz-González, 2010) (°C)	K-Mg (Giggenbach, 1988a,b) (°C)
SHU	50.5	95	139	115	159	392	100	72
AVA	40.3	438	392	456	390	428	443	62
BAK	38.5	368	348	388	351	394	374	57
TOOR	41.8	490	423	505	417	457	494	74
WARM	44.0	435	391	453	389	463	440	80
CAZ	49.0	495	426	511	419	465	499	75
CALE	48.8	337	327	358	332	423	342	66
BRA	60.5	333	324	353	330	372	338	53
GOUD	45.2	288	293	309	302	319	293	43
THE BATHS	43.0	306	306	328	314	361	312	53
BRICKS	27.0	-22	29	-5	50	341	-18	32
FLO	26.8	33	83	52	104	396	38	93
BAD	29.4	8	59	26	80	178	13	56
ALW	32.6	3	54	21	75	156	8	54
CRAC	25.4	29	78	47	100	-30	34	27
PTS	29.1	10	61	28	82	-32	15	29
TGM	37.5	77	123	97	143	299	82	67

Appendix D: *Geothermal gradients (sourced from Dhansay et al., 2017) for the geothermal waters of South Africa*.

Geological domains	**Dhansay et al. (2017) site names**	**Current study geothermal water site names (abbreviated)**	**Heat flow (mW/m^3)**	**Estimated geothermal gradient (°C/km)**	**Method utilised for estimating the geothermal gradient**	**Data source**
Archean granites and gneisses	Badplaas	BPS	0	53.16	Geothermometer (Si)	Kent, 1949
	Natal	NTL	0	45.23	Geothermometer (Si)	Kent, 1949
	Wagendrift	WGD	0	45	Thermodynamics	Kent, 1949
	Baleni	BAL	0	45	Thermodynamics	Kent, 1949
Pongola Supergroup	Sulphur-Spring	SUS	0	47.97	Geothermometer (Si)	Kent, 1949
Transvaal Supergroup	Machadodorp	MDP	0	49.78	Geothermometer (Si)	Kent, 1949
Limpopo Mobile Belt associated with the Soutpansberg Group	Siloam	SILO	0	64.05	Geothermometer (Na-K)	Olivier and Jonker, 2013
	Mphephu	MPU	0	45	Thermodynamics	Olivier and Jonker, 2013
	Tshipise	TSH	0	46.3	Geothermometer (Si)	Olivier and Jonker, 2013
	Sagole	SAG	0	45	Thermodynamics	Olivier and Jonker, 2013
	Evangelina	EVGL	0	50.05	Geothermometer (Si)	Kent, 1949
	Môreson	MRS	0	45	Thermodynamics	Olivier and Jonker, 2013
Waterberg Group	Rhemardo	RHM	0	45	Thermodynamics	Olivier and Jonker, 2013
	Warmbath	BELA	0	50.05	Geothermometer (Si)	Kent, 1949
	Loubad	LBD	0	40.89	Geothermometer (Si)	Kent, 1949
	Amanzintaba	AMZT	0	45	Thermodynamics	Olivier and Jonker, 2013
	Buffelshoek	ZMTB	0	48.38	Geothermometer (Si)	Kent, 1949
Namaqua-Natal Province	Riemvasmaak	RIEV	0	45	Thermodynamics	Olivier and Jonker, 2013
	Grovesbad	SKROEF	0	45	Thermodynamics	Kent, 1949
	Lilani	LIL	0	45	Thermodynamics	Hoole, 2000
	Shu-Shu	SHU	0	45	Thermodynamics	Hoole, 2000

Geological domains	Dhansay et al. (2017) site names	Current study geothermal water site names (abbreviated)	Heat flow (mW/m^3)	Estimated geothermal gradient (°C/km)	Method utilised for estimating the geothermal gradient	Data source
Cape Fold Belt	Avalon	AVA	0	45	Thermodynamics	Olivier and Jonker, 2013
	Baden	BAK	0	45	Thermodynamics	Baden Information Desk 2016, oral communication, Nov 20
	Toorwater	TOOR	0	45	Thermodynamics	Boekstein, 2012
	Warmwaterberg	WARM	0	35.31	Geothermometer (Si)	Kent, 1949
	Calitzdorp Spa	CAZ	0	45	Thermodynamics	Olivier and Jonker, 2013
	Caledon Spa	CALE	0	52.41	Geothermometer (Si)	Olivier and Jonker, 2013
	Brandvlei	BRA	0	52.48	Geothermometer (Si)	Kent, 1949
	Goudini	GOUD	0	45	Thermodynamics	Olivier and Jonker, 2013
	Citrusdal	THE BATHS	0	45	Thermodynamics	Olivier and Jonker, 2013
Uitenhage Group	Bricks	BRICKS	0	0	-	-
Karoo Supergroup	Florisbad	FLO	0	0	-	-
	Badsfontein	BAD	0	45	Thermodynamics	Kent, 1949
	Aliwal	ALW	0	35	Geothermometer (Si)	Kent, 1949
	Cradock Spa	CRAC	0	45.95	Geothermometer (Si)	Kent, 1949
	Knegha Drift	PTS	0	45	Thermodynamics	Kent, 1949
	Thangami	TGM	0	45	Thermodynamics	Hoole, 2000

Appendix E: Measured temperatures (°C), quartz geothermometry temperatures (°C) and circulation depths (km) for the 41 geothermal waters of South Africa.

Geological domains	Geothermal water sites	Measured temp. (°C)	Quartz (°C) (Fournier, 1977)	Yearly air temp. of sampling locality (°C)*	Geothermal gradient (°C/km)#	Circulation depth (km)
Archean granite and gneisses	BPS	49.4	112	21.84	53.16	1.70
	NTL	40.6	116	22.13	45.23	2.07
	WGD	32.5	121	22.13	45.00	2.20
	BAL	41.6	115	25.95	45.00	1.98
Pongola Supergroup	SUS	29.7	99	21.84	47.97	1.61
Transvaal Supergroup	MDP	28.8	81	21.84	49.78	1.18
Limpopo Mobile Belt associated with the Soutpansberg Group	SILO	50.6	133	25.95	64.05	1.67
	MPU	43.4	102	25.95	45.00	1.69
	TSH	54.9	111	25.95	46.3.	1.83
	SAG	44.7	120	25.95	45.00	2.10
	EVGL	30.7	104	25.95	50.05	1.55
	MRS	40.4	45	25.95	45.00	2.70
Waterberg Group	RHM	36.5	99	25.95	45.00	1.62
	BELA	49.0	117	25.95	50.05	1.83
	BELA 2	35.4	118	25.95	50.05	1.84
	BELA3	40.9	112	25.95	50.05	1.72
	LBD1	32.1	65	25.95	40.89	0.96
	LBD2	32.9	65	25.95	40.89	0.96
	LBD3	30.2	63	25.95	40.89	0.92
	AMZT	34.2	97	21.87	45.00	1.67
	ZMTB	31.0	103	24.22	48.38	1.62
Namaqua-Natal Province	RIEV	38.4	105	24.88	45.00	1.77
	SKROEF	45.0	122	24.88	45.00	2.17
	LIL	40.0	120	22.13	45.00	2.17
	SHU	50.5	108	22.13	45.00	1.91
Cape Fold Belt	AVA	40.3	79	22.05	45.00	1.27
	BAK	38.5	75	22.05	45.00	1.18
	TOOR	41.8	86	22.05	45.00	1.42
	WARM	44.0	103	22.05	35.31	2.29
	CAZ	49.0	94	22.05	45.00	1.60
	CALE	48.8	107	22.05	52.41	1.62
	BRA	60.5	95	22.05	52.48	1.39
	GOUD	45.2	81	22.05	45.00	1.30
	THE BATHS	43	70	22.05	45.00	1.08
Uitenhage Group	BRICKS	27.0	47	21.53	27.00	0.93
	FLO	26.8	67	22.29	26.80	1.67

Geological domains	Geothermal water sites	Measured temp. (°C)	Quartz (°C) (Fournier, 1977)	Yearly air temp. of sampling locality (°C)*	Geothermal gradient (°C/km)#	Circulation depth (km)
Karoo Supergroup	BAD	29.4	74	22.29	45.00	1.14
	ALW	32.6	72	21.53	35.00	1.44
	CRAC	25.4	95	21.53	45.95	1.60
	PTS	29.1	83	21.53	45.00	1.37
	TGM	37.5	83	22.13	45.00	1.36

*The World Bank Group (2021)

#Dhansay et al.,(2017)

Appendix F: The geological domains, geothermometry, circulation depths and low-medium enthalpy of the geothermal waters in South Africa.

Geological domains	**Geothermal water sites**	**Measured temp. (°C)**	**Predicted temp. (°C) (Fournier, 1977)**	**Geothermal Gradient (°C/km)**	**Circulation depth (km)**	**Enthalpy (kJ/kg)**
Soutpansberg Group associated with the Limpopo Mobile Belt	MRS	40.4	147.6	45.0	2.7	624
Soutpansberg Group associated with the Limpopo Mobile Belt	SILO	50.6	133.2	64.1	1.7	559
Archean granites and gneisses	WGD	32.5	121.0	45.0	2.2	508
Soutpansberg Group associated with the Limpopo Mobile Belt	SAG	44.7	120.3	45.0	2.1	504
Namaqua-Natal Province	SKROEF	45.0	122.4	45.0	2.2	504
Waterberg Group associated with the Limpopo Mobile Belt	BELA 2	35.4	118.2	50.1	1.8	495
Namaqua-Natal Province	LIL	40.0	119.6	45.0	2.2	495
Waterberg Group associated with the Limpopo Mobile Belt	BELA	49.0	117.5	50.1	1.8	491
Archean granites and gneisses	NTL	40.6	116.0	45.2	2.1	486
Archean granites and gneisses	BAL	41.6	115.2	45.0	2.0	483
Archean granites and gneisses	BPS	49.4	112.1	53.2	1.7	470
Waterberg Group associated with the Limpopo Mobile Belt	BELA3	40.9	112.1	50.1	1.7	470
Soutpansberg Group associated with the Limpopo Mobile Belt	TSH	54.9	110.5	46.3	1.8	466
Namaqua-Natal Province	SHU	50.5	108.0	45.0	1.9	453
Cape Fold Belt	CALE	48.8	107.2	52.4	1.6	449
Namaqua-Natal Province	RIEV	38.4	104.5	45.0	1.8	440
Soutpansberg Group associated with the Limpopo Mobile Belt	MPU	43.4	101.8	45.0	1.7	436
Soutpansberg Group associated with the Limpopo Mobile Belt	EVGL	30.7	103.6	50.1	1.6	436
Waterberg Group associated with the Limpopo Mobile Belt	ZMTB	31.0	102.7	48.4	1.6	432
Cape Fold Belt	WARM	44.0	102.7	35.3	2.3	432

Oral presentation

Safi, M., Motlakeng, T., Ngamlana, S., Maja, F., Ngubana, M., Phahlane, I. and Dhansay, T., 2022. Energy under your feet. Green Energy Day held online by Geological Society of South Africa.

South Africa is a country that emits large amounts of CO_2, in the developing world. Through the Paris agreement, the government has made a commitment to reduce CO_2 emissions. This is achieved by transferring toward affordable and clean energy that includes understanding and accelerating renewable energy generation. Currently SA has tabled renewable energy in the forms of solar, wind and hydro energy excluding geothermal energy.

SA's geological history includes continental collision with consequent subduction and uplift, together with thrusting, faulting, igneous and metamorphic activity however lacks active volcanism. The complex geological settings have produced geothermal waters that are utilised for recreational activity and not for energy. The reason for this is that there are insufficient regional analyses to understand the geothermal energy of South Africa. This paper looks at additional data to support the possible inclusion of geothermal energy into the South Africa renewable energy mix. Here, we present chemical analyses and interpretation of analytical results where water samples were collected from 41 sites.

The chemical signatures between the deep-seated geological structures and the geochemistry of the geothermal waters, where springs controlled by similar regional structures share similar properties. In addition, using the chemistry together with the heat flow we were able to predict the depth of the source of the geothermal waters.

The data suggests that low enthalpy geothermal reservoirs are located at depths of 0.74 km to a depth of 1.77 km from the surface. We propose that these models be proven with additional geophysical modelling and exploration drilling.

Oral presentation

Safi, M., Motlakeng, T., Ngamlana, S., Maja, F., Ngubana, M., Phahlane, I. and Dhansay, T., 2023. Advances made in geothermal energy in South Africa. GeoCongress. Stellenbosch University, Stellenbosch, South Africa.

The South African government published the Integrated Resource Plan of 2019, where the government outlined plans to increase the use of renewable energy. South Africa's renewable energy currently contributing to the energy grid is biomass, solar, hydro and wind. The Integrated Resource Plan of 2019 fails to explore or add geothermal energy as an additional alternate source of energy[1].

Geothermal energy usage worldwide increased by 27% from 2015 to 2020 for installed capacity. Countries such as the USA, Indonesia, Philippines, Turkey and Kenya have the most installed geothermal power generation[2].

The current research focuses on updated physical and new hydrochemical properties of South African geothermal waters to increase the understanding and knowledge of such waters as a potential source of geothermal energy. The analyses of samples from 41 sites involve physical property measurements, cation and anion and stable isotopes. This data will assist in modelling the potential geothermal reservoir characteristics using solute-based chemistry in the geothermal waters (geothermometry) to ascertain the temperature and depth from which such waters originate. The temperature range gives insight into the potential reservoirs in terms of enthalpy range. To have a comprehensive insight into the geothermal waters, updating or adding information on geological settings, hydrogeology, seismic activity, and socio-economic aspects is necessary to delineate sites for potential energy generation.

The hydrochemical data classifies the geothermal waters into four types: Na-Cl, Na-HCO_3, Mg-HCO_3 and mixed. In addition, utilising the chemistry with heat flow data of the geothermal waters to predict the depth of the source of the geothermal waters is possible. The data suggest that low enthalpy geothermal reservoirs are located at depths ranging from 1-3 km from the surface. We propose that these models be proven with additional geophysical modelling and exploration drilling.

References

- Department of Mineral Resources and Energy, 2019. Integrated Resource Plan 2019. Department of Mineral Resources and Energy, Pretoria.
- Huttrer, G. W., 2021. Geothermal power generation in the world 2015-2020 Update report. Proceedings World Geothermal Congress 2020+1. Reykjavík, Iceland, 17pp.